Aalto University
School of Chemical
Technology

School of Chemical Technology
Degree Programme of Materials Science and Engineering

Alberto Espinosa Ruiz

PREVENTION OF TRANSVERSAL CORNER CRACKING IN CONTINUOUS CASTING OF MICRO-ALLOYED STEELS

Final Project (30cr) submitted for inspection, Espoo, 1 August, 2014.

Supervisor **Professor Seppo Louhenkilpi**

Instructor **M.Sc. Heli Kytönen, M. Sc. Pilvi Oksman**

Author Alberto Espinosa Ruiz

Title of thesis Prevention of transversal corner cracking in continuous casting of micro-alloyed steel

Department Materials Science and Engineering

Professorship Metallurgy **Code of professorship** MT-37

Thesis supervisor Seppo Louhenkilpi

Thesis advisor(s) / Thesis examiner(s) Heli Kytönen, Pilvi Oksman

Date 17.07.2014 **Number of pages** 87 + 7 **Language** English

Abstract

Transversal corner cracking during the continuous casting of micro-alloyed steels is well known to be a consequence of the presence of film-like ferrite along the austenite grain boundaries. Surface structure control cooling (SSCC) has been found to be a promising technique in order to prevent transverse corner cracking. It consists of cooling below the Ar_3 temperature and a subsequent heating over the Ac_3 temperature followed by mild cooling. Cracking is prevented by promoting a double phase transformation which results in a ferrite microstructure that is different from the film-like ferrite along the grain boundaries, and a much more uniform microstructure without any chain-like precipitation at the grain boundaries. This technique has been studied and applied to the continuous casting conditions. Experiments based on the SSCC method with a micro-alloyed steel containing Nb, V and Ti have been carried out in order to evaluate the different parameters that are involved in the process. The SSCC based samples show a finer microstructure than the mild cooling samples. In addition, it could be that cooling until 510 °C and holding time at high temperature of 2 minutes are the most optimal parameters to obtain a microstructure with two different austenites, differenced by their carbon content. No other differences were found between the SSCC based and the mild cooling (normal cooling concept in continuous casting) samples.

Keywords Micro-alloyed steel, transverse corner cracking, hot ductility, surface structure control cooling.

Table of contents

Preface

The present study was funded by the Finnish Funding Agency for Technology and Innovation (TEKES). The research was carried out as part of the Finnish Metals and Engineering Competence Cluster (FIMECC)'s ELEMET program. The financial support is kindly acknowledged.

I am especially grateful to my supervisor Seppo Louhenkilpi and to my instructors, Heli Kytönen and Pilvi Oksman, for giving me the opportunity of making my Master's Thesis in the Department of Materials Science and Engineering of Aalto University. I have to say "kiitos" for all your support, help, and advice during the realization of this study. You have done a remarkable effort and without your help, the execution of this work would not be possible.

I also want to show my sincere gratitude to Marko Kekkonen, Risto Toivanen, Ilkka Penttinen and Ari Kruskopf (I hope I do not forget anyone) for your support and help in the parts in which I did not have enough knowledge. I have learned a lot from you.

My sincerest thanks to my mother, Juana Ángeles, to my father, Alberto (I know you are supporting me wherever you are), to my sister, Belén, and to my girlfriend, Laura, for all your endless and lovely support which you have given to me not only during this year but during my whole student life. You have encouraged me in the worst moments and I really feel that you are also part of this work.

This year has been plenty of good moments, and also not so good. Despite the difficult moments, I keep very good memories of my experience in Finland. I do not regret of choosing Aalto University for my studies and I will never forget this year.

Kiitos paljon!

_____

Alberto Espinosa Ruiz

Espoo, Finland, 17.07.2014

LITERATURE PART

1 Introduction

1.1 General

Micro-alloyed steels typically contain less than 0.2 % carbon content, up to 2 % manganese and small additions of niobium, titanium or vanadium among other elements (less than 0.1 % each and less than 0.15 % in total). These steels are characterized by cost-effectiveness due to the small amount of alloying elements, high yield strength (up to 600 MPa), good toughness, weldability and corrosion resistance. Strength is enhanced by fine grained straightening and by precipitation strengthening due to vanadium, titanium and niobium precipitates that appear as carbides, nitrides or carbonitrides, which precipitate in the austenite and then contribute to dispersion hardening during or after austenite to ferrite transformation. [1]–[7] The key advantage is the weight reduction achievable through substitution, which depend both on the difference in strength and in the mode of loading [4]. Some applications of these steels are large bridges, high pressure vessels, boilers, oil and gas pipelines, construction and farm machinery, heavy-duty highway and off-road vehicles, industrial equipment, storage tanks, mine and railroad cars, off-shore structures, power transmission towers, light poles, building beams and panels, lawn mowers, etc. [3], [5], [6]

In the last four decades micro-alloyed steels have been developed a lot, becoming an indispensable type of structural steel owing to their properties. Nonetheless, obtaining micro-alloyed steels with better quality, lower cost and improved properties is still crucial. Despite their benefits, the current total production of micro-alloyed steels, which is evenly distributed between long and flat products, only represents about 12 % of total world steel production (i.e. about 189 million tons from the 1578 million tonnes of world crude steel that were produced in 2013) [4], [7], [8]. The main reason is that precipitation can cause cracking during other processing stages such as continuous casting [5]. Thus, further investigation of the continuous casting process of micro-alloyed steels is still necessary. Moreover, during the 20th Century continuous casting has turned into the most important process in steel production. The demand of steel with better quality and properties and the necessity of reduce costs, energy and time has caused the investigation and development of continuous casting technique and the parameters that are involved on it.

There are still problems during the continuous casting of steels. Transversal corner cracking is very damaging in micro-alloyed steels, and has not been studied deeply yet. Thus, the investigation of transversal corner cracking becomes very important in order to understand the mechanism of this defect and find solutions to minimize and avoid it. “Surface Structure Control Cooling” (SSCC) is a method that has been

found very promising in the minimization and prevention of transversal corner cracking. SSCC allows the formation of a fine equiaxed microstructure at the surface periphery of the solidifying strand during secondary cooling before reaching the unbending zone in continuous casting process. Thus, the micro-alloyed steel's proneness to cracking during continuous casting could be prevented.

1.2 Goals of the final project

This project has two main goals:

- Examine deeply the reasons and causes for corner transversal cracking in micro-alloyed steels
- Find solutions to minimize transversal corner cracking in micro-alloyed steels and to improve their surface structure

In order to achieve these goals, this thesis is divided in two parts. The first one consists of a literature review based on theoretical fundamentals concerning continuous casting of steel process, problems that occur during continuous casting of micro-alloyed steels and corner transversal cracking.

In the second part the SSCC concept is applied and adapted to the continuous casting process. Laboratory trials, microscope analysis and hardness measurements are carried out in order to obtain information about the phenomena involved in the process.

2 Continuous casting of steel

2.1 Continuous casting process

Continuous casting is the most important process in steel production, being used to produce over 90 % of steel in the world including carbon, alloyed and stainless steels with a great number of steel qualities in very wide variety of dimensions. It is the important linking process between steelmaking and rolling, in which molten steel is solidified for subsequent processing. In 1856 the continuous casting method was suggested by Bessemer but it was not implemented in wide scale until 1960s. Before, steel was poured into stationary moulds to solidify as ingots. During 1930s and 1940s the continuous casting process became a common production method for nonferrous metals. However, for steels it was implemented later due to their relatively low thermal conductivity and the required high casting temperatures. In 1980s continuous casting exceeded the conventional ingot steel casting route, turning into the biggest steel casting method. Continuous casting has a lot of benefits compared to the conventional ingot casting route such as improvement of steel quality, better

yield and saving of energy and manpower. [9]–[12] The principle of continuous casting is illustrated in Figure 1.

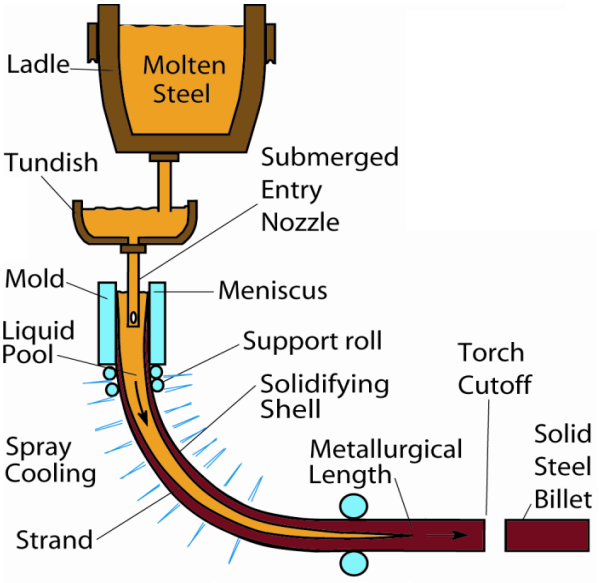

Figure 1. Schematic of steel continuous casting process [9].

The molten steel in a ladle is transferred to the caster. When the process starts, the nozzle at the bottom of the ladle is opened and the steel flows into the tundish at a controlled rate. Then, steel from the tundish flows through a submerged entry nozzle (SEN) into one or several moulds, which are generally water cooled moulds. The steel should be protected from exposure to air over each vessel by slag cover and between vessels by ceramic nozzles. The first solidification occurs at the metal-mould interface, where the molten steel freezes against the mould walls to form a solid shell. The shell thickness increases progressively when the steel is withdrawn through the machine. The withdrawn is carried out at a rate or casting speed that matches the flow of incoming metal, thus the process ideally runs in steady-state. Below the mould exit, the shell thickness must be enough to support the remaining liquid. To minimize bulging due to the ferrostatic pressure there are rolls that support the steel. Between rolls, water and air mist sprays are utilized to cool the surface of the strand in order to maintain its temperature until the molten core is solid. The mould and rolls cooling is called the primary cooling, while the spray cooling is called secondary cooling. At the machine end, when the centre is completely solid, the strand is cut off and transferred to a rolling mill. [9], [11]

The biggest challenge in continuous casting of steel is to cast steel continuously without interruptions and to minimize defects. Although steel cleanliness is mainly determined by the preceding operations, continuous casting also influences it. In addition, solidification control is important to achieve good surface and internal quali-

ty. Research and development in the continuous casting field is still being carried out in order to cast steels with better quality and to develop methods to cast extra difficult steel grades with special problems and requirements such as cracking and high surface quality. Ecological aspects and energy efficiency are nowadays important aspects as well. [9], [11], [12]

2.2 Conventional continuous casting process

Continuous casting is, by far, the most important process in steel production. There exist three main types of casters, result of the development during the years in order to reduce the capital costs and to improve the quality of the steel: simple vertical casters, vertical bending casters and curved casters. The length of the casters is between 500 and 800 m. [10]–[12] The different types of casters can be observed in Figure 2.

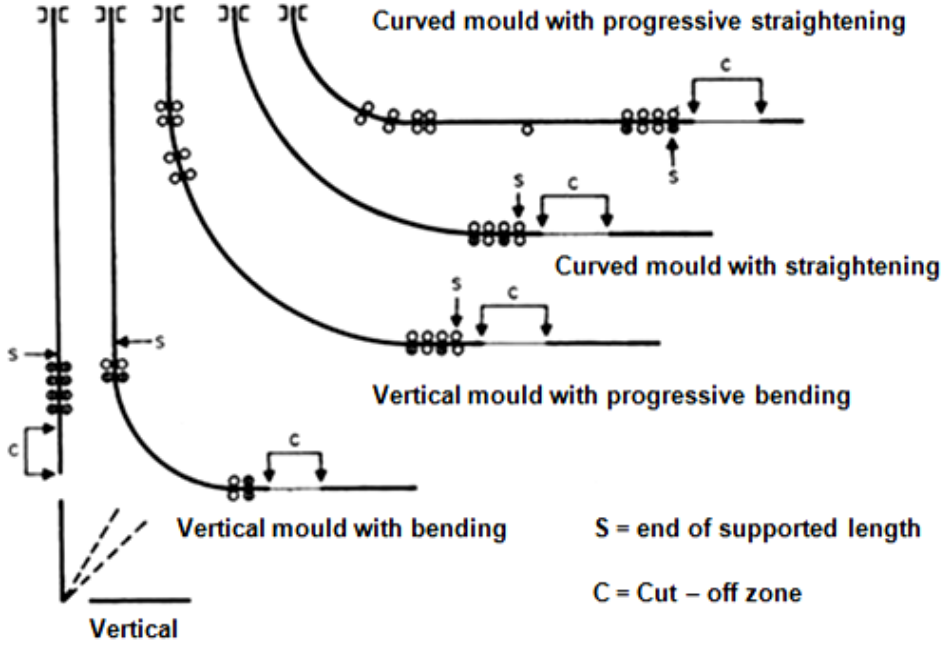

Figure 2. Scheme of the different types of casters [13].

In addition, according to the strand dimensions the casters are typically named as billet, bloom and slab casters. Billets are squares (< 200 x 200mm^2), slabs are rectangular (width 1000-2000mm, thickness 100-200mm) and blooms are between them. There are also round products and other shapes as beam blanks. [9], [11], [12]

2.2.1 Vertical casters

Simple vertical casters were the first industrial continuous casting machines. One advantage of vertical casters is that some defects that appear in the other types such as transversal cracking can be reduced or even eliminated due to there is no bending or straightening of the strand. Thus, these casters are especially suitable for high

surface quality steel and high alloy steel casting. Another advantage is that non-metallic inclusions can float up more easily to the meniscus (the upper liquid surface in the mould) than in the other casters due to the solidification of the molten steel is done in the vertical direction, while in bow type casters some inclusions can may be attached to the inner arc of the strand shell when they are flowing up [11], [14], [15].

However, the main problem in these casters is that the distance between the mould and the point of cutting is limited, what leads to low casting speed and therefore to low production rate. In addition in the case of large strand sizes severe defects such as segregation and cracking can appear due to the high bulging of the solidified strand shell which is caused by the ferrostatic pressure of the liquid steel inside the strand. The higher the machine is, the bigger the risk for bulging. Furthermore, vertical casters have large overall height. [10], [11], [16] In the past 10 years these casters have rarely been used except for a few special steel grades [14].

2.2.2 Vertical bending casters

Further development resulted in vertical bending casters, which consist of bent casters with straight mould, with an arc continuous casting machine and a straight line segment. Three types exist: with bending and straightening of the solid strand, with bending and progressively straightening while there is liquid inside the strand and bending and straightening while there is still liquid inside the strand [11], [13], [14].

These casters, as well as the curved casters, were developed with the target of constructing lower and simpler machines with smaller need for space, high flexibility in production and maintenance and lower investment costs. The vertical mould provides improvement of quality and increases of productivity 1.4-1.5 times because the distance between the mould and the point of cutting is smaller than in straight vertical casters. Moreover, the risk for bulging is smaller than in straight vertical casters as well. In addition, in these casters inclusions can float up better than in curved casters. Due to the need for cleanliness in larger strand, especially with slab, vertical bending casters are nowadays widely used. [10]–[12]

However, vertical bending casters have some disadvantages such as early and considerable deformation of the strand shell, there are no driven rolls in the bending section, their overall height is large and the degree of straightening deformation is high. In addition, the ferrostatic pressure in these casters is higher than that of the curved casters, which could causes bulging effect if the mould cannot withstand it. [10], [16]

2.2.3 Curved casters

Curved casters are bow type casters with a curved mould. Nowadays they are the most common casters. There are two different types: with straightening of the solid strand and with progressive straightening, while there is still liquid inside the strand. [10], [11], [16]

The reasons for their extended utilization are: high speed and high production rate can be achieved, the height is lower, the risk of bulging is smaller owing to the lower ferrostatic pressure of the liquid steel inside the strand and, the most important reason, the strand in this casters leaves the curved mould in an arc without need for further bending and just with straightening at the lower part of the machine when shell is already relatively thick. However, as explained above, a drawback of these casters is that inclusions cannot float up easily to the meniscus. [10], [11], [16]

2.3 Near net shape casting

Near net shape casting (NNSC) means casting close to the final dimension and shape of the final product. Thus, the hot rolling process can be minimized or even omitted and a lot of time, energy and material can be saved. The NNSC methods can be classified as thin slab casting, strip casting and near net shape casting of long products and rapid solidification processes. [11]

2.3.1 Thin slab casting

Thin slab casting is used for slabs that typically have a thickness of 40-80 mm and the casting speed is about 4-20 m/min in order to attain the same production rate as with the conventional caster. [11] The advantages are savings in investment costs and energy owing to less rolling passes in hot rolling and smaller and more compact machine construction [17]. The machine length can be diminished from 800 m of conventional casting machines to 250 m [17], [18]. However, the problem is that is not possible to get very strong work hardening effect than with the conventional thicker slabs. Nowadays, there are many thin slab casters based on conventional slab casters. [9], [17], [18] Figure 3 shows a schematic of the thin slab casting process.

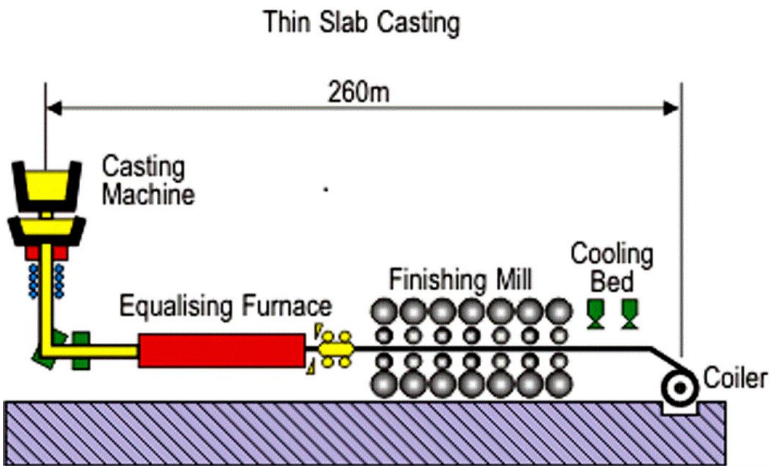

Figure 3. Schematic of thin slab casting process [18].

2.3.2 Strip casting and near net shape casting of long products

Strip casting is used to cast thin sheet or strip, in which hot rolling and intermediate processes can almost be omitted and very thin strip can even be directly introduced into cold rolling. Strip thickness is 5-20 mm and the thickness can be even less than 1 mm. The casting speed is 10-40 m/min. Due to the high casting speed, the cooling rate is high and the solidification takes place in a very short region of the strand rapidly, obtaining a fine microstructure with less segregation than in the cast product. [11] In addition, the total length of the line is only about 60 m. [19]

Strip casting is usually performed by two processes: twin roll process and single process. In twin roll process casting is done between two rolls. Single roll process is usually used when casting very thin strip. The steel melt is poured and dragged on a rotating roll where the steel final thickness is acquired and solidification occurs instantaneously. Advantages of this process are that there are no roughers nor finishers and a reheat furnace is not needed. [11], [19]–[21]

Strip casting has reached industrial applications in United States, for instance by Castrip, for carbon steel grades and for stainless steels, but the methods are still under development and still have not reached industrial applications. The reason is that it is a complex process which involves complex interactions between fluid flow, solidification, shrinkage and stress which leads to quality problems [21], [22]. Figure 4 shows a scheme of a twin drum strip caster.

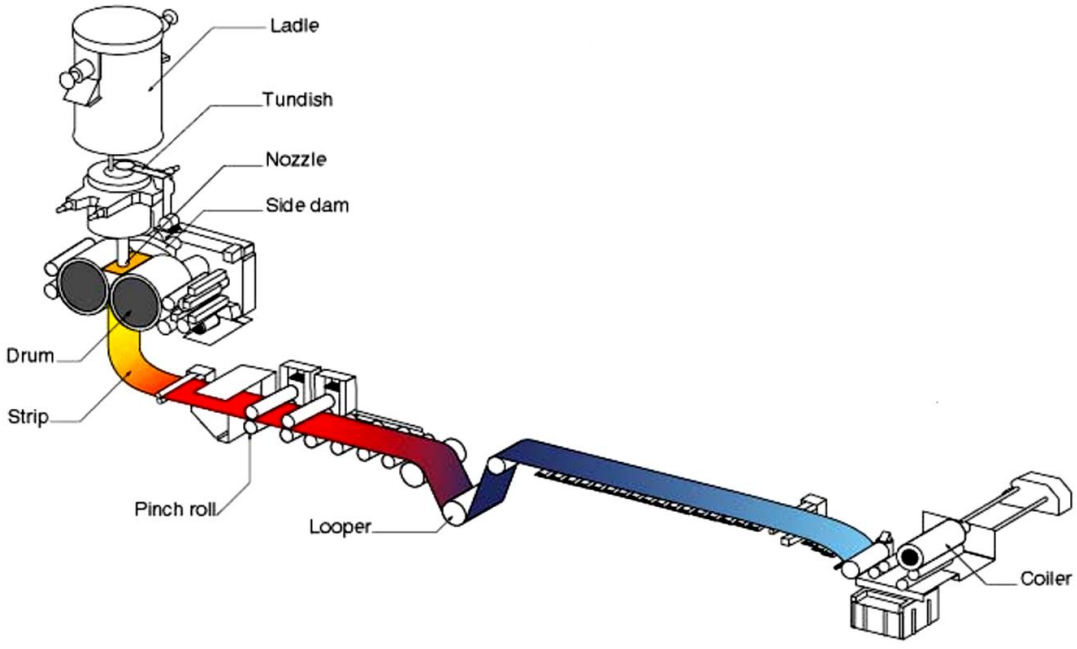

Figure 4. Schematic of a twin drum strip caster [23].

In spite of be only used at pilot-scale, strip casting provides some improvements comparing to conventional methods. Hot rolling can be bypassed, anisotropy is reduced due to the usually weak primary crystallography, a fine microstructure is obtained owing to the high cooling rate, steel sheets which do not have enough intrinsic ductility for rolling can be directly casted and small quantities of high steel grade can be profitably produced. [20], [23]

2.3.3 Rapid solidification processes (RSP)

Rapid solidification process is used to cast very thin strip, much less than 1 mm, with very high cooling rate. Thus, crystallization can be avoided and a non-crystalline metallic amorphous metal can be obtained with special metal alloys. It is applied in the laboratory scale. The aim is typically to cast wire directly. [11]

2.4 Fundamentals of solidification in continuous casting of steel

Solidification control is very important for surface and internal quality. There are many important control parameters in solidification such as steel chemistry, casting speed, mould level, mould powder, mould oscillation, liquid steel temperature, secondary cooling conditions and parameters that affect the flow phenomena in the mould. [10]–[12], [24]

2.4.1 Solidification structures

The cast structure during continuous casting consist of three zones: a chill zone adjacent to the strand surface which structure consist of fine equiaxed crystals, a columnar zone in which dendrites extend towards the inside from the chill zone, perpendicular to the strand surface, and a central equiaxed zone which consist of randomly oriented dendrites (Figure 5). The size of the columnar dendrites is about ten times bigger than that of the equiaxed dendrites. Columnar dendrites have higher risk of internal cracks formation than equiaxed dendrites and a long columnar zone increases the severity of centreline segregation and porosity because columnar grains are very long and thin, with long parallel grain boundaries. [11], [12], [24], [25]

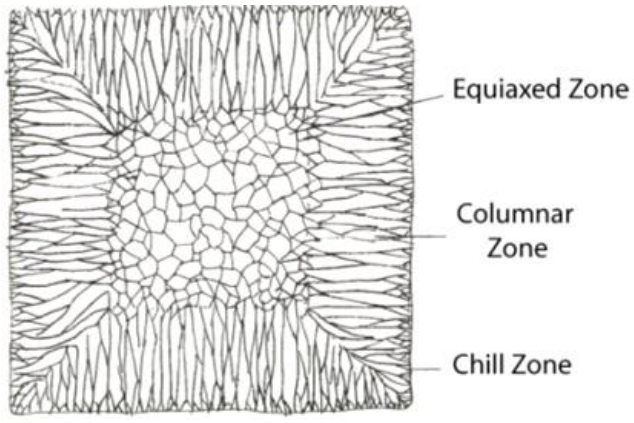

Figure 5. Cast structure during continuous casting [25].

A dendrite is a tree-like structure that grows when the melt is freezing. It has the primary arm or the main branch and also secondary arms, tertiary arms, etc. The driving force for dendrite growth is the undercooling of the melt. When the undercooling increases, the Gibbs free energy difference between the liquid and solid state increases and exceeds the energy barrier. Thus, solidification can take place. The growing morphology is typically dendritic. The reason is that the surface energy of the solid, which is one main reason for the energy barrier, is anisotropic in the case of steels and many other metals. Thus, the growth in certain directions is energetically favoured, typically against the direction of the heat flow. [11], [12], [24]

Other morphologies such as cellular and planar can take place with special compositions and/or cooling conditions that are not typical for steels. Amorphous solidification, which means that the solid is non-crystalline and lacks the long-range order characteristic of a crystal, can be obtained with cooling rate high enough. Anyhow, to suppress nucleation in metallic systems very high cooling rates are required. That cooling rates can only be achieved in special RSP processes. [11]

In continuous casting of steel, the first nucleation takes place at the mould-metal interface. The nuclei grow to the energetically favoured directions forming randomly-oriented dendrites, which in turn form the outer equiaxed zone close to the surface with fine equiaxed dendrites. These dendrites have the favourable growing direction towards the heat flow direction. Then the growth continues against the heat flow forming columnar dendrites. Generally these dendrites can grow to the centreline of the casting if the casting conditions are favourable (typically if the superheat of the steel melt is high, even though other parameters can also affect the grow velocity of the dendrite tip) and during the growing new dendrites might be formed from the higher order arms. This zone is called columnar dendrite zone. However, very often a central equiaxed zone is forming as well, again randomly-oriented equiaxed dendrites. The width of the inner equiaxed zone is related to the amount of superheat in the melt (the lower the superheat, the wider the equiaxed zone). The dendrites are not symmetrical due to many phenomena occur during the dendrite growth such as dendrite engulfing, branching and coarsening. [10]–[12], [24]

Below the solidus the structure is called as grains. Depending on the dendrite alignments just below the solidus a grain can include one or more dendrites. Grain boundary movement can take place after solidification and the final grain structure can be altered by solid state transformations. The grains are typically growing due to the grain surface has extra energy and larger grains have less surface per grain volume compared to smaller grains. At high temperatures the growth can be fast due to fast diffusion, but at low temperatures the growth is small or even non-existent. Inclusions formed during solidification and precipitations formed during cooling prevent the growth due to the pinning effect. Small grain size entails good resistance for

cracking during casting and good mechanical properties in the final product. [11], [12], [24]

2.4.2 Microsegregation

Microsegregation is a phenomenon that takes place during solidification in the scale of dendrites. Microsegregation is the variable distribution of chemical composition on the microscopic level in a microstructure owing to the difference between the liquid and solid composition during solidification. Equilibrium diagrams assume that diffusion is infinite and therefore that the concentration at solidus when all the melt has been solidified is homogeneous and the composition is equal to the nominal composition. However, this is not the reality and in real casting conditions the microsegregation is typically much higher due to small composition gradients that exist after the solidification. High microsegregation, especially of the harmful elements, should be avoided owing to it can leads to hot cracking, formation of inclusions and eventually to macrosegregations. [11], [24], [26]

The degree of microsegregation of a specific element is influenced by three factors: the equilibrium partition coefficient, the diffusion coefficient of the element in the solid phase of the alloys and the cooling rate and dendrite spacing. The equilibrium partition coefficient (K_p) is a coefficient which is defined as $K_p=C_s/C_l$ where C_s is the solidus composition and C_l the liquidus composition. Typically it is smaller than one. [11], [27] The diffusion coefficient of the element in the solid phase of the alloys is the rate at which a diffusing substance is transported through a unit surface in a unit time at a concentration gradient of unity. [28] In steels, the diffusion coefficient of many chemical elements are usually higher in ferrite than in austenite, which entails that the microsegregation typically is much stronger for high carbon steels than for low carbon steels. Diffusion in the steels that contain interstitial elements is fast. In the steels that contain a substitutional element diffusion is slow. [11], [27]

High cooling rate and high arm spacing lead to stronger microsegregation as a separate phenomenon. The effect of the cooling rate is twofold, because the cooling rate and arm spacing are coupled. High cooling rate reduces the diffusion time and cause high segregation but it reduces the arm spacing as well, which leads to reduce the segregation. [11], [27]

Microsegregation itself is not usually a serious defect in the as-cast strand due to the fast homogenization below the solidus and it can be removed by annealing. However, if it is high during solidification it can entail severe defects like hot cracking, formation of inclusions or macrosegregation. In micro-alloyed steels Nb causes more segregation than the other microalloying elements since it is the element that shows higher equilibrium partition coefficient. Ti also segregates, although less strongly. V segregates slightly and Al presents a very small tendency to segregate [11], [24], [27]

2.4.3 Macrosegregation

Macrosegregation is non-uniformity of composition on a large scale, mainly caused by fluid flow. It is found in the central regions of the continuously cast products and it cannot be removed by annealing and it leads to non-uniform mechanical properties. Its severity increases as the columnar zone length increases. [11], [24], [27]

The microsegregated melt which is situated between the dendrites can move either outwards to the surrounding bulk liquid or inwards. The inward flow is due to the shrinkage of the melt during solidification, in order to compensate the density difference between the solid steel and the liquid phase. The inward flow causes a positive macrosegregation (the concentration of the alloying element is higher than the nominal) at the surface region and negative segregation (the concentration of the alloying element is lower than the nominal) at the centre part of the strand. This kind of segregation caused by the inward flow is as-called inverse macrosegregation. It is difficult to avoid owing to the shrinkage is a fundamental phenomenon during solidification, but is typically very small and therefore not a problem. [11], [26], [29]

The segregation caused by outward flow might lead to severe macrosegregation as to centre-line segregation, mesoscopic scale segregations and white band segregations. Severe mesoscopic and centre-line segregations can be formed due to bridge formations caused by the dendrites through which the melt cannot flow very well, especially in billet and bloom casters. The bridges are formed when the microsegregated melt flows into the shrinkage cavity formation in the centre part of the strand. In slab casters the microsegregated melt flows into the voids along the centre-line that have been developed during the shell bulging near the liquid pool end area. Thus, bulging should be minimized as much as possible. In continuous casting typically mesoscopic scale segregation takes place close to the centre-line and it has two names depending of the shape: A-type segregation or freckles, and V-type segregation or channels. These defects are normally not as severe as the centre-line segregation in terms of quality and surface damaging. [11], [26], [29]

2.4.4 Solidification paths

Figure 6 shows the Fe-C equilibrium diagram up to 6.67 %, the carbon content at which Fe_3C (cementite) is formed. The data of this diagram can present little variations depending on the source consulted. At higher C content the product is considered pure graphite. In practical, all steels and cast irons have less than 6.67 wt% C. Three types of ferrous alloys can be distinguished: iron (< 0.008 wt % C), steel (0.08-2.14 wt % C) and cast iron (2.14-6.7 wt % C). [11], [30]

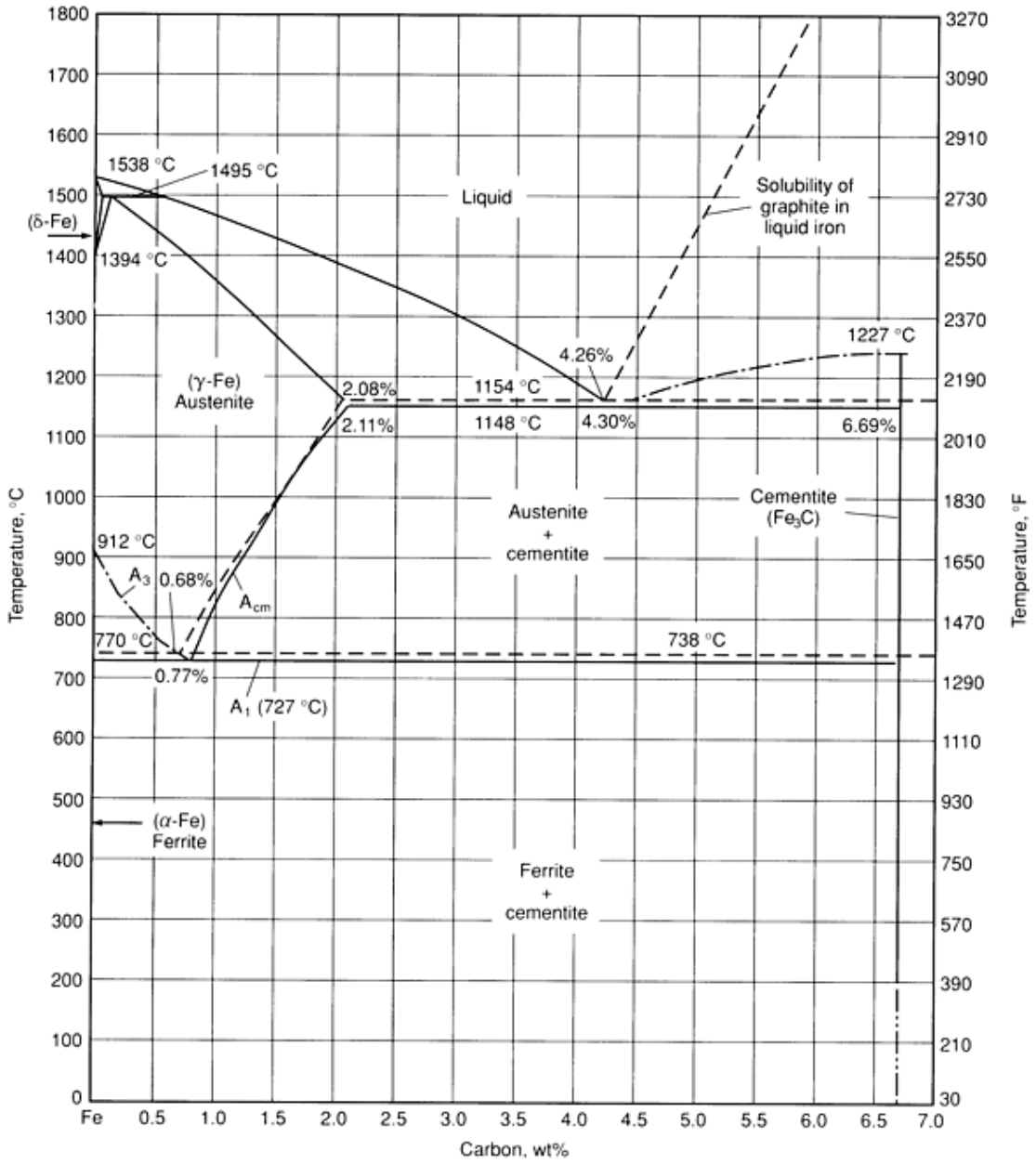

Figure 6. Fe-C equilibrium diagram up to 6.67 wt% C. Solid lines indicate Fe-Fe_3C diagram. Dashed lines indicate iron-graphite diagram [30].

In steel, there are four different solidification paths at high temperature that result from three different important points of the Fe-C equilibrium phase diagram (C%=0.1, C%=0.18, called as peritectic point, and C%=0.51) [11]. Figure 7 shows these points.

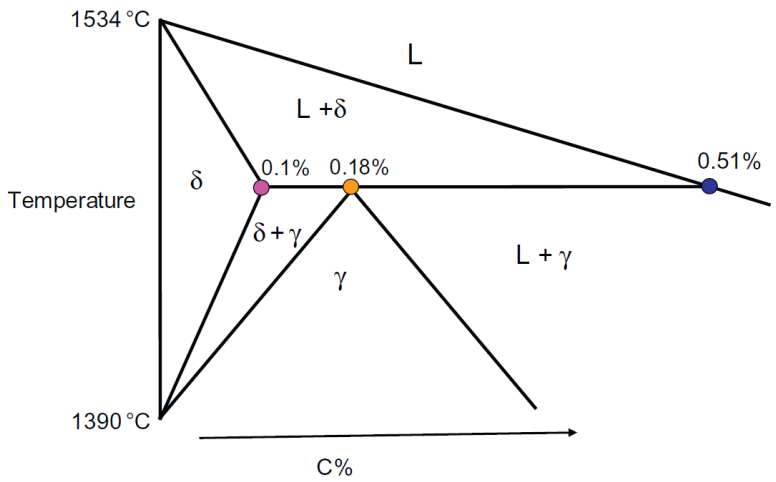

Figure 7. The left uppermost part of the Fe-C equilibrium phase diagram. The three points in the figure divide the solidification of the Fe-C steels into four different areas. The four areas are: 1) C= 0-0.1%, 2) C= 0.1-0.18 %, 3) C= 0.18-0.51% and 4) C>0.51%. [11]

All steels typically solidify according to one of these four solidification paths despite these values are only for binary Fe-C alloy in equilibrium conditions and non-equilibrium conditions and alloying alter these values [11], [19]. Since in this thesis micro-alloyed steels are considered, only areas 1 and 2 are studied.

Area 1 (C=0-0.1 %): Solidification takes place with liquid to δ-ferrite phase transformation, thus the dendrite is fully ferritic at solidus. The diffusion coefficients in ferrite are high and therefore microsegregation is small and these steels are not very sensitive to hot cracking. Below the solidus the δ-ferrite transforms to austenite. During this transformation the steel shrinks about 0.6 %. If this transformation starts close to solidus (in steels close to 0.1 %) the steel can be very sensitive to many types of surface defects due to when shrinkage occurs at a thin shell close to solidus, the shell is not strong enough to resist deformation. The deformation leads to the formation of air gaps between the shell and the mould, which means reduced heat transfer leading to shell reheating and grain growth and uneven heat transfer and shell growth. Thus, these steels are sensitive to hot spots, surface cracking and longitudinal surface cracking. If the δ-ferrite to austenite transformation takes place at lower temperature, not close to solidus, the shell is stronger to resist its deformation. If the amount of ferrite in the strand is big, the strand should well cooled and supported to prevent bulging owing to ferrite phase is quite soft. [11], [19]

Area 2 (C=0.1-0.18 %): Solidification starts with liquid to δ-ferrite phase transformation. Steels which carbon content is C=0.1 % or close to that are very sensitive to surface defects, as occurs to the steels of area 1. When the carbon content is 0.08 % the dendrite is fully ferritic. When it is higher the solidification starts with δ-ferrite

but when temperature decreases to the peritectic temperature above the solidus, the peritectic reaction takes place and the previously solidified δ-ferrite reacts with liquid forming austenite. When the temperature is decreasing, the reaction continues and the austenite is formed between the liquid and the δ-ferrite phases. Thus the austenite grows towards both to the liquid and solid directions. When the carbon content is 0.18 % the peritectic reaction ends due to both the liquid and δ-ferrite disappears at the same time and therefore the solidus structure is fully austenitic. The austenite grain size of these steels will be relatively high and this increases the sensitivity to cracking. The peritectic reaction of the steels with carbon content between 0.1-0.18 % ends when the liquid phase disappears. The remaining δ-ferrite continues to transform to austenite just below the solidus. The more the solidification takes place with liquid to δ-ferrite transformation the smaller the microsegregation is. Thus, low carbon steels are less sensitive to surface defects than higher carbon steels. [11], [19]

It should be noted that the homogenization of the structure below the solidus temperature is in general fast because the diffusion rates are high at high temperatures, even if the microsegregation is strong. This is especially notable with interstitial elements such as C, B, N, O and H. [11]

2.4.5 Austenite decomposition

The austenite decomposition of the Fe-Fe_3C phase diagram is shown in Figure 8.

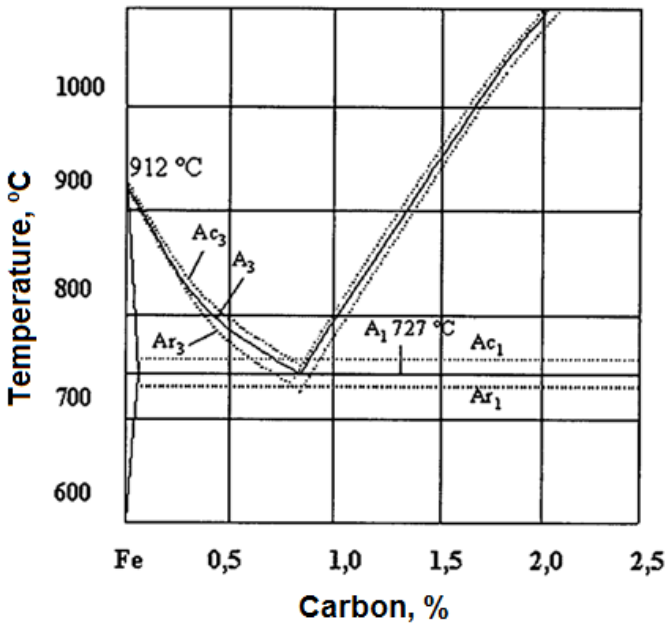

Figure 8. The austenite decomposition part of the Fe-Fe_3C equilibrium phase diagram [31].

There are three important lines: A_3, A_1 and A_{cm}, and the so-called eutectoid point at C=0.77 %. The A_3 line is the starting temperature for the austenite to α-ferrite phase transformation. α-ferrite has the same crystallographic structure that the δ-ferrite. The A_{cm} line is the start temperature for the austenite to cementite transformation, instead of α-ferrite. The A_3 lines can also be marked as A_{3e}, A_{3r} or A_{3c} and similarly for A_1. In this nomenclature e means equilibrium condition, r cooling condition and c reheating condition. Typically $A_{3c}>A_{3e}>A_{3r}$. All carbon steels are fully austenitic already at high temperatures. [11], [19]

Low carbon steels have some ferrite after solidification but it rapidly disappears through the ferrite to austenite phase transformation. Then, austenite is stable until the temperature reaches the A_3 or A_{cm} lines. If the carbon content of the steel is lower than the eutectoid point (0.77 %) the steel cools down through the A_3 line and if the carbon content of the steel is higher through the A_{cm} line. During normal cooling both α-ferrite and cementite are nucleating and forming at the austenite grain boundaries and growing from there to the centre part of the austenite grains. [11], [19]

The ferrite and cementite that are formed prior to the eutectoid transformation are referred to proeutectoid ferrite (Figure 9 (a)) and cementite (Figure 9 (b)). The proeutectoid forms of ferrite grown along austenite grain boundaries, typically during slow cooling, are called grain boundary allotriomorphic ferrite. Other morphological ferrites can appear in special conditions such as Widmanstätten ferrite and acicular ferrite. Widmanstätten ferrite appears when the cooling rate is moderately high and the austenite decomposition is produced with large undercooling (Figure 9 (c)). It typically nucleates at grain boundaries but grows as a needle-like towards the centre of the grain. This microstructure is undesirable due to its properties are worse than other ferrite morphologies. Acicular ferrite appears if the cooling rate is more rapid than slow cooling (Figure 9 (d)). It is formed in the inner part of the austenitic grains typically by direct nucleation on the inclusions, resulting in short randomly oriented ferrite needles which especially increases the toughness. Its nucleation is aided by non-metallic inclusions of a certain type and size, which needs to be numerous enough but not so much because too many particles could cause defects on the structure. [11], [19]

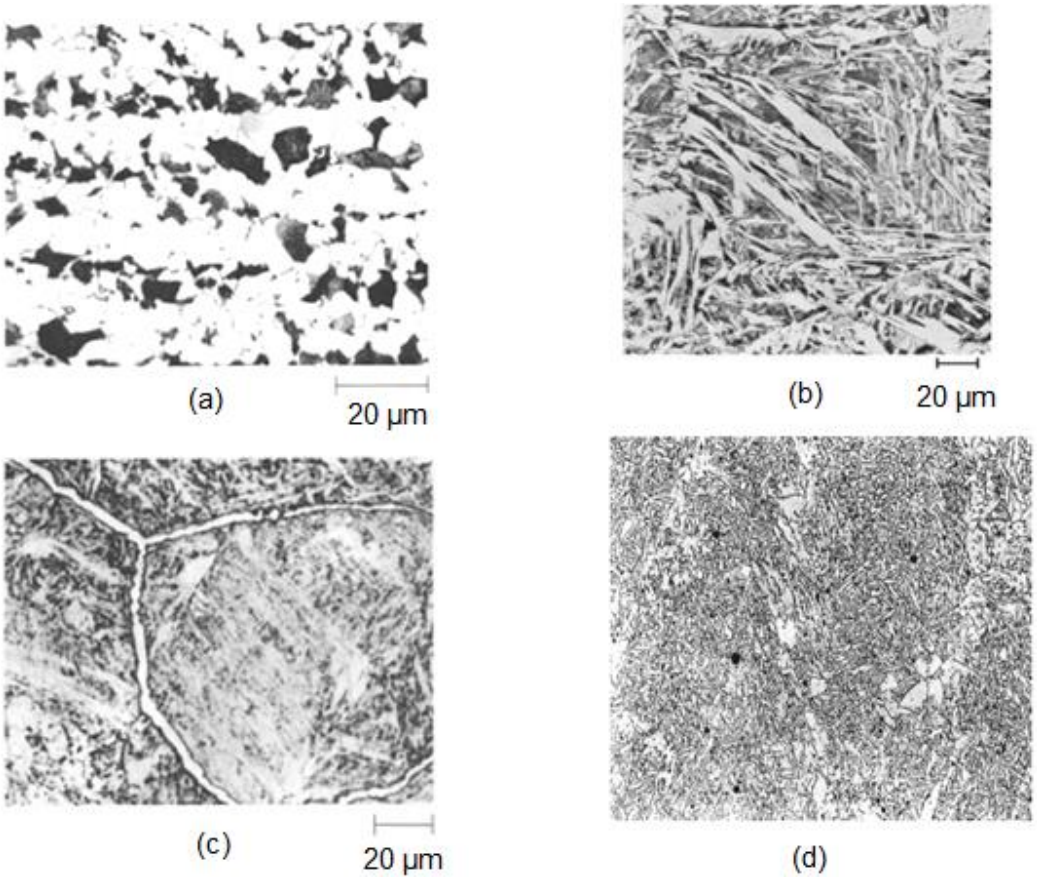

Figure 9. Different microstructures during austenite decomposition. (a) shows a light micrograph of proeutectoid ferrite (white) and pearlite (dark) in a 0.17 C-1.2 Mn-0.19 Si steel [30], (b) shows a light micrograph of Widmanstätten ferrite (large elongated with white crystals) formed in micro-alloyed steel isothermally transformed for 100 s at 600 °C etched with Nital [19], (c) shows a light micrograph of cementite network on prior-austenite grain boundaries in an Fe-1.5 C-1.12 Cr alloy [30] and (d) shows a light micrograph of acicular ferrite in low-carbon weld metal etched with Nital at 500x [19].

Just below the A_3 or A_{cm} lines due to the narrow α-ferrite or cementite film in the austenite grain boundary areas the structure becomes relatively weak especially with the grain boundary cementite. The structure can become even weaker with the presence of certain precipitates (such as AlN, Nb(C.N), etc.) in the ferrite band. These precipitations can also precipitate at the austenite grain boundaries above the A_3 temperature, weaken the austenite grain boundaries. The structure becomes stronger again when the ferrite band grows thicker. [11], [19]

If the carbon content is very low, the A_1 line is not traversed and the structure at room temperature is almost totally α-ferrite with almost zero carbon but with some cementite in the grain boundary. If the carbon content of steel is higher, α-ferrite is

growing until the temperature reaches de A_1 line and then after traversing the A_1 line the remaining austenite transforms to pearlite. This reaction is called as eutectoid reaction, where solid austenite transforms to two solid phases forming a lamellar eutectic structure formed by cementite and α-ferrite lamellas. Depending on the growth the eutectic structure will be coarse when it is slow or fine when it is rapid. Thus, the final equilibrium structure at room temperature of the typical carbon steel is called ferritic-pearlitic. At the eutectic composition only pearlite is formed. [11], [19]

Non-equilibrium microstructures such as bainite, martensite and retained austenite can be also obtained increasing the cooling rate or due to the alloying elements of the steel and the grain size of the austenite. Many systems never reach equilibrium. In order to study the formation of non-equilibrium states the continuous cooling transformation (CCT) diagram, which measure the extent of transformation as a function of time for a continuously decreasing temperature, and the time-temperature transformation (TTT) diagram, which measure the rate of transformation at a constant temperature have been developed and used. [11], [19]

3 Transversal corner cracking in continuous casting of micro-alloyed steel

Transversal corner cracking is a defect that occurs very often in continuous casting of micro-alloyed steels which hinders the production continuity of the slabs and reduce their hot delivery and casting quality [2], [6]. Transversal corner cracks are related to the strong cooling of the edges during cooling [33]. Their length ranges from some millimetres to 15-20 mm and their depth ranges up to 5-10 mm [34]. They are caused due to excessive deformation with low strain rate during the austenite to ferrite phase transformation. It is especially remarkable in micro-alloyed steels with high N content. [35] In addition, the formation of longitudinal shrinkage stresses when the edges of the ingot are excessively cooled has strong influence in the formation of transversal cracks. [34]

Transversal cracks initiate at high temperatures in the mould and are associated with segregation in the vicinity of the oscillation marks. [36]–[38] Microalloying elements do not influence this stage of transversal crack formation [36]. These cracks become larger and more numerous at lower temperatures during straightening or bending operation of casting in the secondary cooling segment. In these operations, usually carried out within the temperature range of 600-1200 ºC, the slab is exposed to strong thermal and mechanical stresses on the top surface and edges. This temperature range coincides with the range where micro-alloyed steels exhibits a ductility minimum, between 700 and 1100 °C depending on the steel chemistry, with the consequent susceptibility to surface cracking. [36], [38]–[44]

In the vertical bending type continuous casters the temperature of the slab corners decreases dramatically from about 1200 ºC to the temperatures range of the ductility trough (700-1000 ºC) during casting because of the intensified cooling due to the two-dimensional heat delivery on slab corners. It causes that when bending is made the fixed side (outer surface) of the slab is exposed to large tensile stress and cracks appear at the troughs. Thus, transversal corner cracks are usually found on the fixed side (outer surface) corner of the slabs and rarely on the narrow surface of the loose side (inner surface). The notch effect of the trough of oscillation marks has an influence as well. In addition, the stress at the corner is greater than that of the centre. The heat is conducted from the molten steel in the slab centre to both slab surface and corner. Thus, their temperatures rise and remain out of the temperatures range of the ductility trough. [2], [34]

Transversal cracks are usually distributed alongside the oscillation marks and along prior austenite grain boundaries due to chain-like precipitates and film-like proeutectoid ferrite. No slag inclusions can be found in cracks. [2] Figure 10 shows the transversal corner cracks on the slab.

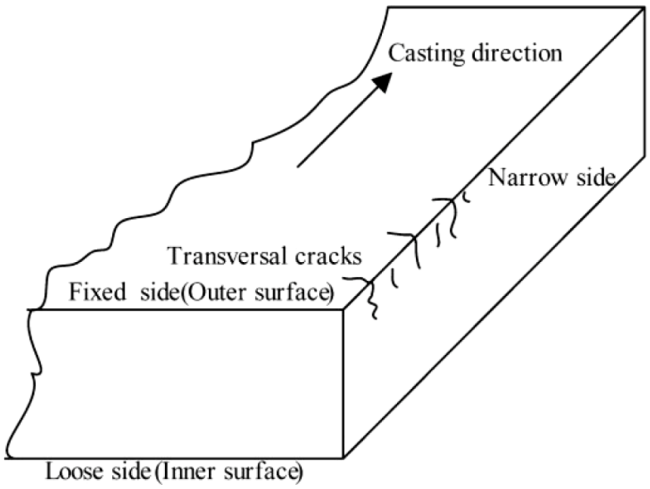

Figure 10. Transversal corner cracks on the slab [2].

There is a relation between transversal cracking and hot ductility. As was mentioned above, the temperature interval where straightening and bending operations are carried out coincides with the temperature interval where micro-alloyed steels exhibits a ductility minimum. When low ductility regions are present, cracking is much more likely to take place. As hot ductility is strongly influenced by microalloying elements additions, this is the way how these elements affect transversal cracking [36]. Hot ductility will be discussed in chapter 4.

4 Hot ductility

The micro-alloyed steels experience a loss of ductility at temperatures generally ranging from 700 to 1000 ºC [44]. Hot ductility is usually measured by the reduction of area of the samples after hot tensile tests performed up to the fracture point. This measurement allows the formation of the so-called hot ductility curves. [38], [42], [44] Hot ductility curves are generally obtained by hot tensile testing of the steel at different temperatures, showing the temperature versus reduction of area at fracture [44]. The advantage of this method is that it is independent of the fracture geometry of the sample [38]. In addition, this method is more sensitive to soft changes in precipitation than yield and flow strength measurements [45]. Depending on the hot tensile test, different authors have given different values of reduction of area to avoid transversal cracking (p.e. Bannenberg suggested 75 % [46], Suzuki et al. Suggested 60 % [47] and Mintz and Crowther suggested 40 % [48], [49]) [36].

The results obtained from the hot ductility curves can be wrong. A large improvement of hot ductility at high temperatures in hot tensile testing can occur due to the onset of dynamic recrystallization, which is not possible during straightening. [48]

In a typical hot ductility curve three regions can be distinguished: the high ductility – low temperature region (region I), the ductility trough or embrittlement region (region II) and the high ductility – high temperature region (region III) [44] A typical hot ductility curve can be observed in Figure 11:

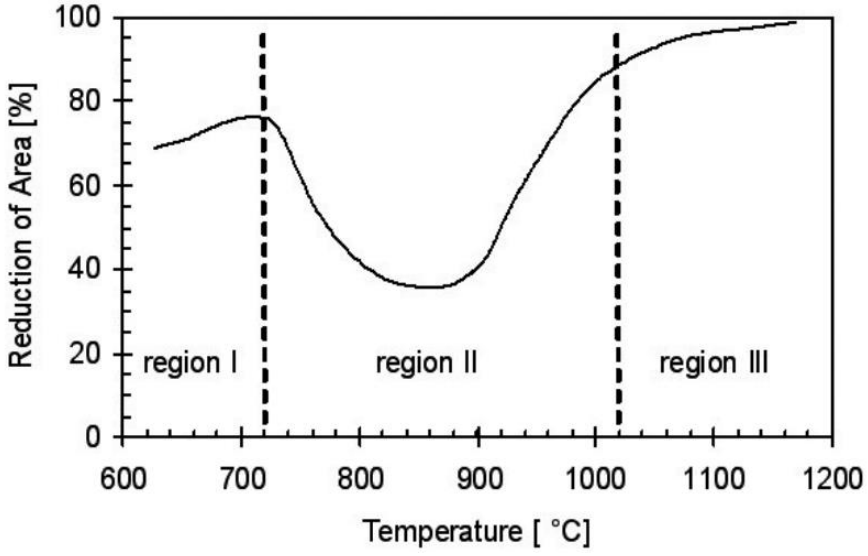

Figure 11. Typical hot ductility curve recorded for a steel showing the embrittlement region at an intermediate temperature range. [44]

4.1 Region I: High ductility – low temperature region

Region I includes temperatures lower than approximately 700 °C. In this region relatively large fraction of ferrite is formed. The recovery rate of the ferrite is higher and the grain size is finer compared to that of the austenite from which the ferrite has been formed. Thus, strain localization in a thin ferrite film at the austenite grain boundaries is restrained. [38], [44] In addition, at these low temperatures higher ductility is observed because the strain in the ferrite decreases and the plastic strain in the austenite increases. The reason is that the strength differential between ferrite and austenite decreases when the temperature is decreasing and thus the concentration of strain at grain boundaries is minimised. [38] Furthermore, the volume fraction of ferrite is higher with decreasing the temperature. As a result, there is not strain concentration. [6]

In general, at temperatures near to 700 °C the ductility is very good if the percentage of ferrite is high. The reason is that at this temperature the recovery in the ferrite occurs with relieve, the flow strain is low and the grain size is large. [38]

4.2 Region II: Ductility trough or embrittlement region

The ductility trough region is associated with intergranular fracture and transversal cracking appears in a temperature range of approximately 700-1000 °C [38], [44].

Ductility is reduced because of the formation of a thin film of ferrite in the austenite to ferrite phase transformation at the austenite grain boundaries that takes place at this temperature range. The strength of the ferrite is lower than that of austenite and therefore ferrite absorbs the majority of the deformation. [2], [39], [43], [44] In ferrite low flow stresses compared to austenite occurs. Thus, there are strain concentrations in the ferrite film that leads to ductile voiding when the ferrite cannot supports the strength generated by stress. Thus, cavities emerge in the films and cracks develop along the grain boundaries leading to their separation. [2], [6], [38] The thickness of the ferrite film has a dominant role on hot ductility. When a thin ferrite film is formed at the austenite grain boundaries is when the ductility is minimal due to microvoid coalescence in the ferrite film. [6] This ferrite film is deformation induced and strain induced ferrite can appears at temperatures above the Ar_3 temperature and often as high as the Ae_3 temperature. Its thickness does not experience significant changes below the Ae_3 temperature until the Ar_3 temperature is reached. Following reduction in the temperature quickly thickens the ferrite film and ductility is fully recovered when approximately 50% ferrite is present before starting the test. [38] This recovery of ductility is due to the decrease of deformation in these regions [11].

In addition, another reason for the ductility loss is the precipitation of second phase particles such fine nitrides as AlN when Nb and Al are present together and Nb(C,N)) or sulphides (MnS) at the austenite grain boundaries. [38], [42]. These precipitates encourage void formation either at ferrite films or during grain boundary sliding and

cause the existence of precipitate free zones adjacent to grain boundaries, which presents weaker resistance to deformation than the rest of the matrix structure [44], [50]. NbC precipitation during austenite to ferrite transformation makes that the carbon content near the grain boundary is lower and therefore film-like proeutectoid ferrite is formed [2]. Fine precipitation can occurs in the matrix leading to significant matrix strengthening as well [38]. Generally finer precipitates leads to lower ductility due to a more effective pinning action of grain boundaries, allowing more time for crack nucleation and linking and enhancing the hot cracking damage [44]. The effect of precipitates is discussed in chapter 5.2.

Voids usually appears firstly at large inclusions and then progressively at smaller particles. The amount of microvoid coalescence increases while lowering the temperature until deformation induced ferrite appears and all the fractures are of this type. [38]

4.3 Region III: High ductility – high temperature region

Region III includes temperatures higher than approximately 1000 ºC. These temperatures lead to the absence of ferrite and to less precipitation in the matrix and at the grain boundaries than at lower temperatures [36], [38]. The precipitation at the grain boundaries of precipitates such as Nb(C,N), V(C,N), Ti(C,N) or AlN can lead to a ductility loss, even at lower strain rates [11].

In addition, the formation of (Mn,Fe)S-O precipitates at the austenite grain boundaries can lead to a ductility loss. The reason is that these precipitates have pinning effect. Thus, the moving of the grain boundaries is prevented and the structure is weak. However, this usually occurs at high strain rates and therefore it is not a major problem in continuous casting since the strain rates are too small. [11], [36]

5 Effect of steel grade

Grain size and precipitates have high importance in hot ductility of micro-alloyed steels, especially the latter [51]. Thus, their effects on hot ductility and therefore in transversal cracking are explained in this chapter.

5.1 Effect of grain size

The grain size has an important influence on transversal cracking. In general, the smaller the grains size of the steel, the better the hot ductility. However, this performance might be different in the micro-alloyed steel due to the effect of the precipitation of carbonitrides and impurities at the grain boundaries. [52]

The austenite grain size is influenced by the austenizing temperature due to austenite grain growth is very retarded by the presence of second phase particles, especially by fine grain boundary precipitates. Many kinds of cracks, such as transversal cracks, are connected with a coarse austenite grain size due to deformation induced

ferrite can lead to a wide and deep ductility trough. In this way the tendency of cracks can be reduced by preventing the formation of coarse austenite grains. [52] Furthermore, grain refinement gives benefits when low-ductility intergranular failures occur. The reason is that refined grain decreases the crack aspect ratio, complicates the propagation of smaller cracks formed by sliding through triple points, increases the specific grain boundary area (which reduces the precipitate density on the grain boundaries) and reduces the critical strain for dynamic recrystallization by increasing the number of nucleation sites. At 850 ºC, grain refinement from 300 to 150 μm is expected to increase the reduction of area value by 15-20 % in tests. [51], [52] The austenite grain size does not influence the precipitation kinetics of NbC [45].

However, a small grain size can also be harmful to hot ductility. Deformation before straightening to refine the grain size has been found not to be feasible due to significant strains are required to recrystallize the coarse as cast grain size. [38], [39]. In addition, hot ductility is worse when there is dynamic precipitation in a fine form in the grain boundaries and in the matrix [38], [39], [49], [51]. Dynamic precipitation is the precipitation that takes place when the precipitation rate is increased when strain is imposed, for instance during deformation. The reason is that favourable nucleation sites are introduced by the deformation process. [36], [38], [52] When the particles are less than 50 nm in size, their ductility is reduced. When the particles are about 10 nm in size they are likely to give rise to serious transversal cracking. [49]

Despite not having influence on the reduction of area measurement, the grain size also has influence in the ease of propagating cracks to a critical depth. Columnar grains, which are associated with certain levels of C and Al, have been found to encourage the growth of transversal cracks. [38]

The ferrite grain size has influence on the strength of the steel. Finer ferrite grain sizes mean higher yield strength, better toughness and better ductility. [3]

5.2 Effect of precipitates

During continuous casting of micro-alloyed steels, many precipitates are formed because these steels contain Nb, T and V. Nb, T and V are strong nitride and carbide formers, which can be formed in different stages and locations such as in the liquid steel upon collision of the particles, in the mushy zone between dendrites because of rapid diffusion during solidification, and inside the grain or at the grain boundaries due to slow solid state diffusion. The role of the precipitates on cracking is very important and mainly depends on their amount, composition, size distribution, location and morphology. [36], [38], [52], [53] The carbides and nitrides precipitate in a chain-like way at the austenite grain boundaries. Thus, the grain boundary binding force will be weakened and movement of the precipitates along the grains will be suppressed, which leads to ductility reduction and cracks propagation along the bounda-

ries. In addition, precipitates determine the depth, position and width of the ductility trough. [2]

The rate of precipitation is increased when strain is imposed, for instance during deformation, because of dynamic precipitation. [36], [38], [52] V precipitates are randomly distributed throughout the matrix whereas Nb(C,N) precipitates are found both within the matrix and at the boundaries [38], [51].

In general, coarse precipitates are favourable to hot ductility. Coarse precipitates means that the particle spacing increases and hence the strength difference between the grain interior and the precipitate free zone is reduced. Therefore the formation and propagation of microcracks is suppressed. [54] Large volume fractions are likely to increase strength and therefore to reduce hot ductility. Thus, it is recommended to minimize the volume fraction of the precipitates [36], [38], [52], [54]. In turn, fine precipitation pin the grain boundaries in the case of grain boundary sliding in the austenite when deformation occurs, allowing the cracks to join up. Moreover, both precipitates and inclusions cause void formation and the increment of their volume fraction at the grain boundaries promotes microvoid coalescence failures. [36], [38], [52] In any case, there must be a balance in precipitates form and function. If they are too large, they cause quality problems because they do not restrict grain boundary movement and the corresponding growth. If they are too fine or dissolved, they do not have any effect. [53] Figure 12 shows the formation of surface cracks and precipitate embrittlement.

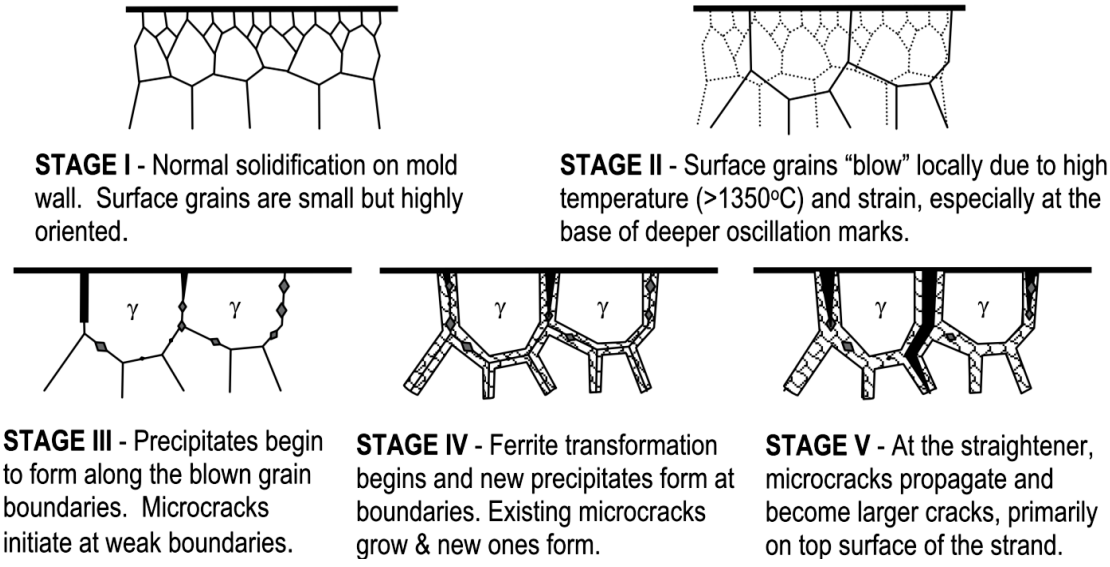

Figure 12. Formation of surface cracks and precipitates embrittlement. [53]

The precipitates also have influence on dynamic recrystallization depending on their size and volume fraction. The greatest effect on delaying recrystallization is achieved

by large volume fraction of fine particles. The volume fraction of precipitates also has influence on the temperature at which ductility begins to recover. [36], [52]

6 Effect of chemical elements on transversal corner cracking of micro-alloyed steel

Apart from Fe and C, many different elements are present in steels. The common alloying elements are Mn, Ni, Cr, Mo, V, Si, B, Al, Ni and Ti but there are many others as well. Their presence affects in many ways. For instance they might increase the strength by solid solution strengthening (C, Cr, Mn, Ni, Mo, Si, Co) or increase hardness by forming carbides (Ti, W, V). [11], [55]

The alloying elements strongly affect the stability of the different phases. Phases and phase relations during solidification and cooling may be affected due to the alloying elements can extend or decrease the phase areas where they are stable and even form new intermetallic phases and carbides. They have influence on the important points of the Fe-Fe_3C equilibrium phase diagram (peritectic, eutectoid, etc.) and lines (A_3, A_1, A_{cm}, etc.). Depending on their influence on austenite and ferrite stability the alloying elements can be divided in austenite stabilizing elements (Mn, Ni, Cu, N, etc.) and ferrite stabilizing elements (Cr, Si, W, Mo, V, P, Ti, Al, etc.). [11], [55]

In this chapter, the influence on transversal cracking of the most common elements added to the micro-alloyed steels is discussed. They are divided in three different categories depending on their influence: microalloying elements, elements with considerable influence and other elements. The composition of the steel analysed in this thesis is shown in chapter 11.

6.1 Microalloying elements

The elements that have highest influence on transversal cracking of micro-alloyed steels are the microalloying elements (Nb, V and Ti). The reason is that Nb, V and Ti precipitates are the responsible of the precipitation strengthening during continuous casting of the micro-alloyed steel. Thus, cracking can take place. Transversal surface cracking is the only defect that is influenced by these elements [36]. As was mentioned in chapter 1.1 micro-alloyed steels typically contain small additions of niobium, titanium or vanadium among other elements (less than 0.1 % each and less than 0.15 % in total).

6.1.1 Niobium

Nb is added to the steel due to its ability to refine the austenite grain size and induce precipitation hardening. Thus, high strength and toughness can be obtained. [3], [56] Its effect in grain refinement is more effective than that of V. Nb additions of 0.01 % increase the yield strength from 35 to 40 MPa. [3]

However, this precipitation causes bad surface quality and makes the casting of these steels more difficult [56]. The Nb containing micro-alloyed steels exhibit very low hot ductility during straightening, suffering transversal surface cracking [40]. The effect of niobium is detrimental, decreasing the minimum ductility and especially broadening the ductility trough to higher temperatures [36], [57]. In addition, Nb has a powerful influence in decreasing the Ar_3 temperature, widening the trough at low temperatures [56]. Nb additions as small as 0.017 % or even smaller are detrimental to hot ductility. Thus, the Nb content should be as low as possible in order to avoid transversal cracks. [2], [36], [38]

The main cause of low ductility at high temperatures is the precipitation of fine Nb(C,N) along the austenite grain boundaries, that are particularly effective in preventing grain boundary mobility and reducing ductility [2], [58]. These precipitates encourage voiding and the extension of the cracks that are formed by grain boundary sliding [58]. When Nb(C,N) precipitation occurs at the temperature at which single phase austenite forms, it enhances grain boundary sliding in the course of straining which leads to low ductility. Intergranular fracture is promoted by the appearance of coarse eutectics and precipitate free zones along the grain boundaries. [6], [57], [58] Nb(C,N) precipitates can precipitate as fine particles at both grain boundaries and grain interiors [40], [58].

It has also been suggested that Nb(C,N) precipitates delay the initiation of dynamic recrystallization by pinning the boundaries. Therefore the cracks are allowed to be formed by grain boundary sliding and to join. [6], [36], [44], [58] It has been observed that Nb begins to precipitate at the austenite grain boundaries at 1100 ºC, but it seems to influence the ductility only under 950 °C owing to the limited kinetics of the reaction, what makes the precipitation out of equilibrium and probably incomplete [2], [42]. The maximal susceptibility for cracking is observed in the range of 800-900 ºC in Nb containing steels [37].

In Nb-Ti micro-alloyed steels very large precipitates, that play any useful role in refining grain size, can be found. These precipitates are complex Nb-rich (Nb,Ti)(C,N) precipitates, which precipitate at 900-1000 ºC. Their precipitation path is that first small nuclei are formed during solidification and/or in high temperature region and then the nuclei grow during isothermal holding with equilibrium composition at about 1000 ºC. The precipitates have three different morphologies: semi-dendritic, dendritic and rod-like shapes. Most of them are quite small semi-dendritic precipitates. [1], [54] Hot ductility can be improved by reducing their volume fraction or coarsening their size [54].

In Nb bearing steels reducing the cooling rate (p. e. from 4 to 1 °C/s) improves ductility because it makes the ductility trough narrower and shallower but in the Nb-free steels the cooling rate has no influence [57].

6.1.2 Vanadium

The addition of V to the steel contributes to strengthening by forming precipitates. Fine V(C,N) precipitate particles from 5 to 100 μm in diameter are formed during cooling. V additions increase yield strength depending on C content and cooling rate. It averages 5 to 15 MPa per 0.01 % V. [3]

However, the presence of V in the steel has a harmful effect on hot ductility. The higher is the V content, the worse the hot ductility. [58] The effect of V is less detrimental to ductility than that of Nb, even for a steel with 0.1 % of V [36], [38], [49], [57]–[59]. The reason is that V has higher solubility in the austenite compared to Nb. Thus, V precipitates in a coarser form and a greater volume fraction of precipitate is required to deteriorate the ductility. V precipitates are more randomly distributed as well. In addition, V containing steels have little VN precipitation, while Nb containing steel has a lot of Nb(C,N) precipitation because V precipitates are not as stable as Nb precipitates. [3], [36], [49], [51], [58], [59] In steels with V<0.1 % any problem has been found [57]. The most effective intra-granular nucleation of ferrite is provided by the precipitation of VN [4].

The maximal susceptibility for cracking is observed in the range of 800-900 ºC in V containing steels [37]. Steels that contain both Nb and V shows better ductility at temperatures lower than approximately 900 °C but significantly worse ductility at higher temperatures than that of Nb containing steels [49], [60]. There are two possibilities for this: One is that V addition to Nb bearing steel increases the carbonitride solubility because it decreases the activity coefficient of C and N, slowing down the precipitation kinetics. The other is that the precipitation in the austenite is coarser and fewer due to the V presence. The solubility of (Nb,V) (C,N) is higher than that of NbC. Thus, recrystallization is delayed, increasing the strength and worsening hot ductility. [60]

Work on V-N and V-Nb steels showed that there is a ductility trough in the temperature range of 700 to 1000 ºC with a minimum at 800 ºC. The hot ductility is better at the onset of dynamic recrystallization temperatures, which are 950 ºC and 1050 ºC respectively. Thus, it is higher for the V-Nb steel compared to the V-N steel. This temperature is higher with the V and N content increasing due to N favours more precipitation of VN, retarding recrystallization at the deformation temperature. [60] V additions to Nb containing steels improve hot ductility by changing the morphology of the (Nb)(C,N) precipitates to coarser precipitates [36], [59].

For V containing steels with less than 0.005 % N transversal cracking does not occur, although at high levels of V and N (for instance 0.15 %V, 0.02 %N) transversal cracks appear [36].

6.1.3 Titanium

Ti additions to the micro-alloyed steels can form a number of compounds that provide grain refinement, precipitation strengthening and sulphide shape control. Ti is a strong deoxidizer, so it can be used only in aluminium deoxidized steels in order to ensure that Ti is available for the formation of other compounds than titanium oxide. [3] It does not grain refine the as cast structure but it seems to be the most effective microalloying element in reducing transversal cracking [38], [49].

The effect of Ti on the hot ductility of the micro-alloyed steels depends on the Ti:N ratio which in turn controls the precipitate size [36], [44], [49], [57] The precipitate volume fraction is increased when increasing the Ti content for a given N content [49]. Ti additions of 0.02-0.04 % reduce transversal cracks and Ti content of 0.15 % is required to completely avoid transversal cracking [36]. In addition, transversal cracking is considerably reduced for steels which Ti content of 0.015-0.020 % when the N content is lower than 0.0045 %. [38], [49]

However, at the stoichiometric ratio for TiN (3.4:1), when the maximum volume fraction of precipitate can form, it has highly detrimental effect due to the precipitation of fine TiN particles at the boundaries [36], [49], [57]. In Nb-Ti steels with high Ti content and about 0.005 %N the equilibrium volume fraction of precipitates is much larger than that of a Nb steel [54]. Work done by Luo et al. [54] shows that in a Nb-Ti steel with high Ti content half of the particles precipitate below 1150 ºC. Thus, the ductility trough is extended to higher temperatures and ductility is worsened because a large volume fraction of fine precipitates could form in the straining stage. [54] The Ti micro-alloyed steels without Nb does not possess any higher minimum reduction of area values than the Nb bearing steel. In these steels the Ti/N ratio is 2.8, rather near the stoichiometrc ratio, and fine TiN precipitation can appears which is detrimental to ductility. [57]

In C-Mn-Nb-Al steels small addition of Ti improves hot ductility and reduces transversal cracking [4], [36], [38], [40], [44], [49], [56] at low Ti/N ratios (≤ 2) and at low cooling rates (≤ 1°C/s) [36], [49], [57]. The reason is that the Ti containing particles precipitates at the lowest temperature so that they are fine (<10 nm) [49]. The reason for the beneficial effect is that Ti-rich (Ti,Nb)(C,N) relative coarse and finely dispersed precipitates are formed at high temperatures by Ti additions as low as 0.005 % - 0.007 %. Thus, the formation of AlN precipitates, which are more detrimental, is prevented and the amount of N available to form Nb(C,N) is reduced. In addition, TiN particles can act as preferential nucleation locations for Nb and V precipitates and therefore the Nb(C,N) phase is able to occur at higher temperatures obtaining coarser precipitates that are too coarse to diminish hot ductility significantly. By the time the temperature drops to 1200°C most of the Nb has already precipitated as NbC. Thus Nb(C,N) precipitation cannot occur at lower temperatures. [4], [6], [38], [44], [49], [52] Moreover, large precipitates of (Nb,Ti)(C,N) are formed, which is beneficial

to hot ductility [6]. In these steels, dendritic particles of (Nb,Ti)(C,N) of 50 nm size richer in Nb have also been found because TiN and Nb(C,N) are mutually soluble [49]. In Nb-Ti the supersaturation of Nb in the austenite is reduced due to the Nb contained in the (Ti,Nb)(C,N) and to the delay of the precipitation of strain-induced NbC forming in the matrix of Nb-Ti steel [45]. In Nb containing steels with C content less than 0.08 % the addition of Ti makes that no scarfing is necessary [38], [49].

In V containing Nb free steels with similar Ti and N content very fine TiN particles that had precipitated out at low temperatures have been found [49].

In steels with 0.005 % N, optimum ductility can be achieved with a low Ti content, about 0.01 %, to limit the precipitate volume fraction or high Ti level, about 0.04 %, to have a Ti:N ratio of 4-5:1 to favour precipitation at high temperatures and excess Ti to encourage growth. [49]

6.2 Elements with considerable influence

In addition to the microalloying elements, there are other elements that are commonly presented in the micro-alloyed steel and have effect on transversal cracking: Al, B, Ca, C, Cu, H, Ni, N, P and S. S, P and the Mn/S ratio have especially importance in surface cracking. Furthermore C, S and P have big influence in internal cracking. [36]

6.2.1 Aluminium

In micro-alloyed steels Al can be harmful due to AlN precipitation, which leads to an embrittlement of the steel [33]. In Nb containing steels, the presence of Al even in relatively small amounts might deepen and widen the ductility trough especially when N content is increased due to the precipitation of AlN at the austenite grain boundaries in addition to that of Nb(C,N). Furthermore, Nb(C,N) precipitates are finer, which deteriorates the hot ductility. [36], [38] It has been estimated that the Al content in these steels should be lower than 0.03 % [38].

In Ti containing steels the Al level should be restricted to very low levels to avoid AlN precipitation although for a steel with Ti:N ratio of 2:1 and Al level of 0.03-0.04 % the hot ductility is better. It has been suggested that the reason is that Al associates with the N and instead not producing a precipitate, this effectively increases the amount of Ti in solution, what encourages the growth. [49]

6.2.2 Boron

Boron is used to increase the hardenability of the steel. It has a beneficial effect at temperatures where the austenite and ferrite phases coexist improving the hot ductility because the precipitation of $Fe_{23}(B,C)_6$ in the matrix that acts as preferential sites for ferrite intergranular nucleation and less ferrite is available to form at grain boundaries. [40], [61] In addition, $Fe_{23}(B,C)_6$ contains N and therefore its precipitation reduces the amounts of N and C available for the precipitation of Nb(C,N) leading to an

increment in the density of mobile dislocations [40]. Thus, the interior austenite grain is more deformable owing to the soft intergranular ferrite and the number of cracks and voids at grain boundaries is diminished [40], [61]. However, B additions must be controlled because if it precipitates in a fine form the ductility can be very poor. Hot ductility is improved by increasing the B/N ratio when decreasing the cooling rate and at the stoichiometric ratio (0.8:1) the best ductility has been found with high cooling rates. [48]

At austenitic phase temperatures the beneficial effect of boron is not clear. [40], [61] It has been suggested that boron addition improves hot ductility by several factors such as preferential BN precipitation, retardation of the austenite to ferrite transformation (avoiding the formation of ferrite films at the austenite grain boundaries) and increasing resistance to grain boundary sliding during straightening operation resulting in better creep ductility. The best improvement in deformability is observed in Ni_3Al. In addition strong B segregation, which mainly appears at boundaries between new recrystallized grains and deformed original grains, delays the nucleation and growing of new grains. The migration of the new grains is delayed because of the solute drag force and thus the recristallization is delayed as well. However, the segregation of B impurities at the grain boundaries could deteriorate the hot ductility. Soluble B can segregate towards boundaries at high temperature and can occupy proper nucleation sites preferentially and lower austenite grain boundary energy. Thus, the decomposition of the austenite is suppressed and grain boundary cohesion is increased. Boundary cohesion is also favoured because of the strong tendency of B to segregate to the grain boundaries but not to cavity surfaces. Moreover there is a shift of the ductility trough to lower temperatures due to the boron addition. The most likely reason is the decrease in the formation temperature of pro-eutectoid ferrite at austenite grain boundaries. [61]

At 900 and 1000 ºC there is dynamic recrystallization which contributes to high ductility together with the grain boundary sliding phenomena. At 700 and 800 ºC these phenomena are not observed. At 800 ºC boron micro-alloyed steels exhibit a region of hot ductility loss, thus the hot ductility is worse at this temperature than at 700, 900 and 1000 º C. The recovery of hot ductility at 700 ºC is due to the high volume fraction of ferrite since there is no recrystallization. In addition, it has been found that the onset of the dynamic recrystallization is lowered as the B content is higher. In certain steels an increment of B from 62 to 105 ppm leads to a reduction of area greater than 60 %, which means a further improvement in hot ductility. [61]

B addition to Nb-containing steel makes that the grain interior can undergoes a considerable amount of deformation and relieve the stress at grain boundaries. [40]

6.2.3 Calcium

The effect of Ca is beneficial because its presence entails a reduction in the total amount of S in the steel thereby reducing the amount of S in solution or precipitated

in a finer form during cooling after solidification [38], [49], [50], [57]. The modification of the inclusions cannot be account as the reason for the improved hot ductility in calcium treated steels. Precipitation patterns and grain sizes are not modified by Ca addition in the as cast specimens. [50]

In Nb-containing steels Ca addition improves hot ductility [36], [40] although Nb(C,N) precipitations remain [50]. When Ca is added to the melt, cleaner steel can be produced, which can lead, to better hot ductility. The reason is that the sulphides can be removal from the liquid by flotation due to the solubility of the sulphide is reduced and the sulphide is precipitated in the liquid ahead of solidification. Thus, less S is available for further precipitation at the austenite grain boundaries. [50] However, it has also been reported that calcium silicide is related with uneven oscillation marks, promoting cracking [36].

The recommended Ca/S ratio is 2 to obtain fully modified calcium sulphides-calcium aluminates [50], [57]. The cracking tendency becomes lower with increasing Ca/S ratio between 0.5-1.6. [57]

6.2.4 Carbon

The carbon content is very important due to its influence in the austenite to ferrite transformation. An increasing C content increases the width of ductility trough and the transversal cracking tendency is highest at 0.1-0.15 % C. These contents are connected with the peritectic reaction, which leads to uneven thickness in the solidified shell during the transformation from δ-ferrite to austenite. This transformation leads to a contraction which favours the formation of a gap between the shell and the mould. That gap in turn reduces the heat transfer coefficient and gives rise to hot spot areas that lead to the occurrence of a thinner shell in those areas which exhibit a lower strength. Moreover this carbon content is characterized by a coarser austenite grain size which also reduces hot ductility. [32], [38], [39], [42], [52] Reducing the C content below the peritectic range is positive to hot ductility owing to it means moving away from the peritectic range [48].

In C-Mn-Nb-Al steels with Nb content lower than 0.03 % and C content higher than 0.05 %, the influence on the position of the ductility trough is small. The reason is that Nb(C,N) precipitates have majority influence due to there is a little further increase in the volume fraction precipitated. [38]

6.2.5 Copper

Cu residues remain in the steel due to it cannot be preferentially oxidised during normal steelmaking and it builds up progressively in the subscale layer, producing hot shortness [49]. It is recommended that the Cu level should be low. Cu contents greater than 0.15 % have been found to give poor surface quality and cracking. [48] Additions of 0.2-0.3% of Cu promote transversal cracking in Nb containing steels [36].

However, the work of Comineli et al. [62] on steel with 0.1 % C, 1.5 % Mn, 0.015 % Ti and 0.03 % Nb showed that the hot ductility of Cu-free steel compared with a steel with 0.3 %Cu at a cooling rate of 3.3ºC/s was equal but at slower cooling rate, 0.4ºC/s, ductility was much better especially for the Cu containing steel in the temperature range 800-1000 ºC, which had significantly coarser precipitation. [62]

6.2.6 Nickel

The effect of nickel in the micro-alloyed steels is harmful because it promotes cracking. Low carbon steels containing Ni are more prone to surface defects caused by slab surface cracking than other steels grades. [57]

Despite not affecting the precipitation of Nb, Ti and Al [48], Ni additions of 0.2-0.3% promote transversal cracking in Nb containing steels [36]. In Cu free steels small Ni additions (< 0.5%) do not influence hot ductility but at higher levels (1-2%) it improves hot ductility due to coarse precipitation. [48], [57]

The addition of Ni to Ti containing steels deteriorates hot ductility leading to transversal cracking. Although it has been suggested that Ni additions do not introduce any change in ductility [49], Kato et al. [63] found that increasing the Ni content from 0 to 5 % in Nb-Ti containing steel with 0.2 % Cu lead to widen the trough about 100 ºC, which can be owing to a reduction in the Ae_3 and Ar_3 temperatures due to the high Ni addition [63].

6.2.7 Nitrogen

The effect of N is detrimental to the hot ductility only when it is present with Al or microalloying additions due to the formation of nitrides or carbonitrides can seriously affects hot ductility. The N levels, as well as the Al level, have to be as low as possible. Typical N levels are < 0.008 %. [36], [49], [64] Increasing N content to 0.01 % causes serious deterioration in ductility [56]. Low N content micro-alloyed steels with carbon levels in the peritectic range (0.08-0.17 %) do not show transversal cracking problems until the Al level is > 0.04 % [64].

The effect of N in C-Mn-Nb-Al steels depends on the N level, whether it is above or below 0.005 % [49]. (original article by Ouchi and Matsumoto [65], as given by [49]). It has also been proposed that if the N level is kept below 0.004 % its effect on transversal cracking is minimized [36]. Other target that has been suggested as recommendable to the N content is 0.003 % and it is unlikely to be reduced due to it us needed to provide grain refinement by AlN precipitates. In any case, increasing the N content leads to transversal cracking due to it increases the amount of Nb(C,N) and AlN precipitated. [38] In Nb containing steels the nitrides precipitate before the carbides. If the N content is high, then the composition of the precipitate approaches to nitrides more than to carbides, encouraging the precipitation of Nb(C,N) in the austenite instead of that of NbC. Deterioration in hot ductility is progressive in the range 0.004-0.011 % N and changes in ductility are very small. They have suggested that

an increment in the N content only have a small influence on the volume fraction of Nb(C,N) that is precipitated and that the detrimental influence of N on transversal cracking is related to the enhancement of AlN precipitation. [49] (original article given in reference [66], as given by [49]). In addition, in these steels the formation of AlN interacts with the precipitation of Nb(C,N). Nb(C,N) is not affected by AlN due to the maximum rate for Nb(C,N) precipitation is achieved at 950 °C and that for AlN is achieved at 815 °C .Thus Nb(C,N) precipitates much before cooling and is not affected by AlN. However, it has also been proposed that Al could slow down the diffusion of N atoms. Thus the formation of the Nb(C,N) phase could occur at lower temperatures, and then in a finer form. Experimental results supports that in Nb bearing steels the hot ductility is considerably reduced by Al due to a finer precipitation of Nb(C,N) particles rather than by the formation of AlN precipitates. [44], [49]

The role of N is very important in the precipitation strengthening in V containing steels. It determines the V(C,N) density and hence the size of precipitation strengthening. The reason is that VN is much less soluble than VC. The solubility product of VN is approximately two orders of magnitude lower than that of VC. Thus, the first formed V(C,N) is N-rich and the C content starts to increase only when all N has been consumed. In addition the V(C,N) precipitation can be easily controlled by N additions due to all the N content in the steel is normally dissolved in the ferrite before V(C,N) precipitation. [59] Therefore the effect of N is more is more pronounced on V containing steels than that in Nb containing steels although Nb-containing steels have worse hot ductility. [49], [56], [64] When the N content cannot be low, a combination of Nb and V gives better ductility. C-Mn-V-Al steels are susceptible to transversal cracking if the V and N content is very high. Raising these contents leads to deterioration on the ductility. When the product $[V_t]$ x $[N_t]$ is grater than $1.2*10^{-3}$ (for example 0.1 %V and 0.012 %N) the ductility is as low as in Nb-N steels. In these steels no AlN precipitation has been found owing to VN can form preferentially to AlN. [49], [56], [64] In V-N steels increasing the N content favours VN and V(C,N) precipitation. Thus, recrystallization at the deformation temperature is retarded and the ductility trough becomes wider and deeper. [60]

In Ti micro-alloyed steels the Ti will combine preferentially with N. Any remaining N will combine with Al. N levels should be low in order to keep high Ti/N ratio (4-5:1) which encourages precipitate coarsening and improves ductility. In these steels low nitrogen should reduce the precipitation temperature for TiN and lead to a smaller volume fraction of finer precipitates. [57], [64]

In high N containing steels small Ti additions are required to avoid transversal cracking because they lead to reduce the fraction of fine particles. The slow secondary cooling allows the formation of coarse precipitates that have no influence on the ductility. If there is enough Ti to combine with all the free N, the steel has good ductility

at temperatures above 750 ºC and transversal cracking is not observed. [56] In addition, low Al content is also recommended to prevent further AlN precipitation [64].

6.2.8 Phosphorus

P remains residually in the steel. Small additions of P improve the hot ductility and the apparition of transversal cracks during straightening will be more unlikely. One possible reason is that P segregates to boundaries and vacant sites and therefore prevents the precipitation of fine Nb(C,N). [36], [49] Nonetheless, if the P content is high enough to segregate in the austenite grain boundaries then interdendritic liquid will be present at a temperature well below the bulk solidus temperature and it will leads to transversal cracking. The reason is that when P segregates to the austenite grain boundaries, it stabilizes the liquid film. [49]

6.2.9 Sulphur

The effect of sulphur is detrimental and can be detected only in as-cast specimens [57]. One of the best methods to reduce transversal cracking is reducing S content. The S present in the boundary regions is what gives embrittlement, any sulphides situated within the matrix only have little influence on hot ductility [38].

The total S content shows the quantity of coarse sulphides inclusions in the steel, which are either MnS, (CaMn)S or CaS depending on the content of Ca, Al and O. S can impair hot ductility by weakening the grain boundary regions due to the formation of fine solid state sulphide precipitates and sulphur segregation on the boundary and interfaces. [38], [57] Intergranulate failure is encouraged by FeMnS precipitates formed at the boundaries because they lead to the formation of precipitate free zones. FeMnS precipitates are formed in both low (0.6 %) and high (1.4 %) Mn steels when the cooling rate is slow enough to allow the intense segregation of S to the interdendritic boundaries. In micro-alloyed steels the MnS inclusions are not expected to influence the hot ductility by failure by grain boundary in the austenite due to MnS inclusions are often an order of magnitude larger than the AlN or Nb(C,N) precipitates. [38] However, if the S level is very low, < 0.005 %, transversal cracking increases in Nb containing steels [36].

FeS is not a problem in micro-alloyed steels owing to the high Mn/S ratio [38]. Fe oxysulphides are able to precipitate and strengthen the matrix in a similar manner to Nb(C,N) [49], [57]. Maehara and Nagamichi [67] have proposed that unprecipitated S segregates to grain boundaries and Nb(C,N) matrix interfaces facilitating decohesion and microvoid formation at grain boundary precipitates during straining. They recommended that the S content should be below 0.001 % to avoid this problem. [49], [57]

Sulphide inclusions reduce hot ductility in the temperature range 750 ºC-Ae_3 by delaying the onset of dynamic recrystallization and therefore encouraging grain boundary sliding [50].

6.3 Other elements

There are other elements that are normally presented in the steel but their influence is not very remarkable, such as Sb, Mn, Sn, Ce, Y and Zr.

The Mn content has influence on the AlN precipitation in the way that in low Mn steels the AlN precipitation is easier due to Mn increases the solubility of carbonitrides in the austenite [49]. Mn additions to V containing steels enhances strengthening owing to it lowers the austenite to ferrite transformation temperature and therefore it results in a finer precipitate dispersion. It has a greater effect than in Nb steels. [3]

Sn remains residually in the steel and must be kept as low as possible [48], [49]. This residual level, about 0.05%, can leads to worse ductility due to grain boundary segregation. Maximum segregation has been found at a cooling rate of 10 ºC/s and thus cooling rate should be slow. [48] It is very detrimental to hot ductility in combination with Cu owing to the formation of precipitates at the austenite grain boundaries. Their influence becomes higher as the C content advances to the peritectic range. Sb remains residually in the steel. The effect of Sb is likely to be nearly as detrimental as that of Sn due to it reduces the solubility of Cu in the austenite. [49]

Moreover, the addition of Ce, Y or Zr to Nb containing steels improves their hot ductility [40].

7 Effect of casting parameters on transversal cracking of micro-alloyed steel

7.1 Casting speed

The casting speed is limited in order to ensure that the shell of the steel has enough thickness to withstand the ferrostatic pressure of the liquid core during solidification and to be compatible with the steelmaking facilities supporting the caster. Typically casting speeds are between 0.6 and 1.3 m/min. [38] The influence of casting speed on oscillation mark can be beneficial or not depending on the oscillation strategy [37]. Steady casting speed helps to decrease or avoid cracking [32]. Surface temperature of the strand can be significantly increased by a small increase in casting speed. It is beneficial if the straightening procedure is carried out on the high temperature-high ductility region due to a reduction in the amount of precipitation and the consequently reduction of transversal cracking. [38]

7.2 Casting temperature

The casting temperature strongly affects surface cracking. Low degree of superheat is beneficial to avoid cracking. If the degree of superheat in liquid steel is higher than 30 ºC, the risk of cracking is high. [32] The degree of superheat should not exceed

20-25 ºC, depending on the C content and the strain rate. In addition, the minimal superheat temperature should be controlled at a range between ± 2 to 4 ºC during continuous casting in order to improve hot ductility and surface quality. [68]

7.3 Cooling rate

Cooling rate is the factor that has highest influence on the second phase precipitation and the precipitation of proeutectoid ferrite from the austenite matrix [41]. Thus, cooling rate influences hot ductility and, consequently, transversal cracking. It has been suggested the higher the cooling rate, the worse the ductility. An increase on the cooling rate might reduce the grain size, which leads to the formation of finer precipitates or inclusions, whereas a reduction on the cooling rate leads to the coarsening of Nb(C,N) precipitates and to the reduction in the thermal stresses in the strand. Thus, a reduction on the cooling rate would beneficial in order to reduce transversal cracking. [38], [49], [52], [54] It has also been found that at slow cooling rates (0.5 to 1 °C/s) increasing the cooling rate when the strain rate is slow deteriorates the ductility because S segregation has already taken place so that precipitation of sulphides can occur. Thus, a finer distribution of sulphides at the austenite grain boundaries is produced, which are more detrimental to the ductility. [49]

However, it has also been found that soft cooling is detrimental for surface cracking, while the effect of intensive and medium cooling is positive [37]. Intensive cooling process makes that inclusions and micro-alloyed elements rarely aggregate in the grain boundary because they do not transfer to the grain boundary and the high degree of supercooling that is achieved. Thus, to find chain-like precipitations is difficult. When cooling rate is increased, the amount of carbonitrides that precipitate from the austenite matrix can be controlled and therefore the width of the film-like proeutectoid ferrite becomes smaller. The reason is that austenite transforms more rapidly to ferrite and there is a lack of ferrite precipitating in the boundary due to a large amount of ferrite nucleates and precipitates in the grain owing to the ferrite in the austenite cannot rapidly transfer and separate out along the grain boundary. In addition, the second phase precipitates extends finely and diffusedly in the grains. Therefore, ferrite grains are finer and the thermomechanical properties of the slab are improved. Furthermore the difference of incubation time between the grain boundary and the grains in the austenite to ferrite transformation decreases. In addition, increasing cooling rate leads to the decrease of starting temperature of the phase transformation. The reason is that the atomic diffusion velocity is lower, the degree of supercooling is higher and free energy between the old and the new phases is lower. The perfect cooling rate to achieve a finer microstructure after phase transformation, without film-like proeutectoid ferrite and chain-like precipitation and in which precipitations extends dispersedly is 3-6 ºC/s for a Nb-V-Ti containing steel. Moreover, with increasing cooling rate the size of the ferrite grains after phase transformation becomes finer. [41]

In Nb-Ti steels reducing the cooling rate improves hot ductility in the temperature range of 850-1000 ºC [6]. In these steels the higher the cooling rate, the lower the amount of Nb and Ti in the (Nb,Ti)(C,N) precipitates [1]. Cooling rates below 1.7 ºC/s have a beneficial effect in Nb-Ti steels, which is more significant with a cooling rate of 0.4 °C/s [38], [57]. It is suggested as being a result of the precipitation of Nb(C,N) on the coarse TiN particles at high temperatures, reducing the amount of soluble Nb that could precipitate dynamically in a form of fine Nb(C,N) particles [49], [57]. This effect is not detected in plain Nb steel [57]. In addition, at low cooling rates the Nb(C,N) precipitates are grower due to they have enough time to grow. As a result the interparticles space decreases. Hence, the strength difference between the grain interior and the weak precipitation-free zone decreases, therefore suppressing microcracks formation and propagation. Fast cooling rates leads to produce fine Nb(C,N) precipitates at the austenite grain boundaries. Thus, interparticle spacing is smaller and pinning is more effective, allowing cracks to join up easily reducing hot ductility. In the temperature range of 650-800 ºC the effect of the cooling rate is not appreciable. The reason is that large fractions of ferrite appear at the austenite grain boundaries that allow recovery and minimize the effect of the cooling rate. At 650º C there is an important improvement of hot ductility at high cooling rate (10ºC/s) due to austenite transforms faster to ferrite and when the ferrite in the austenite cannot quickly transfer and separate out along the grain boundary and therefore at lower temperatures a larger amount of ferrite will nucleate and precipitate in the grain. In these steels the higher cooling rate lowers the Ar_3 temperature, moving the ductility trough to lower temperatures. [6]

For steel with V content of 0.15 % it has been proposed that the optimum cooling rate for strengthening is 2.83 ºC/s. If it is lower the V(C,N) precipitates coarsen excessively and are less effective in strengthening. If it is greater more V(C,N) remains in solution and only a small fraction of V(C,N) precipitates. [3]

At the edge sections of the slab slower cooling should be provided. The reason is that the corners have different temperatures during bending and unbending. Thus, the temperature of the metal should be kept from dropping to the brittleness interval. [34]

7.4 Multiple points bending

Multiple points bending is a method in which the straightening is carried out by multipoint straightening. It might do not improve hot ductility owing to strain rate is reduced, which reduces hot ductility. Furthermore, there is more time to dynamic precipitation. In Nb bearing steels stress relaxation between bending points is minimal. [36] In addition, transversal cracking might not be prevented increasing the number of bending points, but the depth to which they can propagate below the surface is very diminished due to the lower applied surface strain in the region of limited ductility [38].

7.5 Oscillation marks

In continuous casting most cracks appears in the vicinity of the oscillation marks on the surface of the strand, perpendicularly to casting direction, due to the up and down oscillations that take place in the mould [37], [38]. Depending on the type of the oscillation marks strain is concentrated on different areas [37].

Before it was thought that oscillation marks should be minimised in order to minimize cracks [2]. The explanation was the following: Generally the frequencies are between 60 and 120 cycles/min, which leads to depths in the ranges 0.1-1 mm and 5-10 mm respectively. These ripples are regions of high interdendritic segregation of elements such as P, which is detrimental to hot ductility and therefore increase the risk of transversal cracking. In addition there is a gap between the strand and the water cooled mould which is bigger in the surface ripples. This gap diminishes the heat transfer favouring a thinner shell and coarser grain, which are also detrimental. Moreover, the oscillation marks can act as notches, making the material more brittle due to the introduction of high localised stress concentration. It has been found that in the temperature range 800-1000 increasing the depth of the notch generally reduces the elongation. The radius of the notch was found not to be important. [38]

Nonetheless recent studies have shown that the depth of the oscillation marks is not related to the incidence of cracks. Thus, marks are just one of several factors that have influence on transversal cracks. [2] What is more, crack susceptibility has also been found to decrease with increasing oscillation mark depth. A possible reason is that austenite nucleation and growth occurs in the mould. Thus, more severe cracking could takes place in the case of shallower marks due to friction forces. Oscillation mark depth can be decreased with higher frequency, lower stroke and lower negative strip time for peritectic steel grades. [37]

7.6 Slab measurements

The slab thickness has been found not to affect crack formation in the mould nor in the secondary cooling zone during continuous casting. However, the slab width has influence in crack formation. When the slab width is about 1900 mm there is a maximum of defective slabs. Above this temperature, the higher the width of the slab the lower the amount of defective slabs is. [34]

7.7 Strain rate

Increasing the strain rate improves the hot ductility in the range of the strain rated applicable to straightening operations, which are about 10^{-3}-10^{-4}/s. The upper temperature boundary of the hot ductility curve is displaced to lower temperatures and thus the trough is narrower. Increasing the strain rate improves hot ductility for the following reason: there is insufficient time for strain induced precipitation, the amount of grain boundary sliding is reduced, the formation and diffusion controlled growth of voids next to the precipitates and inclusions at the grain boundaries is not possible

due to there is not enough time and higher strain rate prevents the formation of deformation induced ferrite. [38]

For Nb-bearing steels increasing strain rate, which means increased casting speed for a specific caster, improves hot ductility [68].

7.8 Temperature of the straightener

The temperature of the straightener also has influence on transversal cracking. During straightening the inner arc supports tensile stress and the positive camber supports compression stress. If the temperature of straightening the slab is in the temperature range of the ductility trough cracks will increase. Thus, the intensity of cooling water must be controlled and asymmetry of the temperatures must be avoided in order to minimize cracking. [32]

At lower temperatures surface cracking is not reduced because of the effective gauge length over which the constant total strain is applied is increased, lowering the average strain rate and allowing the occurrence of more precipitation, worsen the hot ductility. At higher temperatures surface cracking is reduced because stress relaxation occurs. Higher straightening temperatures can be achieved by increasing the casting speed or reducing the amount of secondary cooling. [38]

7.9 Thermal stresses

Thermal stresses must be minimised in order to minimize the likelihood of cracking [38]. Thermal cycling along continuous caster can generates cracks, even if there is not any bending or unbending strain. The minimisation of mechanical loads decreases surface cracking, which is demonstrated by the lack of surface cracks in the corner regions of soft cooled strand. [37]

8 Prevention of transversal corner cracking

8.1 Secondary cooling strategy

Secondary cooling strategy is important in avoiding transversal cracking. One method to avoid surface quality problems in conventional continuous casting is to carry out bending and straightening operations out at temperatures either above (soft cooling) or below (hard cooling) the zone of the ductility trough (700-1000 ºC) [2], [32], [35], [36], [39], [41], [42].

It has been suggested that the temperature range when straightening is made should be either 30 ºC below the Ar_3 temperature (when a large amount of ferrite exist before deformation, about 40 %) or above the temperature at which dynamic recrystallization starts to take place (due to the ferrite film no longer forms and there are few coarse precipitates that not influence hot ductility) [48]. In addition, secondary cooling must be as uniform as possible to prevent thermal stresses. When soft

cooling is used, it is important to maintain the cross section above the critical range, especially slab corners. When hard cooling is used, it is important to maintain all cooling nozzles to avoid regions within the critical range. [36]

Cracking has not been prevented completely because of the difficulty of unique thermal profile across the slab due to unique subscale formation. This difficulty especially takes place in the corners, where it is very difficult to avoid the trough range because heat is transferred from both the narrow and the wide sides. This problem is enhanced in Nb bearing steels [35], [39], [41], [42]. This secondary cooling strategy is only possible with the bow type continuous casters but not at the vertical bending type continuous casters due to at that range of temperatures the intensive cooling before bending is carried out. [2]

Other method to combat edge cracks is to adjust the area sprayed by the secondary cooling zone to provide softer cooling of the slab's edge sections, especially when bending and unbending are carried out. [34] Corner cracks might be eliminated if no water is applied to the corner sections of the slab [68].

Slab quenching has also been suggested as a strategy to avoid transversal cracking. In this technique slab surface rapidly is cooled down below the transformation temperature. Thus, fine grain structure is obtained in the surface which restricts the formation and propagation of cracks. [36]

8.2 Steel composition

Other path to reduce surface cracking susceptibility is by controlling the steel chemistry. As mentioned before, the steel composition has high influence on cracking, especially microalloying elements. The objective is to obtain fewer crack sensitive compositions provided the required properties are ensured by other mechanisms or by elements that modify the precipitation type and size [42]. The target is to control the separation of the fine grain [32]. Some options are minimizing Nb, replacing Nb by V and N additions, adding V to Nb bearing steels and considering Ti additions [36].

8.3 Machine operation

In the machine operation, important aspects are the type of mould powder used, the viscosity, the oscillation marks and ensure good and uniform fluxing [36]. The importance of the oscillation marks has been mentioned before.

It has been suggested that an increment in the $W/(\Delta * v)$ ratio (where W is the width, Δ is the conicity of the mould and v is the casting speed) diminishes the amount of slabs with cracks. Thus, for a determined slab width, decreasing either the casting effect or the conicity of the mould has positive effect on cracking. [34]

Superheat control like the one that was explained before (20 to 25 ºC of superheat and variation of $\pm$ 2 to 4 ºC) along with secondary cooling control improve hot ductility. By this control, a reduction of area of only 20 % was established as the limit to crack-free slabs in Nb-bearing steels. This value is much lower than others that have been published. [68]

In Shougang steel plant the following measures were applied in order to reduce transversal corner cracks. They remained the superheat degree lower than 25 ºC, maintained the stability of the casting speed and fluid level of the crystallizer, decreased the cooling intensity and increased the casting speed. They obtained successfully results, since they achieved increasing the straightening temperature to approximately 950 ºC, reducing transversal corner cracks. [32]

8.4 Surface conditioning

Conditioning of the surface, such as mechanical scarfing and hot scarfing, are used to remove cracks from the slabs surface. The negative point of these measures is that the costs are increased and some defects might not be completely repaired or missed. [34]

9 Surface structure control cooling

SSCC is a technique that improves hot ductility and aids in preventing slab surface transversal cracking. It consists in an intense cooling of the strand surface just below the mould and further reheating by the heat contained in the product in the secondary cooling. The strand is cooled with high cooling rate from the solution treatment temperature to the quenching temperature (T_1), below the A_{r3} temperature (1). It is held there for a short time (2) and reheated by the latent heat of solidification released by the internal liquid steel to the reheating temperature (T_2), over the A_{c3} temperature (3). The following step after reheating is the same than in mild cooling (4). Mild cooling is the normal cooling concept in continuous casting. As a result, a double transformation takes place, bringing a finer austenite and ferrite grain size and about a ferrite microstructure with a film-like ferrite-free layer at the strand surface. The distribution of the grain is much more uniform and any chain-like precipitation occurs in the prior austenite grain boundary. New grain boundaries are created which do not coincide anymore with the carbonitrides and/or sulphides, therefore eliminating their embrittling effect. [35], [39], [42], [43] Figure 13 shows an example of the SSCC thermal story.

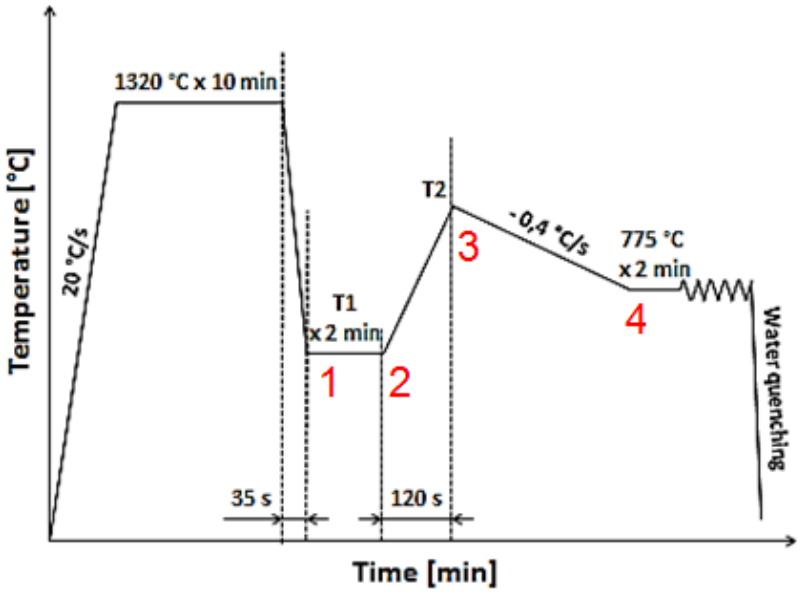

Figure 13. Thermal story of SSCC [43].

Because of the high cooling rate, there is uniform dispersion or solution of the micro-alloyed elements precipitates in the matrix. Ferrite and very fine precipitates, even less than 20nm in diameter, precipitate simultaneously both inside and at the austenite grain boundary. The minimum temperature during initial intensive cooling must be lower than Ar_3 to avoid cracking susceptibility. Ferrite starts to precipitate when the temperature reaches below the Ar_3 temperature and the precipitates precipitate simultaneously. [35], [39], [42], [43] In addition, high cooling rate makes that the difference of incubation time between the grain boundary and the grain decreases. Austenite transforms more rapidly to ferrite with an increase in the cooling rate. When the ferrite is not able to rapidly transfer in the austenite and separate out along the grain boundary, a large amount of it nucleates and precipitates in the grain. Thus, there is a lack of ferrite precipitating in the grain boundaries because it has been consumed. [41] This microstructure is different from the film-like ferrite along grain boundaries microstructure obtained in conventional cooling, where grain boundary precipitates are formed at the last stage of secondary cooling due to the slow cooling rate. Thus, one of the reasons for the occurrence of a ductility trough and slab surface transversal cracking is avoided. [35], [39], [42], [43] In the reheating process some micro-alloyed elements precipitate but it is difficult for them to transfer, and therefore, aggregate precipitation increases that leads to the dispersed propagation of the precipitates. In addition, during reheating ferrite transforms again to austenite. It is difficult for the austenite to grow and coarsen due to the rather low reheating temperature. In the subsequent cooling the microstructure turns into finer after phase transformation. [41] Work carried out by Kato et al. [35] showed that the austenite grain size close to the slab surface is the same under mild cooling and under SSCC.

Thus, phase transformation has never completed during the thermal cycle and therefore the change in the microstructure is not a due to the refinement of the austenite grain by recrystallization. [35]

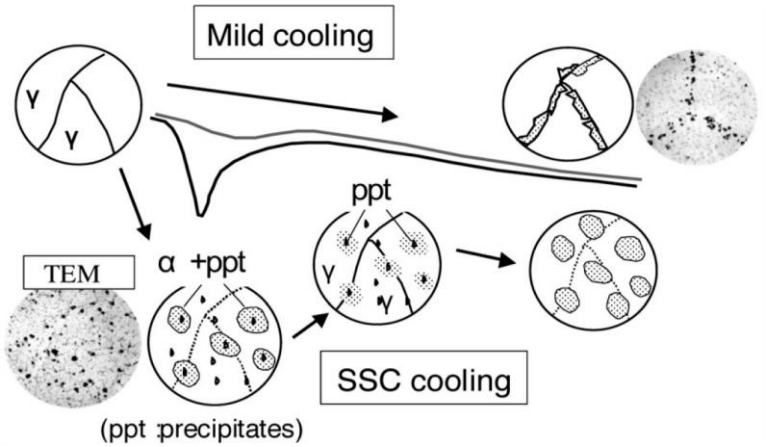

Figure 14. Scheme of the mechanism of microstructure formation [35].

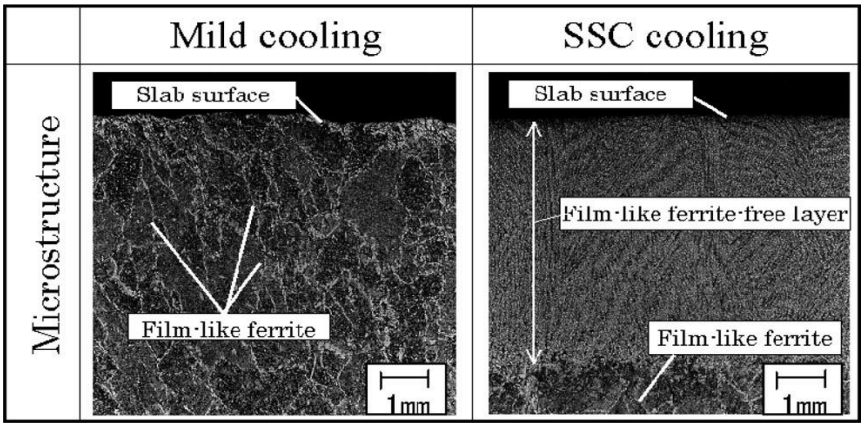

Figure 15. Microstructure of slab surface in continuous casting in conventional/mild cooling and SSC cooling [35].

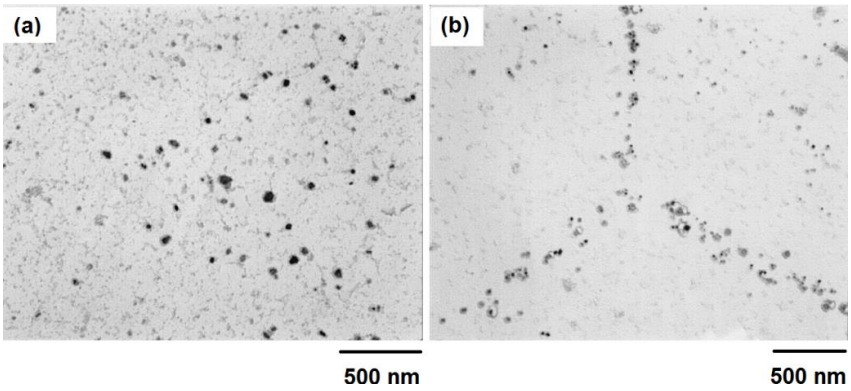

Figure 16. Distribution of precipitates at the austenite grain boundary and matrix under SSC cooling (a) and mild cooling (b) [39].

T_1 has been found to be the most important temperature for the improvement of the mechanical properties. When T_1 is less than 600 °C the RA values increase, being more than 20 % higher than in mild cooling at 550 ºC due to the double phase transformation. [43]

The cooling rate has a strong influence on the thickness of the film-like ferrite-free structure. An increase of the thickness of the film-like ferrite-free layer, which increases with higher cooling rate, reduces transversal cracking. It has been confirmed that cracking is surely prevented when the thickness of the film-like ferrite-free layer is over 3 mm. [35]

In C-Mn steels with low S content the ductility in the temperature interval 700-1100 °C is excellent due to finer austenite grain is achieved (50 μm) after the double phase transformation what during the subsequent cooling leads to a rapid transformation from austenite to fine ferrite pearlite. [42]

In Nb containing steels the ductility drop associated with the austenite to ferrite transformation is suppressed but there is even widened brittleness in the austenitic range owing to finer precipitation of Nb and dislocation accumulation during hot deformation of austenite with a finer initial grain size. The final amount of precipitates is higher than in conventional cooling due to some fine precipitation probably occurs during the self reheating. [42]

EXPERIMENTAL PART

10 General

In the experiments the SSCC concept was applied to micro-alloyed steel samples. In this concept, the samples go through consecutive cooling and heating periods (described in Chapter 9 in the literature part).

Two main phenomena that were looked for:

- A double phase transformation during the heat treatment. This means that during the cooling, austenite firstly transforms to ferrite. Then, during the reheating ferrite transforms again to austenite. This double phase transformation should bring a finer austenite and ferrite grain size and an about ferrite microstructure with a film-like ferrite free layer at the grain boundaries.

- The growth of new grains from the precipitates located at the grain boundaries. The ferrite would grow at the grain boundaries at temperatures lower than the Ar_3 temperature and when it transforms back to austenite in the subsequent reheating the austenite would grow around the precipitates. Thus, new finer grains would be created around the precipitates during the reheating process. Two different kinds of grains would be obtained, differenced in their size: the bigger former grains and the smaller new grains created around the precipitates. Figure 17 shows this phenomenon. It must be noted that this phenomenon is different from the formation of precipitates inside the grains used in the previous work, in which the cooling rate was much higher and then the precipitates were distributed throughout the matrix. [35], [39], [42], [43].

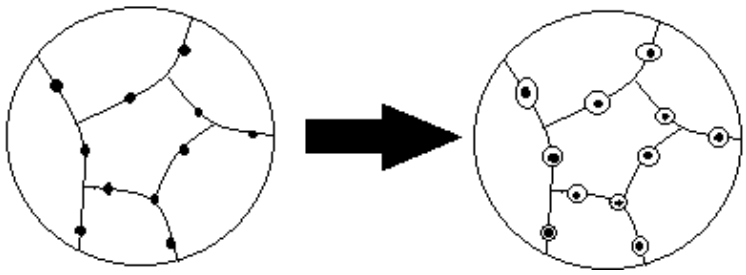

Figure 17. Growth of new grains from the precipitates during the reheating process.

The parameters used in the SSCC experiments were chosen so that they could be applied to a real continuous casting process. The cast strand is the most vulnerable to transversal cracking in the straightening segments where mechanical stresses are induced and grain boundaries are weak due to the presence of film-like ferrite. Thus, there should be enough time to apply the SSCC concept for the corners so that they would be strong enough to withstand the mechanical stresses occurring in the

straightening segments. The micro-alloyed steel grade used in the experiments was cast in the vertical-bending slab caster with a casting speed of 1.0m/min. As the distance from the meniscus to the straightening segments is approximately 15 meters, the total time for each experiment has been calculated in order to be around 15 minutes with this casting speed.

The cooling rate used in this study was much slower (2 - 3.5 °C/s) than in the previous investigations (20 °C/s) [35], [39], [42], [43]. In addition, limitations in the equipment used in the experiments made that the highest cooling rate that can be achieved during the heat treatments was about 3.5 °C/s. This difference in the cooling rate makes that the precipitates will be mainly located at the grain boundaries, instead of being located inside the grains. Furthermore, the size of the precipitates will be bigger as a consequence of the lower cooling rate. In addition, the grain size will be coarser than in the previous studies [35], [39], [42], [43] since the cooling rate is lower.

In order to evaluate all the phenomena involved in the process the samples were metallographically prepared. They were analysed by optical microscope and some of them by scanning electron microscope. In addition, hardness measurements were carried out.

11 Sample description before the experiments

The micro-alloyed steel samples used in these experiments were cut off from the wide surface of an as-cast slab. The dimensions of the obtained slab piece were 15x3x3cm^3. The chemical composition of the steel is shown in Table 1.

Table 1. Chemical composition of the micro-alloyed steel (in wt %).

C	Si	Mn	P	S	Nb	V	Mo	Ti	Cr
0.147	0.457	1.43	0.014	0.0015	0.045	0.094	0.007	0.013	0.046
B	Ni	Al	Ca	H	N	Co	Cu	Pb	Sn
0.0003	0.04	0.034	0.0002	0.00017	0.0042	0.013	0.019	0.003	0.003

The slab piece was cut in smaller pieces of approximately 1x1x1 cm^3 and a hole of 2 mm of diameter was drilled in the corner of the samples. The samples are shown in Figure 18.

Figure 18. Micro-alloyed steel samples of size 1x1x1 cm^3.

12 Heat treatment experiments

12.1 Experimental setup

The experiments were carried out in a furnace Entech ETF 50-175V. The furnace has two openings, one on the top and one on the bottom. Table 2 shows the elements and the characteristics of the furnace.

Table 2. Elements and characteristics of the furnace.

Furnace type	Entech ETF 50-175V
Maximum temperature	1750 °C
Heating elements	Kanthal Super™ 1900 Molybdenum disilicide ($MoSi_2$)
Programmable controller unit	Eurotherm 903P
Furnace tube	Alumina

The furnace atmosphere during the experiments was argon with a purity of 99.999 % and the flow rate was 0.05 l/min. The argon is blown from the top of the furnace.

The temperature profile of the furnace is vertical and it was measured before the experiments. The sample temperature during the experiments was measured by a B-type thermocouple (Pt-30%Rh vs. Pt-6%Rh). The thermocouple is located inside the alumina furnace tube so that the tip of the thermocouple is just under the bottom of the steel sample. The thermocouple is located in the bottom opening of the furnace and allows the movement of the sample through the different temperatures depending on the thermocouple position. Figure 19 depicts the temperature profile in the furnace depending on the thermocouple position.

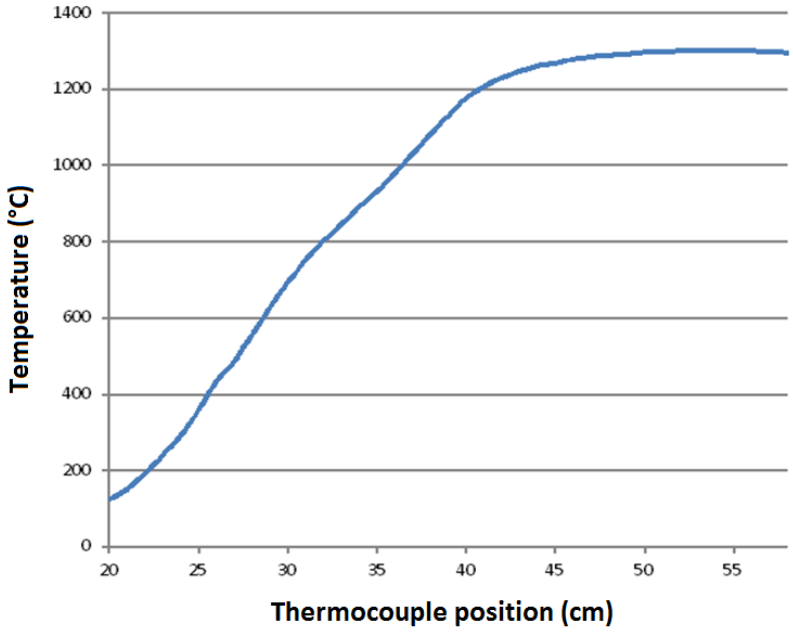

Figure 19. Temperature profile of the furnace.

The sample was hung in the end of an alumina tube with a platinum wire which is tied around the alumina tube and goes through the drilled hole of the samples, joining them together. This platinum wire was protected with alumina tube. Figure 20 shows this holding of the samples. In the opposite end, the tube is located inside a lid which has a hole. The diameter of the alumina tube and the hole of the lid are almost equal but the alumina tube is a little bit smaller so that the upward and downward movement of the alumina tube when moving the sample inside the furnace can be performed.

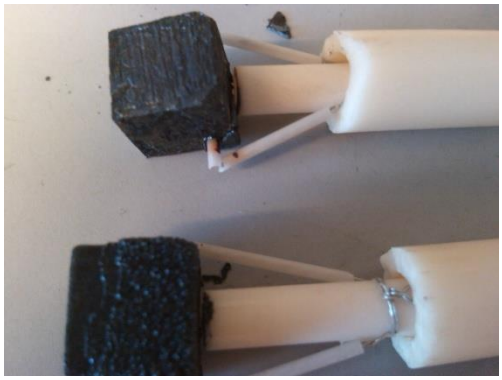

Figure 20. Holding of the samples.

In order to hold the sample inside the furnace during the experiments, a support plate made of aluminium silicate fibre Al_2O_3 55%, SiO_2 44% was used. This plate has

a hole in the middle, so that the thermocouple tip can be in contact with the bottom of the sample. Figure 21 shows a schematic picture of the equipment used in the experiments.

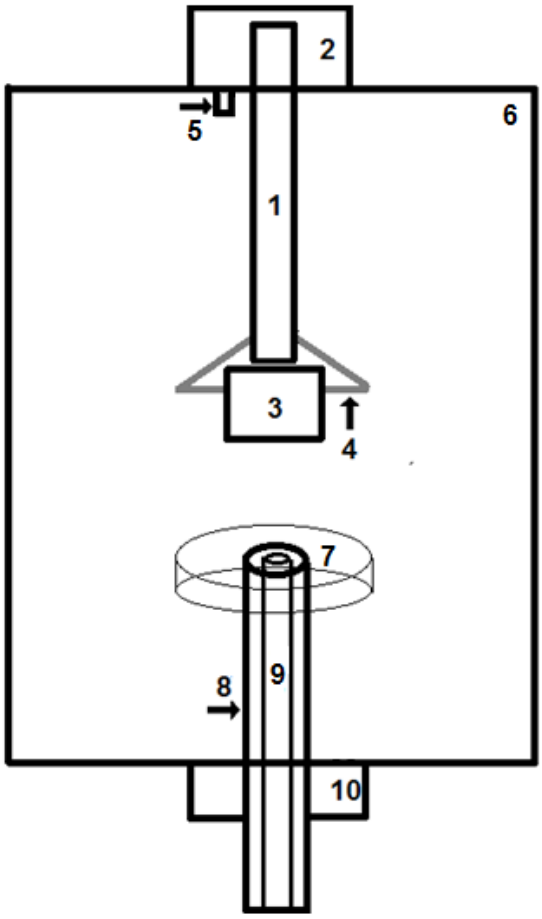

1. Alumina tube for sample holding
2. Upper lid
3. Sample
4. Platinum wire
5. Argon nozzle
6. Furnace wall
7. Plate
8. Alumina tube
9. Thermocouple
10. Lower lid

Figure 21. Schematic of the equipment used in the experiments.

12.2 Experiments

The sample is introduced in the furnace from the top opening and it is put over the sample plate. Thus, the contact between the tip of the thermocouple and the bottom of the sample is allowed and the sample temperature is measured during the experiment. Then, the upper opening of the furnace is covered with the lid to seal the furnace. The different temperatures of the samples are achieved by moving the furnace's alumina tube which contains the thermocouple inside. The temperature increases as the tube is moved upwards and decreases as the tube is moved downwards. The larger and faster is the tube movement, the higher the rate.

When the experiment finished, the lid was removed and the sample was taken out from the top opening of the furnace and quenched in water. After that, the platinum

wire which joins together the sample and the alumina tube was removed and sent for further metallographic preparation.

It should be emphasized that the temperature control during the experiments was not extremely accurate due to the manual performance. The accuracy that has been achieved is to control the temperature ± 10 ºC from the given temperature during the holdings.

12.3 Experiment parameters

All the samples were first heated up to the 1300 ºC and held for 2 minutes at this temperature. 1300 ºC is approximately the temperature below the mould during the continuous casting. There is no melting of the steel at this temperature. In addition, the (Nb, V) (C, N) precipitates are dissolved but the Ti (C,N) precipitates are not dissolved because their melting point is greater than 1300 ºC. Thus, the Ti (C, N) precipitates are expected to be larger than the (Nb, V) (C,N) precipitates. Figure 22 shows the calculated precipitates during cooling at a cooling rate of 3ºC /s. The calculation was made with IDS software. IDS is a solidification and microstructure model developed by the Research Group of Metallurgy at Aalto University School of Chemical Technology.

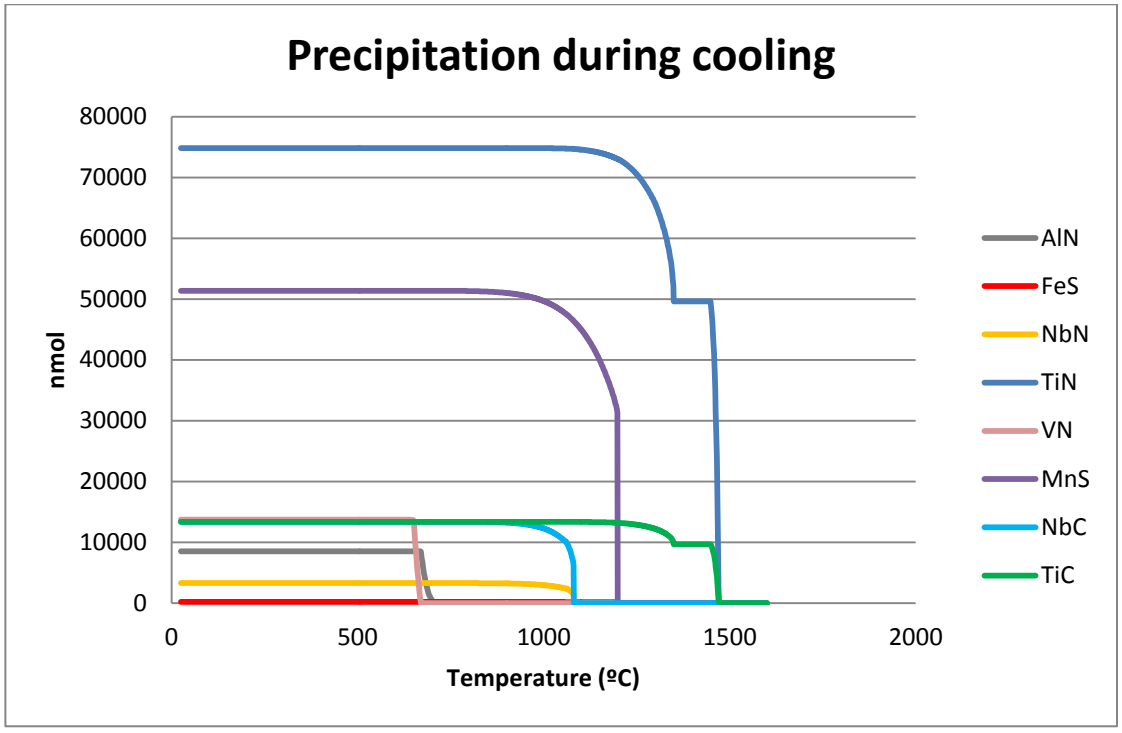

Figure 22. IDS calculation of precipitation during cooling at a cooling rate of 3ºC /s.

Figure 22 shows that mainly titanium carbides but also titanium nitrides start to form above 1400 ºC. Niobium carbonitrides start to precipitate at approximately 1100 ºC.

There are more niobium carbides than niobium nitrides. Furthermore, vanadium nitride starts to precipitate above 600 ºC.

In addition, the grain will experience a big growth due to the high temperature. After this heating, three different heat treatments were tested: mild cooling treatment, SSCC based treatment and SSCC based followed by mild cooling treatment. Finally the samples were quenched in water. Mild cooling refers to normal cooling process in continuous casting.

The A_3 temperature is very important in these experiments because it is the starting temperature for the austenite to α-ferrite phase transformation. It can also be marked as A_{3e}, A_{3r} or A_{3c} depending on if it is equilibrium condition (A_{3e}), cooling condition (A_{3r}) or heating condition (A_{3c}). In the experiments the A_{r3} and A_{c3} temperatures are used, not A_{e3}, because the heat treatments consist on cooling and heating. Thus, the equilibrium condition is not achieved in these experiments.

For the estimation of the Ar_3 the temperature an equation given by Mintz et al. [69] was used. This equation is:

$$Ar3(°C) = 862 - 182\%C - 76.1\%Mn + 1121\%S - 1804\%Nb - 0.084CR(°C/min) + 1168\%Ti - 2852\%N \quad (1)$$

The compositional range covered by the equation is 0.04-0.75 %C, 0.31-2.52 %Mn, 0.01-1.22 %Si, 0.001-0.032 %S, 0.002-0.11 %P, 0.0012-0.014 %N, 0-1.55%Al, 0-0.042 %Nb and a cooling rate of 10-200 °C /min [69]. Since the steel used in this thesis fits inside the limits, the Ar_3 temperature was estimated based on this formula. The value obtained for Ar_3 is shown in equation 2.

$$Ar3\ (ºC) = 650.13 - 0.084\,CR \quad (2)$$

This temperature was also calculated by software package IDS, obtaining a value of 717 °C.

For the estimation of the Ac_3 temperature Andrews's equation (3) and Park's equation (4) were considered [70].

$$Ae3(°C) = 910 - 203 \cdot \sqrt{C} + 44.7 \cdot Si - 15.2 \cdot Ni + 31.5 \cdot Mo + 104 \cdot V + 13.1 \cdot W - 30 \cdot Mn + 11 \cdot Cr + 20 \cdot Cu - 700 \cdot P - 400 \cdot Al - 120 \cdot As - 400 \cdot Ti\,. \quad (3)$$

$$Ae3(°C) = 955 - 350 \cdot C - 25 \cdot Mn + 51 \cdot Si + 106 \cdot Nb + 100 \cdot Ti + 68 \cdot Al - 11 \cdot Cr - 33 \cdot Ni - 16 \cdot Cu + 67 \cdot Mo. \quad (4)$$

The results of the Ar_3 and Ac_3 temperature estimations for the steel used in these experiments are compiled in Table 3.

Table 3. Ar_3 and Ac_3 temperature estimations.

Temperature	Reference	Temperature value
Ar_3	Mintz et al. equation	650,13 - 0.084 CR (ºC/min)
Ar_3	IDS	717
Ac_3	Andrews equation	791,37
Ac_3	Park equation	897,828

12.3.1 Mild cooling experiments

In the mild cooling experiments, the samples at room temperature were placed in the furnace at the position which equals 1300 ºC and held there for 2 minutes. Then the samples were cooled down at 1 ºC/s to a certain temperature and finally they were quenched in water. Figure 23 shows the thermal history for mild cooling.

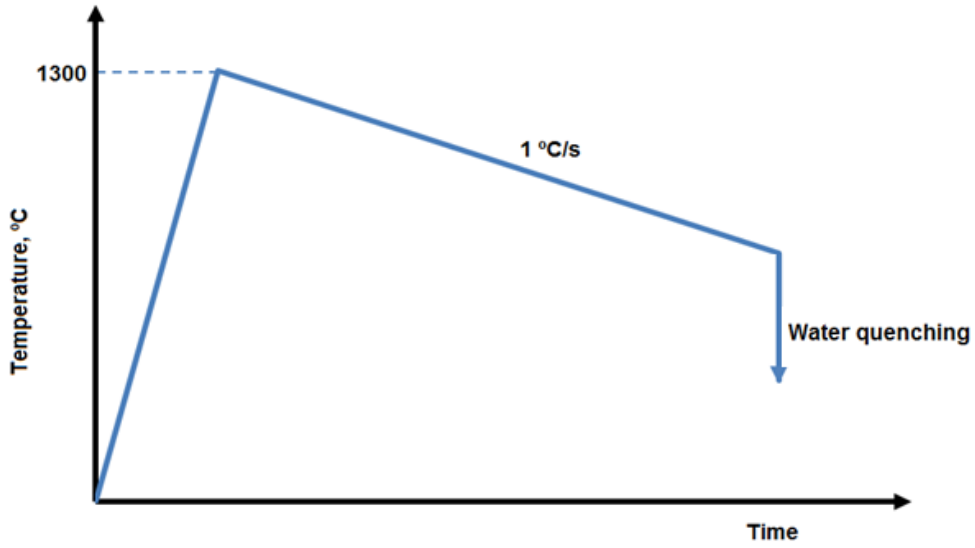

Figure 23. Thermal history for mild cooling.

Two different temperatures after cooling were used (910 and 750 ºC) (Table 4).

Table 4. Mild cooling experiments.

Sample number	Final temperature (ºC)
1	750
2	910

These experiments were made in order to check the microstructure under the mild cooling path at different temperatures. The expected microstructure was fully martensite for both samples.

12.3.2 Low temperature (T_1) experiments

Low temperature (T_1) (Figure 24) experiments were performed in order to see if the temperature (T_1) is low enough to obtain ferritic structure i.e. if the Ar_3 temperature was reached as it would be needed for the further SSCC process. In this heat treatment, the samples at room temperature were placed in the furnace at the position which equals 1300 ºC and held there for 2 minutes. Then the samples were cooled down until the T_1 temperature. The cooling rate was 3.5 ºC/s in the beginning and was progressively reduced until 2 ºC/s in the end of the cooling. The samples were held for a certain time at the T_1 temperature (H_1) and then they were quenched in water. Figure 24 shows the thermal history of these samples.

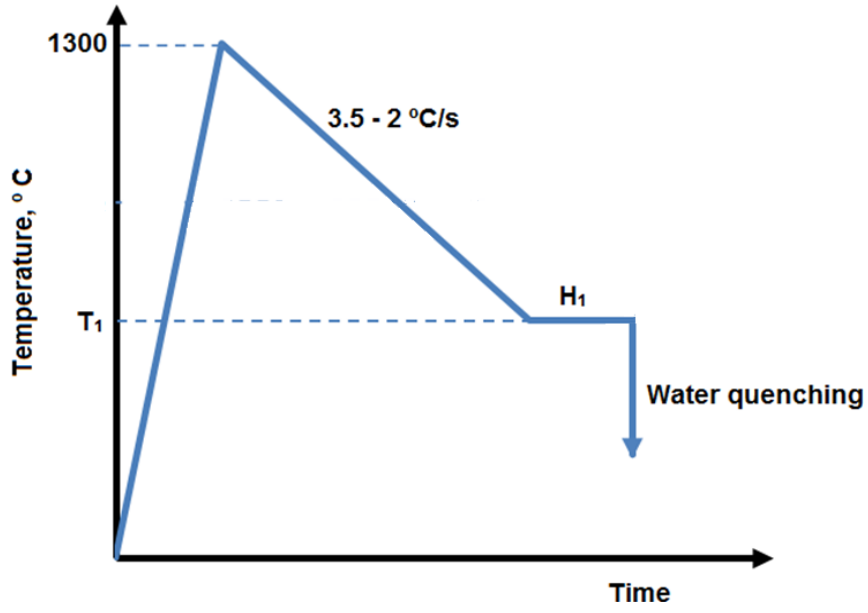

Figure 24. Thermal history for low temperature samples.

Three different T_1 temperatures (510, 610 and 650 ºC) and two different holding times (0 and 5 min) were used. The experiments which were carried out under this heat treatment are shown in Table 5.

Table 5. Low temperature experiments.

Sample number	T_1 (ºC)	H_1(min)
3	510	0
4	510	5
5	610	5
6	650	5

These experiments were carried out in order to check the microstructure after the cooling at low temperature. Thus, the microstructure expected was martensite with some ferrite at the grain boundaries. The morphology of the ferrite growth was observed as well. The lower the temperature and the higher the holding time, the higher was the expected amount of ferrite.

12.3.3 SSCC based experiments

In SSCC based heat treatment, the samples at room temperature were placed in the furnace at the position which equals 1300 ºC and held there for 2 minutes. Then the samples were cooled down until the T_1 temperature (lower than the Ar_3 temperature). In the beginning, the cooling rate was 3.5 ºC/s and it was progressively reduced down to 2 ºC/s in the end of the cooling. The samples were held for a certain time at the T_1 temperature (H_1) and then they were reheated to the T_2 temperature (higher than the Ac_3 temperature), where they were held for a certain time (H_2). Finally, the samples were quenched in water. Figure 25 shows the thermal history of the SSCC based heat treated samples.

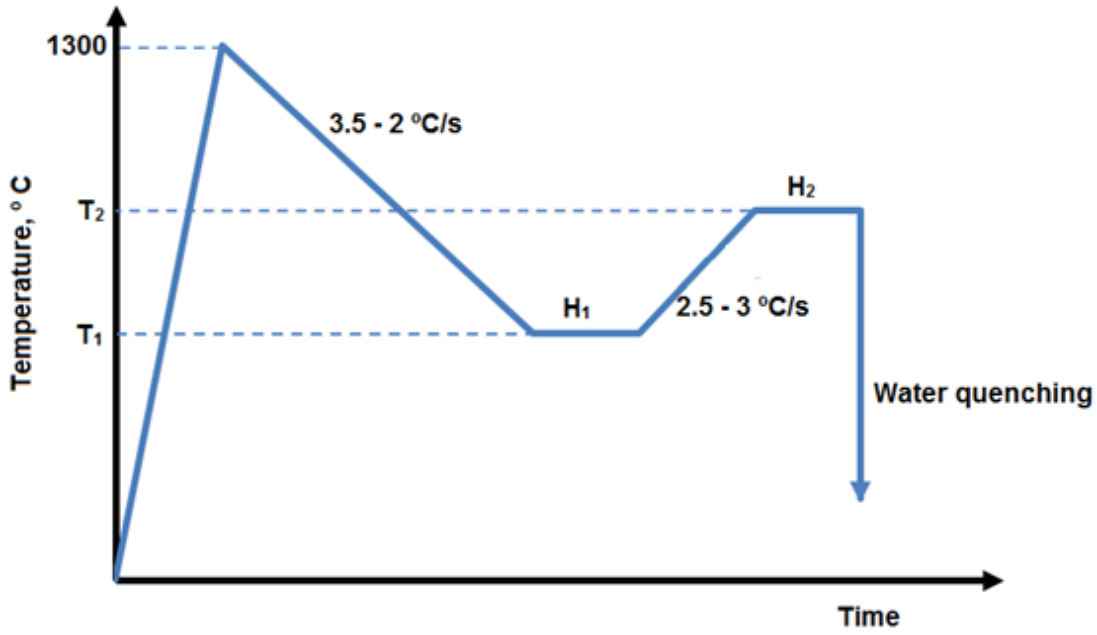

Figure 25. Thermal history for SSCC based heat treatment.

Three different T_1 temperatures (510, 610 and 650 ºC), two different holding times (H_1) at low temperature (2 and 5 min), three different T_2 temperatures (810, 915 and 975 ºC) and two different holding times (H_2) at high temperature (2 and 5 min) were used. The experiments which were carried out under this heat treatment are shown in Table 6.

Table 6. SSCC based experiments.

Sample number	T_1 (ºC)	H_1(min)	T_2 (ºC)	H_2(min)
7	510	2	810	2
8	510	2	810	5
9	510	2	915	2
10	510	5	915	2
11	510	5	915	5
12	610	2	915	2
13	610	5	915	2
14	650	2	915	2
15	650	5	915	2
16	650	2	915	5
17	610	5	975	2
18	610	5	975	5

The aim of these experiments was to observe the effect of the different temperatures and holding times, both at low and high temperature, on the microstructure of the samples and to check if the aimed phenomena were achieved.

12.3.4 SSCC based + mild cooling experiments

In this heat treatment, the samples at room temperature were placed in the furnace at the position which equals 1300 ºC and held there for 2 minutes. Then the samples were cooled down until the T_1 temperature. In the beginning, the cooling rate was 3.5ºC/s and it was progressively reduced down to 2 ºC/s in the end of the cooling. The samples were held for a certain time at the T_1 temperature (H_1) and then they were reheated to the T_2 temperature, where they were held for a certain time (H_2). After that, the samples were cooled down at 1 ºC/s until 750 ºC. Finally, the samples were quenched in water. Figure 26 shows the thermal history of the SSCC based + mild cooling heat treated samples.

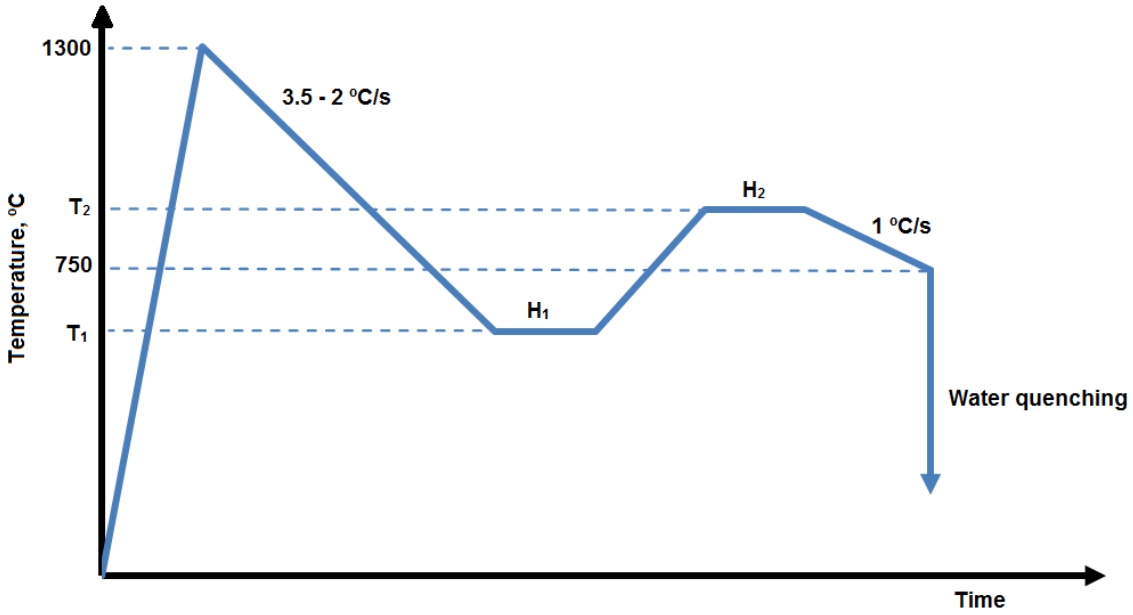

Figure 26. Thermal history for SSCC based + mild cooling heat treatment.

Two experiments were carried out under these conditions, using two different holding times at high temperate (2 and 5 min). They are shown in Table 7.

Table 7. SSCC based + mild cooling experiments

Sample number	T_1 (ºC)	H_1(min)	T_2 (ºC)	H_2(min)
19	610	5	975	2
20	610	5	975	5

These experiments were performed in order to compare the microstructure after the heat treatment with that of the mild cooling samples and to check if the phenomena were achieved.

13 Metallographic specimen preparation

After the heat treatment, the samples were mounted in epoxy resin by mixing epoxy resin (EpoFix resin by Struers, Figure 27 a) and epoxy resin hardener (EpoFix resin by Struers, Figure 27 b) in a proportion of 7.5:1. The sample was held in a mould, which has been previously impregnated with vaseline to facilitate the removal, (Figure 34 c) and then the mixture is added. Then the specimens are introduced in a vacuum chamber for 15 minutes (Figure 27 d) in order to remove the air bubbles that can be formed during the specimen preparation. After approximately 9 hours, the specimen is ready for further grinding and polishing (Figure 27 e).

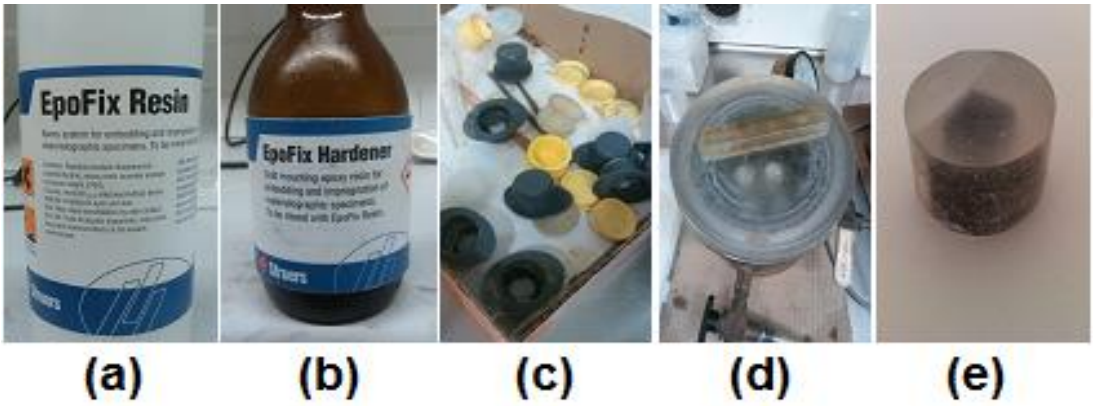

Figure 27. Specimen preparation equipment: epoxy resin (a), epoxy resin hardener (b), moulds (c), vacuum chamber (d) and specimen after the preparation (e).

Grinding was done using water cooled silicon carbide paper and the grit sequence used was 150, 240, 400, 800, 1200, 2500 and 4000. This was followed by polishing with 1 µm diamond paste. After each grinding step the samples were rinsed with water and dried with compressed air and after polishing the samples were rinsed with water, cleaned with ethanol and dried with compressed air. Figure 28 shows the grinding and polishing equipment.

Figure 28. Grinding equipment (left) and polishing equipment (right).

After the grinding and polishing, the samples were etched using 2% Nital. After the etching, the samples were first rinsed with water, cleaned with ethanol and finally dried with compressed air.

14 Optical microscopy

Optical microscopy (OM) is a technique used to examine materials using visible light to provide a magnified image of the micro- and the macrostructure. Grain boundaries, phase boundaries, inclusion distribution and mechanical deformation can be observed by OM. Despite the development of electron microscopes, the optical microscope remains the most important tool for the study of microstructure. [71], [72]

There exist two basic forms of light-optical microscopes: biological and metallurgical microscope (Figure 29). Metals and other materials that cannot easily be made thin enough to be optically transparent are examined by the metallurgical microscope. In this microscope the image is formed by light reflected from the surface of the specimen, which is usually immersed in a chemical etch in order to provide a perfectly smooth surface. Most etches preferentially dissolve the regions between individual grains of the specimen leaving a grain-boundary groove which is visible as a dark line. [71], [72]

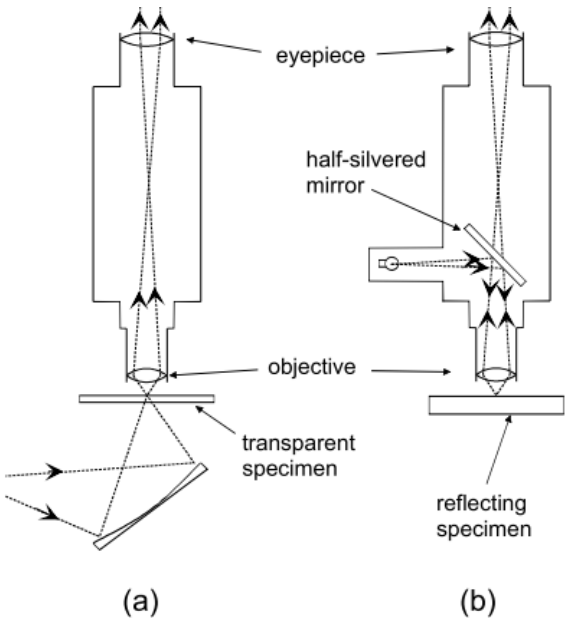

Figure 29. Schematic diagrams of (a) biological microscope and (b) metallurgical microscope. [71]

The resolution is limited by diffraction and it can be improved by decreasing the wavelength of the radiation. The wavelength can be decreased by using oil-immersion or, for greater improvement, by using ultraviolet radiation. For sample preparation grinding, polishing and etching is required. [71], [72]

The limitations of the light-optical microscopy is its resolution limit (about 1 μm), the limited depth of field (cannot focus on rough surfaces), and that it does not give direct chemical or crystallographic information about microstructural characteristics. [72]

In this study the optical microscope Leica DMR was used for analysing the samples after their metallographic preparation. A camera is connected on the top of the microscope in order to take pictures of the samples. Figure 30 shows this device.

Figure 30. Leica DMR optical microscope.

15 Scanning electron microscopy

Scanning electron microscopy (SEM) is a relatively easy handling and destruction-free technique that is used for materials characterization and quality control and to obtain information about chemical composition, crystalline structure, orientation and texture of the materials. In addition, topographical, morphological and composition information can be obtained. Moreover microstructure, fractography and surface contaminations can be analysed. Scanning electron microscopes (SEMs) use the different signals that are generated under electron bombardment at the surface of solid specimens to create an image due to the significant amount of kinetic energy that is dissipated by electron-sample interactions when the incident electrons are decelerated in the solid sample. These signals are secondary electrons, backscattered electrons, diffracted backscattered electrons, characteristic x-rays, long-wave radiation in the ultraviolet and visible region of the spectrum and heat. [73]–[75]

The essential components of SEMs include: electron source (gun), magnetic electron lenses, apertures, scanning coils, detectors for all signals of interest, display/data output devices, vacuum chamber and computer. SEMs always have at least one detector, typically a secondary electron detector, and most have additional detectors for other signals. [71]–[75]

In SEM areas from 1 cm to 5 µm in width can be imaged. In addition, selected point locations of the sample can be analysed which is especially useful in qualitative and semi-quantitative analysis. [71], [74]

Depending on the nature of the samples and the required data, sample preparation can be minimal or more complex. Minimal preparation consists of the preparation of

a sample that fits into the SEM chamber and some accommodation in order to prevent charge build-up on electrically insulating samples. [71], [73], [74]

In this study the scanning electron microscope Tescan Mira 3 was used in order to take pictures of the samples.

16 Hardness measurements

The hardness of the steel samples was measured using a Vickers hardness test following the test procedure ASTM E-384, which specifies a range of light loads using a diamond indenter to make an indentation which is measured and converted to a hardness value. This test is mostly used for small parts, thin sections or case depth work. Sample preparation is required in order to allow the sample to fit into the hardness tester. In addition, the surface of the specimen must be smooth to permit a regular indentation shape and good measurement and to ensure that the sample can be held perpendicular to the indenter. [76]

The Vickers hardness test consists of indenting the test sample with a diamond indenter. The form of the indenter is a right pyramid with a square base and an angle of 136 degrees between opposite faces subjected to a load of 1 to 100 kgf (kgf = kilogram force) which is usually applied for 10 to 15 seconds. Figure 31 shows a schematic of the indentation. After the removal of the load, the two diagonals of the indentation are measured using a microscope and the area of the sloping surface of the indentation is calculated. Dividing the kgf load by the square mm area of indentation the Vickers hardness is obtained. The Vickers hardness can be calculated from the formula, but usually conversion tables are used. [76], [77]

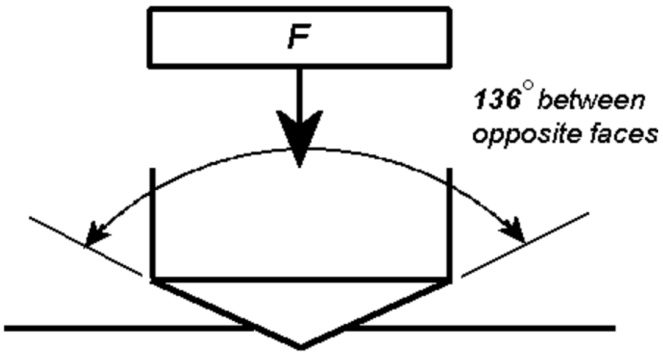

Figure 31. Schematic of indentation in Vickers hardness test [77].

The advantages of the Vickers hardness test are that the measurements are extremely accurate and just one type of indenter is used for all types of metals and surface treatments. However, the Vickers hardness test device is more expensive than that of Brinell or Rockwell hardness test. [77]

In this study the Vickers hardness measurement of the samples were carried out following the test procedure ASTM E-384. The Vickers hardness tester used is the Vickers/Knopp/Brinell hardness tester Innovatest Nexus® 4000, shown in Figure 32. The applied load was 200 g. In order to have more accuracy and reliable results, at least 5 tests were carried out for each sample. Then, the average measurement was calculated.

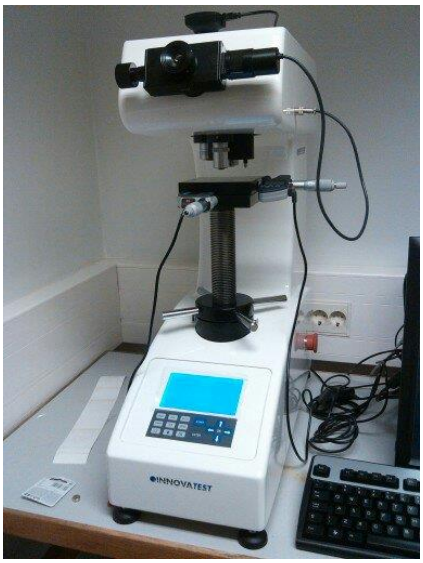

Figure 32. Vickers/Knopp/Brinell hardness tester Innovatest Nexus® 4000.

17 Results

17.1 Optical microscope pictures

The pictures of the samples taken with the Leica DMR optical microscope are shown in the following figures. Only the most representative pictures of the samples are showed in this study. More pictures can be found in Appendix A.

17.1.1 Micrographs of the mild cooling experiments

The micrographs of the mild cooling experiments are shown in Figure 33.

Sample 1: Mild cooling 750 ºC (Mag. 20x)

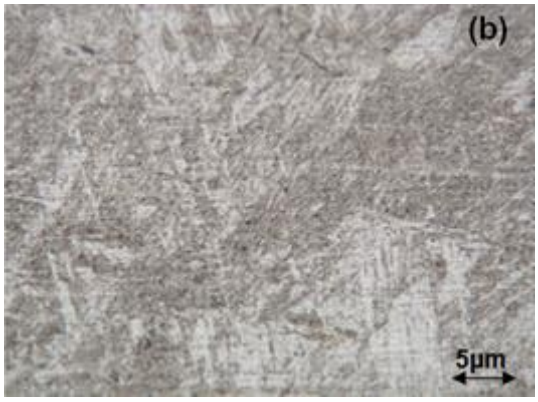

Sample 2: Mild cooling 910 ºC (Mag. 20x)

Figure 33. Micrographs of samples 1 (a) and 2 (b).

A completely martensitic microstructure is clearly observed, as was expected. The reason for this is that during the cooling, the Ar_3 temperature has not been achieved yet (since it is lower than 750 ºC) and therefore the phase before the water quenching was austenite, which after the water quenching transforms to martensite. Very large grains can also be observed in this structure, as a consequence of the low cooling rate (1ºC /s). In addition, the initial heating to the 1300 ºC causes the apparition of large grains due to the fact that at high temperatures the grain growth is very fast, especially over the 900 ºC. The precipitates are not visible with the optical microscope due to that they are smaller, but theoretically they are located at the grain boundaries.

17.1.2 Micrographs of the low temperature (T_1) experiments

The micrographs of the low temperature (T_1) experiments are shown in Figure 34.

Sample 3: T_1 = 510°C, H_1 = 0 min (Mag. 50x)

Sample 4: T_1 = 510°C, H_1 = 5 min (Mag. 50x)

Sample 5: T_1 = 610°C, H_1 = 5 min (Mag. 20x)

Sample 6: T_1 = 650°C, H_1 = 5 min (Mag. 50x)

Figure 34. Micrographs of samples 3 (a), 4 (b) , 5 (c) and 6 (d).

It can be observed that in sample 3 rounded ferrite has grown, probably around the grain boundaries because it is the preference location for the ferrite to growth. In sample 4 ferrite can also be observed in the grain boundaries, but less clearly than in sample 3 (the reason for clearer structure could be that the settings in the microscope has been different and more topographical picture has been obtained from sample 3). Theoretically there should be more ferrite in sample 4 than in sample 3 since the holding time at 510 °C was longer in sample 4. Samples 4 and 5 seem to have Widmanstätten ferrite as a result of the cooling rate used in the experiments and an orientated growth of the ferrite. It is difficult to confirm which sample has higher amount of ferrite, but theoretically sample 4 should contain more ferrite than sample 5 due to the temperature achieved with sample 4 was lower (510 ºC for sample 4 and 610 ºC for sample 5). The microstructure observed in sample 6 is mainly martensitic. No ferrite is observed, maybe because there is no ferrite or because the amount is so small that it cannot be observed with the optical microscope.

Furthermore, the grains observed in these four samples are large due to the initial heating up to 1300 ºC.

Thus, based on these micrographs it can be concluded that ferrite has been formed in the samples that have been cooled down to 610 ºC and to 510 ºC but no ferrite has been formed when cooling down to 650 ºC or maybe the amount of ferrite is very small. In addition, the growth of the ferrite seems to be unidirectional. The reason for the differences in the colours of the samples (grey vs. brown) is that the steel was very sensitive for etching times (brown samples were over-etched).

17.1.3 Micrographs of the SSCC based experiments

The micrographs of the SSCC based experiments are shown in Figures 35 and 36.

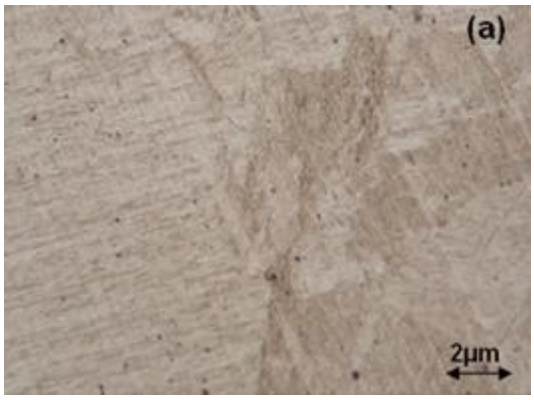

Sample 7: T_1 = 510 ºC, H_1 = 2 min, T_2 = 810 ºC, H_2 = 2 min (Mag. 50x)

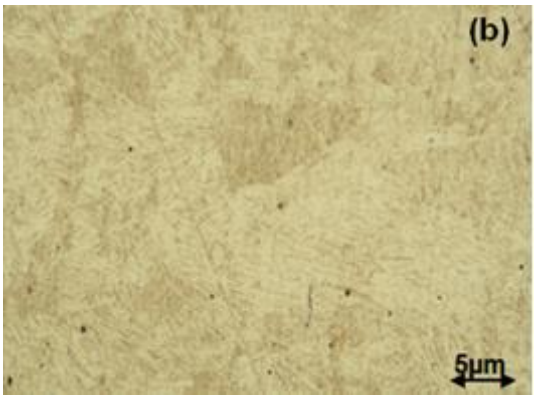

Sample 8: T_1 = 510 ºC, H_1 = 2 min, T_2 = 810 ºC, H_2 = 5 min (Mag. 20x)

Sample 9: T_1 = 510 ºC, H_1 = 2 min, T_2 = 915 ºC, H_2 = 2 min (Mag. 20x)

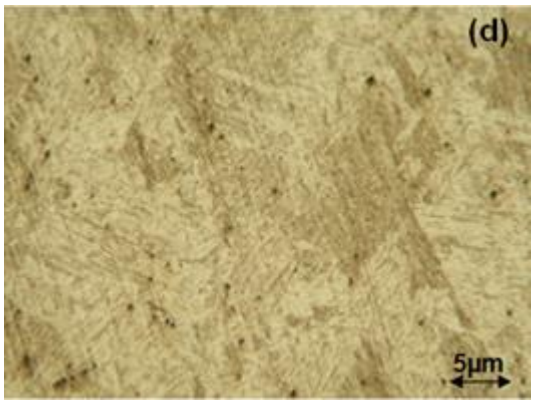

Sample 10: T_1 = 510 ºC, H_1 = 5 min, T_2 = 915 ºC, H_2 = 2 min (Mag. 20x)

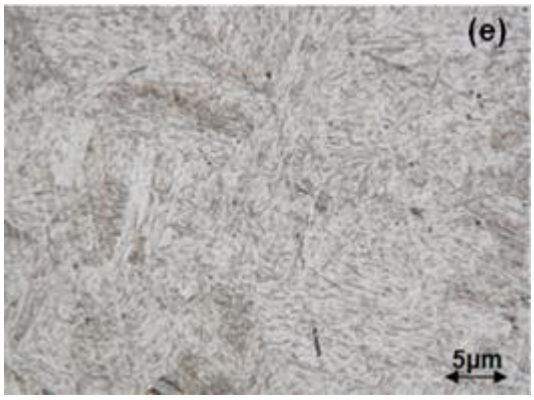

Sample 11: T_1 = 510 ºC, H_1 = 5 min, T_2 = 915 ºC, H_2 = 5 min (Mag. 20x)

Sample 12: T_1 = 610 ºC, H_1 = 2 min, T_2 = 915 ºC, H_2 = 2 min (Mag. 20x)

Figure 35. Micrographs of samples 7 (a), 8 (b), 9 (c), 10 (d), 11 (e) and 12 (f).

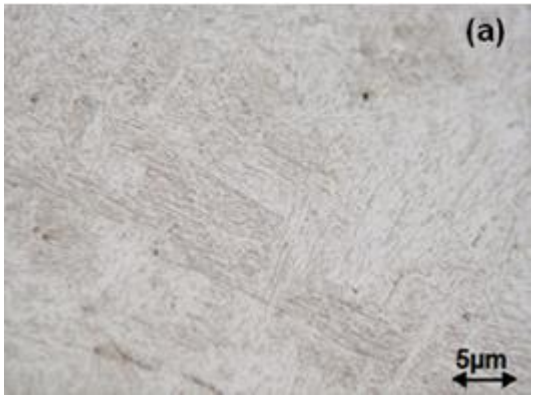

Sample 13: T_1 = 610 ºC, H_1 = 5 min, T_2 = 915 ºC, H_2 = 2 min (Mag. 20x)

Sample 14: T_1 = 650 ºC, H_1 = 2 min, T_2 = 915 ºC, H_2 = 2 min (Mag. 20x)

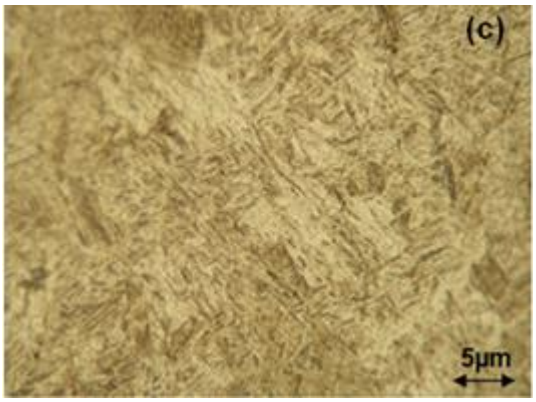

Sample 15: T_1 = 650 ºC, H_1 = 5 min, T_2 = 915 ºC, H_2 = 2 min (Mag. 20x)

Sample 16: T_1 = 650 ºC, H_1 = 2 min, T_2 = 915 ºC, H_2 = 5 min (Mag. 20x)

Sample 17: T_1 = 610 ºC, H_1 = 5 min, T_2 = 975 ºC, H_2 = 2 min (Mag. 50x)

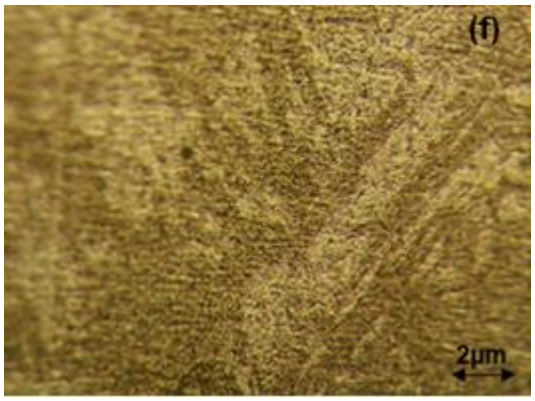

Sample 18: T_1 = 610 ºC, H_1 = 5 min, T_2 = 975 ºC, H_2 = 5 min (Mag. 50x)

Figure 36. Micrographs of samples 13 (a), 14 (b), 15 (c), 16 (d), 17 (e) and 18 (f).

It can be seen that the microstructure after the water quenching of all the SSCC based samples is martensitic. This martensite proceeds from the austenite phase which the samples had before they were quenched in water. No ferrite is observed. This means that all the ferrite that could be formed after the cooling has been transformed to austenite during the reheating and the holding at high temperature.

No grains with different size are observed in these pictures. This indicates that the phenomenon of new grain growth from the precipitates located at the grain boundaries has not happened. If it had happened, two different kinds of grains could be observed. Large grains, which would be the prior austenite grains, and smaller grains which would come from the growth from the precipitates. The double phase transformation phenomena which brings an about ferrite microstructure without a film-like ferrite was clearly not observed either.

As can be deduced from the pictures, all the ferrite that appeared at low temperature has transformed to austenite. During the austenite to ferrite transformation throughout the cooling, the carbon content of the austenite is higher than that of the ferrite. Thus, when this ferrite transforms back to austenite during the reheating it could happen that this new austenite has lower carbon content than the former austenite and therefore this phenomenon would be reflected in two different martensites after the water quenching, with different carbon content. This would happen if the time above the Ac_3 temperature (when the ferrite starts to transform to austenite) is not long enough to allow the carbon to diffuse throughout the sample and then homogenise the carbon content of the martensite. They could be distinguished because the martensite with lower carbon content would look darker than the other martensite. In addition, the martensite which proceeds from the new austenite could have more round form since it would be formed from the ferrite, which is more rounded.

However, this phenomenon is not observed in the pictures. The samples show a martensitic structure which does not suggest that there are two martensites with different carbon content. Only three SSCC based samples, samples 7, 9 and 10, could somehow suggest this kind of microstructure. These three samples have the T_1 temperature, 510 ºC, and the same holding time at high temperature, 2 minutes. In these samples the microstructure is martensitic but there are some areas in which the tonality of the martensite can suggest that this phenomenon has taken place. In addition, some rounded martensite was observed.

Nevertheless, it must be emphasized that it is very unlikely that this phenomenon has happened. The most probable phenomenon that has taken place is that the ferrite formed at low temperature has transformed to austenite and the carbon content of the sample has been balanced throughout the samples and therefore no different martensites exist in their microstructure.

Comparing the microstructure of the SSCC based samples with the mild cooling samples probably the only difference is that the SSCC based samples has a much finer microstructure. The reason for this can be that the cooling rate of the SSCC based samples is higher but also the double phase transformation could have caused that smaller grains are obtained in these samples.

17.1.4 Micrographs of the SSCC based + mild cooling experiments

The micrographs of the SSCC based + mild cooling experiments are shown in Figure 37.

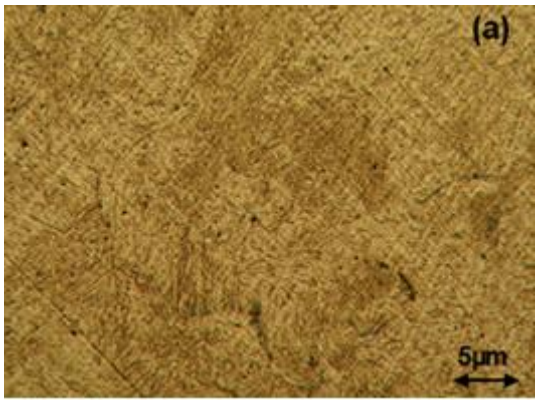

Sample 19: T_1 = 610 ºC, H_1 = 5 min, T_2 = 975 ºC, H_2 = 2 min (Mag. 20x)

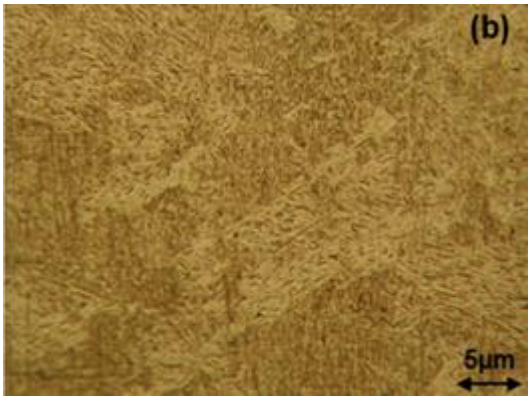

Sample 20: T_1 = 610 ºC, H_1 = 5 min, T_2 = 975 ºC, H_2 = 5 min (Mag. 20x)

Figure 37. Micrographs of samples 19 (a) and 20 (b) at magnification of 20x.

The microstructure of these samples is fully martensitic. It seems that the ferritic structure obtained after the cooling has been destroyed with the reheating to 975 ºC, giving an entirely martensitic microstructure.

Making a comparison between these samples and sample 1 (mild cooling sample until 750 ºC), the microstructure is similar. The only difference is the grain size. The microstructure of these samples is much finer than that of the mild cooling samples. However, it probably is due to the higher cooling rate of these samples, not due to the heat treatment (similarly to the SSCC based samples).

17.2 SEM micrographs

SEM micrographs from samples 2 and 10 are shown in Figures 38 and 39. Sample 2 is a mild cooling sample and sample 10 has gone through SSCC based heat treatment.

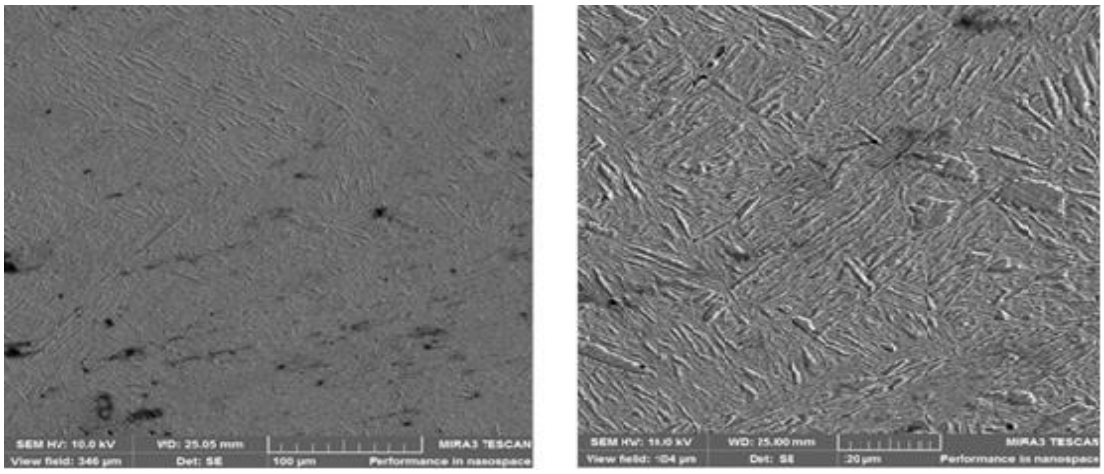

Figure 38. SEM micrographs of sample 2 at 600x (left) and 2000x (right)

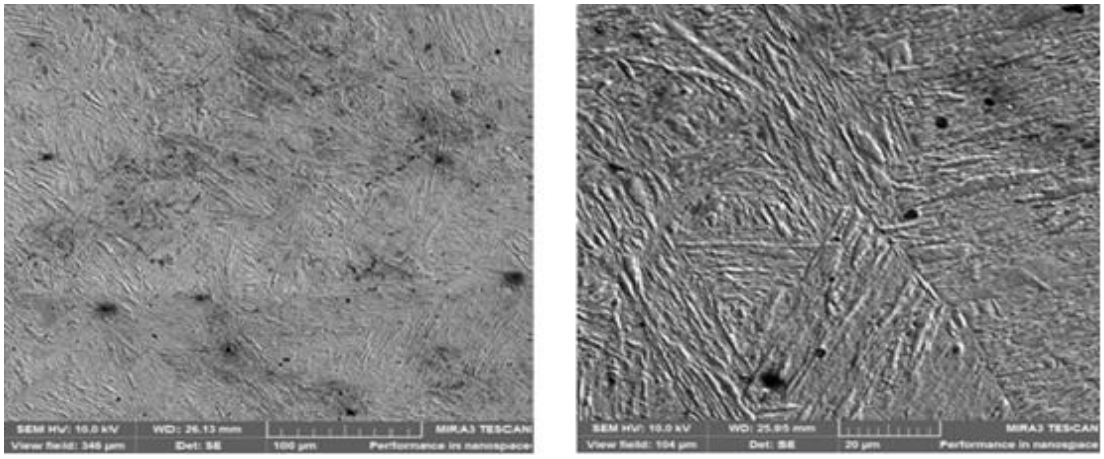

Figure 39. SEM micrographs of sample 10 at 600x (a) and 2000x (b)

The SEM micrographs reveal that the only difference between samples 2 and 10 is that the microstructure of sample 10 much finer and the grain size is smaller than that of sample 2. However, there is some inconsistency in the SEM results, thus these results are not very reliable.

17.3 Hardness measurements

The results of the hardness measurements are given in Table 8.

Table 8. Hardness measurements.

Sample	Meas. 1	Meas. 2	Meas. 3	Meas. 4	Meas. 5	Meas. 6	Meas. 7	Average
1	427	461	426	440	425	437	435	436
2	432	415	409	453	445	437		432
3	433	441	352	392	405	360		397
4	376	415	430	426	413	439		417
5	395	379	350	340	450	440	428	397
6	445	420	455	400	413			427
7	454	450	440	446	443			447
8	437	426	416	460	421			432
9	444	440	440	459	415	458		443
10	403	436	428	413	440			424
11	460	469	470	478	439	451		461
12	420	419	460	434	432			433
13	452	416	450	412	435			433
14	403	443	440	443	410			428
15	444	458	449	465	461			455
16	410	426	421	420	440			423
17	410	417	405	411	440	419		417
18	442	426	396	421	400	395	433	416
19	450	448	431	437	451			443
20	424	423	442	408	427			425

The hardness measurements of the samples confirm that the microstructure of all the samples is mainly martensitic. In addition, there is not a considerable difference

between the hardness of the samples. Thus, no conclusions can be deduced from the hardness measurement.

Nevertheless, it can be observed that the standard deviation of the low temperature samples (samples 3, 4, 5 and 6) is very big. The reason is that the Vickers hardness test is not a micro-hardness test. Then, it was not possible to measure the hardness of a specific phase or place. Thus, if the indentation is made over a martensitic area the value will be high but if it is made over a ferritic area the value will be low. This difference in the values can be checked from the measurements of these samples. This confirms that ferrite has grown in the grain boundaries. It can be observed that the lower the T_1 temperature (see Figure 28), the lower the hardness as a result of the higher amount of ferrite. The hardness value of the sample 6 is the same in the rest of the samples, which confirms that there was no ferrite in this sample (or very low amount).

However, the measurements of the sample 4 are strange since it seems to be harder than the sample 3 (due to sample 4 has higher amount of ferrite). It could be due to the indentations have been made over martensitic areas of sample 4 or because the unidirectional growth of the ferrite in sample 4 makes that its hardness is higher. The most probable option is the first one.

Comparing the results with the values of the graph showed in Figure 40, which shows the martensite hardness depending on the carbon content, the hardness measurements confirm that the carbon content of the steel is 0.147 or, at least, that it is close to that.

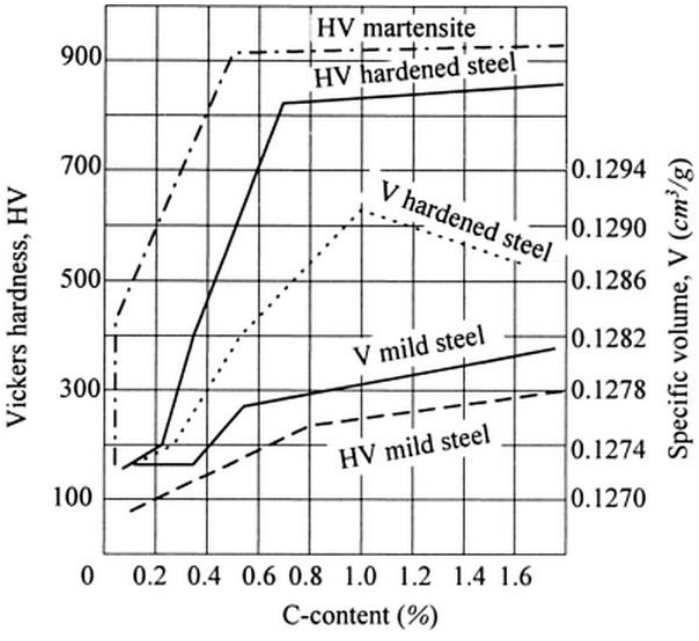

Figure 40. Hardness of steels in various states vs. carbon content [78].

18 Discussion

The microscopic analyses of the heat treated samples showed that the aimed phenomena were not achieved. It seems that the precipitates did not have any effect on the microstructure evolution of the heat treated samples. New grains were not generated from the precipitates during the process in any experiment (or if it happened, these new grains were so small that they could not be observed). It could be that the precipitate size plays a key role in promoting this effect. In this way maybe smaller precipitates, which would precipitate at higher cooling rate, are needed to encourage this phenomenon. In addition, it could be necessary that sufficient supercooling has to be achieved in order to let the ferrite grow not only at austenite grain boundaries but also inside the grain. With high cooling rate, fine precipitates and ferrite would precipitate at the same time. The simultaneous formation of precipitates and appearance of ferrite could be favourable to achieve the growth of the grains around the precipitates. In the reheating the ferrite would transform to austenite again and in the following stage of cooling the ferrite grain would originate from this fine precipitates. Nonetheless, as mentioned before the continuous casting conditions do not allow using very high cooling rates (for example 20 °C/s, as was used in previous work [35], [39], [42], [43]). The only effect of the precipitates could be that they cause an orientated growth of the ferrite when the temperature is lower than the Ar_3 temperature.

In addition, the double phase transformation that brings an about ferrite microstructure with film-like ferrite free grain boundaries did not take place. It is clear that all the ferrite that appeared at low temperature was transformed back to austenite during the reheating. However, this austenite has not been transformed again to ferrite. The reason is that the final temperature of the SSCC based and SSCC based + mild cooling experiments is over the Ar_3 temperature and then the austenite to ferrite transformation cannot take place.

The low temperature samples showed that a temperature of 610 ºC after the cooling is enough to allow the ferrite to appear. The ferrite starts to nucleate mainly in the grain boundaries when the Ar_3 temperature is achieved during the cooling. It starts to appear with rounded shape and it seems to grow in an orientated way later on because Widmanstätten ferrite can be observed. The reason for this orientated growth could be the presence of the precipitates. As the precipitates are located at the grain boundaries, the areas which are close to the grain boundaries but outside of them have lower amount in the elements that form the precipitates (Nb, Ti, V, C and N). The lack of these elements could be the reason for this orientated growth.

A phenomenon that could distinguish the SSCC based samples from the mild cooling samples is that the transformation during and after the reheating of the ferrite to austenite gives a new austenite with lower carbon content than the former austenite. However, this is very unclear and it is just an assumption based on the theory. It

seems that, in case that this phenomenon takes place, the lower T_1 temperature (510 ºC) is favourable and that a holding time at the T_2 temperature (both 810 ºC and 915 ºC) of 2 minutes aids in the appearance of this phenomenon. The reason could be that the samples cooled down until 510 ºC have the highest amount of ferrite and that if the holding time at high temperature is longer than 2 minutes then the carbon content of the whole austenitic structure is equalised and then this microstructure disappears. Furthermore, it seems that lower T_1 temperature and shorter holding time H_1 is more effective than higher T_1 temperature and longer holding time in promoting this effect. In addition, the microstructure observed in the SSCC based samples was much finer than that of the mild cooling samples. It could be as a consequence of the higher cooling rate of the SSCC based samples but it could be also as a consequence of the double phase transformation. In this context, the double phase transformation could give finer grains, which is beneficial to the hot ductility. If this finer microstructure is due to the double phase transformation and not due to the higher cooling rate, then the SSCC process would improve the hot ductility of the analysed steel.

It could be that very high T_2 temperatures and long holding times at this temperature are not favourable for the process, maybe because the microstructure achieved at low temperature is removed. However, this is only an assumption since the aimed phenomena were not achieved in these experiments.

Furthermore, it is possible that very accurate conditions are needed to allow the aimed phenomena to take place. There might have been problems of precision during the experiments. The control at a constant temperature during the holding stages of the experiments was not very accurate because it was manually controlled and due to the temperature profile of the furnace. There was a very big temperature difference within 1 cm (50 – 100 ºC) and therefore the temperature through the sample was most probably not even. This made that the temperature of the sample was varying and was not completely constant (it was controlled in a range of ± 10 °C). The heating and cooling rates were very difficult to control as well. In addition, the removal of the sample from the furnace to quench the sample in water took several seconds. Thus, changes in the microstructure could take place during this time. Previous work [35], [39], [42], [43] used Gleeble thermo-mechanical and simulators, which are more precise and simulate more accurately the desired conditions.

19 Conclusions

Transversal corner cracking has been found as a problem which is very difficult to prevent. This cracking mainly occurs due to the presence of a film-like ferrite and precipitates at the grain boundaries during the straightening in continuous casting. Many strategies have been used already but none of them has completely solved the problem. Surface structure control cooling (SSCC) is a new method that seems to be

very promising in preventing transversal corner cracking. This method consist of cooling until a temperature below the Ar_3 temperature with high cooling rate, a holding there and a subsequent reheating to a temperature above the Ac_3 temperature. After this, a normal cooling takes place. As a result a double phase transformation takes place, giving a microstructure with finer grains and with the precipitates distributed throughout the matrix or with lower cooling rates at the grain boundaries. In SSCC method precipitates induce non-directional ferrite growth around them resulting in a stronger structure than in the case of normal mild cooling in continuous casting. As a consequence of this mild cooling ferrite starts to grow in the grain boundaries in a film-like form which is very sensitive for cracking especially in the presence of stresses.

In order to apply this method to the continuous casting of the micro-alloyed steel, several experiments have been carried out. In these experiments, the parameters have been adapted to the real continuous casting conditions and the effect of the different temperatures and holding times has been tested. Thus, the cooling rate used in the experiments is much lower than which were used in the previous work [35], [39], [42], [43]. As a consequence, in the experiments of this study the precipitates should form at the grain boundaries and not necessarily inside the grains. The samples were analysed with the microscope in order to check if new grains have been created from the precipitates and if a double phase transformation which avoid the film-like ferrite in the grain boundaries has occurred.

The results show that new grains were not created from the precipitates and that the double phase transformation did not take place. There are three samples that somehow suggest that the ferrite obtained at temperatures lower than the Ar_3 temperature transforms to austenite during the reheating. This new austenite could have less carbon content than the former austenite. Thus, a microstructure with two different austenites, differenced in the carbon content, would be obtained. However, it is necessary to stand out that this is just an assumption based on theory and it is possible that it has not happened. In case that this effect occurs, it seems that a temperature of 510 °C (with higher ferrite content at low temperature) and a holding time of 2 minutes (longer time seems to eliminate this effect because carbon would have more time to diffuse and then the carbon content of the austenite would be the same in all the parts of the sample) are the optimal parameters. In addition, the SSCC gives a finer microstructure than the mild cooling. It is not clear if this effect is due to the higher cooling rate only or also due to the phase transformations that are involved in the process.

Furthermore, some recommendations for future work are proposed in order to achieve better and clearer results that clarify the phenomena involved in the process.

20 Future work

For future work, I would recommend to use more accurate equipment because these heat treatments probably require high precision. Thus, more sophisticated equipment would be helpful, such as thermo-mechanical simulator Gleeble. Furthermore, I would recommend melting the sample in order to improve the results. I think that by melting the samples the continuous casting conditions are better simulated. In addition, all the precipitates will be dissolved (in the experiments of this thesis the Ti (C,N) precipitates were not dissolved, according to the calculation showed in Figure 22) and therefore the precipitates would be smaller which probably would aid in achieving the desired phenomena.

More experiments at low temperature are necessary in order to check the growth morphology during the holding at low temperature (T_1) and to understand the mechanism of this growth.

In addition, I suggest performing more SSCC based + mild cooling experiments with a lower final temperature at which the ferrite is able to appear. The comparison of that microstructure with the microstructure of the mild cooling samples cooled until the same temperature (both with normal cooling rate and with the cooling rate used in the SSCC experiments) is important in order to check if there is any difference in the grain size and in the ferrite growth due to the double phase transformation of the SSCC process. For instance, temperatures that could be used are 610 ºC and 550 ºC.

Furthermore, a SEM investigation would be helpful in order to check precisely the microstructure and precipitations and the phenomena that take place at the grain boundaries of the samples.

References

[1] H. Jo, K. B. Kang, and C. G. Park, “Effects of cooling rate and isothermal holding on the precipitation behavior during continuous casting of Nb – Ti bearing HSLA steels,” vol. 49, pp. 1081–1086, 2003.

[2] F. J. Ma, G. H. Wen, P. Tang, X. Yu, J. Y. Li, G. D. Xu, and F. Mei, “Causes of transverse corner cracks in microalloyed steel in vertical bending continuous slab casters,” vol. 37, no. 1, pp. 73–79, 2010.

[3] J. R. Davis and Davis & Associates, Eds., “High-Strength Low-Alloy Steels,” in *Alloying. Understanding the basics*, 1st ed., Ohio: ASM International, 2001, pp. 121–255.

[4] M. Korchynsky, “A New Role for Microalloyed Steels − Adding Economic Value,” in *Proceedings of the 9th International Ferro Alloy Conference Infacon 9*, 2001, p. 11.

[5] K. Xu, B. G. Thomas, M. S. Dyer, J. G. Speer, and D. K. Matlock, “Model of Microalloy Precipitation during Continuous Casting and Reheating,” pp. 1–11, 2011.

[6] Z. Su, “Effects of Cooling Rates on Microstructures and Mechanical Properties of Nb-Ti Microalloyed Steel,” vol. 17, no. 6, pp. 653–657, 2012.

[7] Key to metals, “Application of Microalloyed HSLA Steel: Part One,” 2011. [Online]. Available: http://www.keytometals.com/page.aspx?ID=CheckArticle&site=kts&NM=347. [Accessed: 20-Feb-2014].

[8] Worldsteel association, “Crude steel production,” 2014. [Online]. Available: https://www.worldsteel.org/statistics/crude-steel-production.html. [Accessed: 20-Feb-2014].

[9] B. G. Thomas, “Continuous Casting,” in *Yearbook of Science and Technology*, McGraw-Hill, 2004, p. 6.

[10] H. F. Scherwe, Continuous casting of steel. Fundamental principles and practice. Düsseldorf: Stahleisen, 1987, p. 194.

[11] S. Louhenkilpi, “Continuous casting of steel,” in *Treatise on process metallurgy*, 1st ed., vol. 3, S. Seetharaman, A. McLean, R. Guthrie, and S. Sridhar, Eds. Oxford, UK: Elsevier, 2014, pp. 373–434.

[12] A. Smirnov, V. Pilyuschenko, A. Minaev, S. Momot, and Y. Belobrov, *Continuous casting of steel*, Second edi. Donetsk, 2004, p. 267.

[13] Metalpass, “Continuous casting equipment,” 2002. [Online]. Available: http://www.metalpass.com/metaldoc/paper.aspx?docID=21. [Accessed: 26-Feb-2014].

[14] SEHM, “The role their advantages and disadvantages of vertical continuous casting machine,” 2013. [Online]. Available: http://www.semcgroup.com/news-detail_82.html.

[15] H. J. Jun, K. B. Kang, and C. G. Park, “Effects of cooling rate and isothermal holding on the precipitation behavior during continuous casting of Nb–Ti bearing HSLA steels,” *Scr. Mater.*, vol. 49, no. 11, pp. 1081–1086, Dec. 2003.

[16] H. Okumura, “Recent trends and future prospects of continuous casting technology,” *Nippon steel Tech. Rep.*, no. 61, p. 6.

[17] Key to metals, “Thin slab casting.” [Online]. Available: http://www.keytometals.com/page.aspx?ID=CheckArticle&site=ktn&NM=306. [Accessed: 26-Feb-2014].

[18] B. Smith and M. Sexton, “Steel plant developments,” *Materials World*, 2001. [Online]. Available: http://www.azom.com/article.aspx?ArticleID=913. [Accessed: 26-Feb-2014].

[19] G. Krauss, *Steels. Processing, structure and performance*, 1st editio. Colorado, USA: ASM International, 2005, p. 613.

[20] S. Wilmotte, J.-P. Birat, and R. Steffen, “State of the art and developments in near-net-shape casting of flat steel products,” European Comission, Düsseldorf, Germany.

[21] G. Li and B. G. Thomas, “Transient thermal model of the continuous single-wheel thin-strip casting process,” *Metall. Mater. Trans. B*, vol. 27, no. 3, pp. 509–525, Jun. 1996.

[22] P. Campbell, R. Wechsler, G. Gillen, W. Blejde, and R. Mahapatra, “The Status of Twin-Roll Strip Casting Technology – Castrip Process,” in *SCANMET II – 2nd International Conference on Process Development in Iron and Steelmaking*, 2004, p. 12.

[23] D. Raabe, “Strip casting of steel.” [Online]. Available: http://www.dierk-raabe.com/strip-casting-of-steel/. [Accessed: 26-Feb-2014].

[24] J. K. Brimacombe, I. V. Samarasekera, and J. E. Lait, *Continuous casting: vol. 2. Heat flow, solidification and crack formation*, vol. 2. Chelsea: Iron & steel society of AIME, 1984, p. 238.

[25] B. G. Thomas, “Metals processing,” in *Structure, Processing, and Properties of Engineering Materials*, A. Wesley and J. Adams, Eds. .

[26] I. Ohnaka, “Casting,” in *ASM Metals Handbook*, 9th ed., ASM International, 1988, p. 1256.

[27] A. Kundu, “Grain Structure Development During Casting , Reheating and Deformation of Nb-Microalloyed steel,” College of Engineering and Physical Sciences. University of Birmingham, 2011.

[28] Dictionary.com, “Diffusion coefficient,” *Collins English Dictionary - Complete & Unabridged 10th Edition*. [Online]. Available: http://dictionary.reference.com/browse/diffusion+coefficient. [Accessed: 05-May-2014].

[29] D. M. Stefanescu, *Science and engineering of casting solidification*, Second edi. Columbus, OH: Springer, 2009, p. 402.

[30] “Properties and selection: Iron steels and high performance alloys,” *ASM Metals Handbook*. ASM International, p. 1063, 1990.

[31] S. Kivivuori and S. Härkönen, “Lämpökäsittelyn perusteet,” in *Lämpökäsittelyoppi*, Tampere: Teknologia teollisuus, 2004, pp. 10–24.

[32] M. Qingshen, J. Zhonghang, L. Wenbin, Y. Xiaoshan, L. Yan, and XuLi, “Cause and Measures of Transverse Corner Crack in Hull Structural V-Containing Steel CC Slabs,” in *International Seminar 2005 on Application Technologies of Vanadium in Flat – Rolled Steels*, 2005, pp. 75–78.

[33] B. Patrick, M. W. Short, R. Walmsley, B. Barber, K. Harste, K.-H. Tacke, and I. Steinert, “Crack prevention in continuous casting,” Luxembourg, 1998.

[34] O. B. Isaev, V. V Kislitsa, and A. V. Fedosov, “Studies of the conditions of formation of transverse corner cracks on the surface of continuous-cast slabs,” *Metallurgist*, vol. 55, no. 9–10, pp. 720–723, 2012.

[35] N. Baba, K. Ohta, Y. Ito, and T. Kato, “Prevention of slab surface transverse cracking at Kashima n°2 caster with Surface Structure Control (SSC) cooling,” *La Rev. Métallurgie-CIT*, pp. 174–179, 2006.

[36] D. N. Crowther, “The effects of microalloying on cracking during continuous cracking,” Moorgate, Rotherham, UK.

[37] Y. Le Papillon, M. Konig, W. Jäeger, B. Weisgerber, and M. Jauhola, “Determination of high temperature surface cracks formation criteria in continuous casting and thin slab casting,” Luxembourg, 2003.

[38] B. Mintz, S. Vue, and J. J. Jonas, “Hot ductility of steels and its relationship to the problem of transverse cracking during continuous casting,” *Int. Mater. Rev.*, vol. 36, no. 5, pp. 187–219, 1991.

[39] T. Kato, Y. Ito, M. Kawamoto, A. Yamanaka, and T. Watanabe, “Prevention of Slab Surface Transverse Cracking by Microstructure Control,” *ISIJ Int.*, vol. 43, no. 11, pp. 1742–1750, 2003.

[40] F. Zarandi and S. Yue, “The Effect of Boron on Hot Ductility of Nb-microalloyed Steels,” *ISIJ Int.*, vol. 46, no. 4, pp. 591–598, 2006.

[41] F. J. Ma, G. H. Wen, P. Tang, X. Yu, J. Y. Li, G. D. Xu, and F. Mei, “In situ observation and investigation of effect of cooling rate on slab surface microstructure evolution in microalloyed steel,” *Ironmak. Steelmak.*, vol. 37, no. 3, pp. 211–218, 2010.

[42] G. Walmag, A. Schmitz, and C. Marique, “A new secondary cooling concept for avoiding surface cracks during casting of peritectic and micro-alloyed steels.”

[43] M. Lückl, S. Ilie, J. Six, and E. Kozeschnik, “Surface Microstructure Control during Continuous Casting of Micro- Alloyed Steel,” in *Materials Science and Technology*, 2013, pp. 433–438.

[44] M. Vedani, D. Ripamonti, A. Mannucci, and D. Dellasega, “Hot ductility of microalloyed steels,” *La Metall. Ital.*, pp. 19–24, 2008.

[45] S. G. Hong, K. B. Kang, and C. G. Park, “Strain-induced precipitation of NbC in Nb and Nb ± Ti microalloyed HSLA steels,” *Scr. Mater.*, vol. 46, pp. 163–168, 2002.

[46] N. Bannenberg, B. Bergmann, H.-A. Jungblut, and N. Mueller, “Procedures for successul continuous casting of steel microalloyed with Nb, V, Ti and N,” in *Microalloying proceedings*, 1995, p. 12.

[47] H. G. Suzuki, S. Nishimura, and S. Yamaguchi, “Physical simulation of the continuous casting of steels,” in *Proc. Conf. on Physical Simulation Techniques for Welding, Hot forming and Continuous Casting*, 1988.

[48] B. Mintz and D. N. Crowther, “Hot ductility of steels and its relationship to the problem of transverse cracking in continuous casting,” *Int. Mater. Rev.*, vol. 55, no. 3, pp. 168–196, 2010.

[49] B. Mintz, “The influence of composition on the hot ductility to the problem of transverse cracking,” *ISIJ Int.*, vol. 39, no. 9, pp. 833–855, 1999.

[50] B.Mintz, Z. Mohamed, and R. Abu-shosha, “Influence of calcium on hot ductility of steels,” *Mater. Sci. Technol.*, vol. 5, no. July, pp. 682–688, 1989.

[51] D. N. Crowther and B. Mintz, “Influence of grain size and precipitation on hot ductility of microalloyed steels,” *Mater. Sci. Technol.*, vol. 2, no. November, pp. 1099–1105, 1986.

[52] S. Moon, “The influence of Austenite grain size on hot ductility of steels,” University of Wollongong, 2003.

[53] K. Xu and B. G. Thomas, “Prediction of Grain Size , Precipitation and Crack Susceptibility in Continuous Casting,” in *AISTech 2009 Steelmaking Conference Proceeding*, 2009, vol. 1, p. 12.

[54] H. Luo, L. P. Karjalainen, D. a. Porter, H.-M. Liimatainen, and Y. Zhang, “The Influence of Ti on the Hot Ductility of Nb-bearing Steels in Simulated Continuous Casting Process.,” *ISIJ Int.*, vol. 42, no. 3, pp. 273–282, 2002.

[55] M. Maalekian, “The Effects of Alloying Elements on Steels (I),” Graz, 2007.

[56] K. M. Banks, A. Tuling, and B. Mintz, “The influence of N on hot ductility of V- , Nb- , and Nb-Ti- containing steels using improved thermal simulation of continuous casting,” *J. South. African Inst. Min. Metall.*, vol. 111, no. October, pp. 711–716, 2011.

[57] D. Karjalainen, L.P. , Kinnunen, H., Porter, “Hot ductility of certain microalloyed steels under simulated continuous casting conditions,” *Mater. Sci. Forum Vols.*, no. 284–286, pp. 477–484, 1998.

[58] Z. Mohamed, “Hot ductility behavior of vanadium containing steels,” *Mater. Sci. Eng.*, vol. 326, pp. 255–260, 2002.

[59] R. Lagneborg, T. Siwecki, S. Zajac, and B. Hutchinson, “The Role Of Vanadium In Microalloyed Steels,” Stockholm, Sweden, 1999.

[60] B. Chen and H. Yu, “Hot ductility behavior of V-N and V-Nb microalloyed steels,” *Int. J. Miner. Metall. Mater.*, vol. 19, no. 6, pp. 525–529, 2012.

[61] E. López-Chipres, I. Mejía, C. Maldonado, A. Bedolla-Jacuinde, and J. M. Cabrera, “Hot ductility behavior of boron microalloyed steels,” *Mater. Sci. Eng.*, no. 460–461, pp. 464–470, 2007.

[62] O. Comineli, H. Luo, H.-M. Liimatainen, and L. P. Karjalainen, “Influence of Cu alloying on hot ductility of C-Mn-Al and Ti-Nb microalloyed steels,” in *IX Conference on materials science & technology*, 2003, p. 6.

[63] T. Kato, N. Kasai, M. Kawamoto, Y. A., and T. Watanabe, “Formation mechanism of slab surface transverse cracking in continuously cast Ni bearing steel,” *Tetsu-to-Hagane*, vol. 84, pp. 856–860, 1998.

[64] B. Mintz, “Influence of nitrogen on hot ductility of steels and its relationship to problem of transverse cracking,” *Ironmak. Steelmak.*, vol. 27, no. 5, pp. 343–347, 2000.

[65] C. Ouchi and K. Matsumoto, “Hot ductility in Nb-bearing high-strength low-alloy steels,” *Iron steel Inst. Japan*, vol. 22, no. 3, p. 181, 1982.

[66] B. Mintz and J. M. Arrowsmith, “Influence of microalloying additions on hot ductility of steels,” in *Sheffield Int. Conf. on Hot Working and Forming Processes*, 1979, pp. 99–103.

[67] Y. Maehara and T. Nagamichi, “Effects of sulphur on hot ductility of niobium containing low carbon steels during low strain rate deformation,” *Mater. Sci. Technol.*, vol. 7, no. October, pp. 915–922, 1991.

[68] S. G. Jansto, “Steelmaking and continuous casting process metallurgy factors incluencing hot ductility behavior of niobium bearing steels,” Brno, Czech Republic, 2013.

[69] B. B. Mintz, J. R. Banerjee, and K. M. Banks, “A regression equation for the Ar3 temperature for coarse grained as-cast steels,” London, England, 2011.

[70] A. A. Gorni, *Steel forming and heat treating handbook*, no. February. São Vicente SP, Brazil, 2014, p. 171.

[71] R. F. Egerton, Physical principles of electron microscopy. An introduction to TEM, SEM, and AEM. New York: Springer, 2005, p. 202.

[72] “Materials characterization,” in *ASM Metals Handbook*, 9th ed., ASM International, 1986, p. 761.

[73] G. F. Vander Voort, Ed., “Metallography and Microstructures 2004,” in *ASM Metals Handbook*, ASM International, 2004, p. 1184.

[74] S.Swapp, “Scanning electron microscopy (SEM),” 2013. [Online]. Available: http://serc.carleton.edu/research_education/geochemsheets/techniques/SEM.html. [Accessed: 20-Dec-2013].

[75] M. Master, “Scanning electron microscope. Advantages and disadvantages in imaging components and applications,” 2013. [Online]. Available: http://www.microscopemaster.com/scanning-electron-microscope.html. [Accessed: 20-Dec-2013].

[76] Newage, “Vickers hardness testing,” 2010. [Online]. Available: http://www.hardnesstesters.com/Applications/Vickers-Hardness-Testing.aspx. [Accessed: 17-May-2014].

[77] Gordon England, “Vickers hardness test.” [Online]. Available: http://www.gordonengland.co.uk/hardness/vickers.htm. [Accessed: 17-May-2014].

[78] M. Tisza, “Non-equilibriuim crystallization of iron-carbon alloys,” in *Physical metallurgy for engineers*, 2nd ed., ASM International, 2002, p. 405.

Appendix A. Microstructure of the samples

Micrographs of samples 1 and 2.

Sample 1: Mild cooling 750 ºC (Mag. 20x)

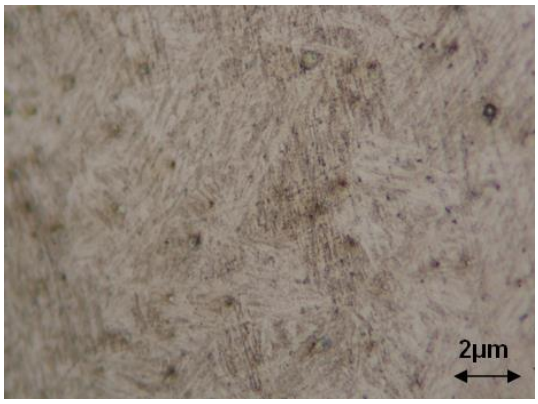

Sample 1: Mild cooling 750 ºC (Mag. 50x)

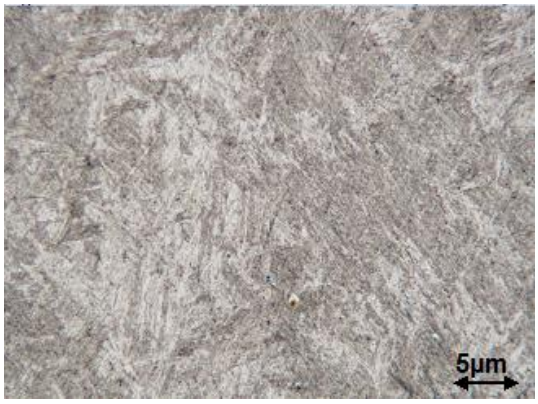

Sample 2: Mild cooling 910 ºC (Mag. 20x)

Sample 2: Mild cooling 910 ºC (Mag. 20x)

Micrographs of samples 3, 4 and 5.

Sample 3: T_1 = 510°C, H_1 = 0 min (Mag. 20x)

Sample 3: T_1 = 510°C, H_1 = 0 min (Mag. 20x)

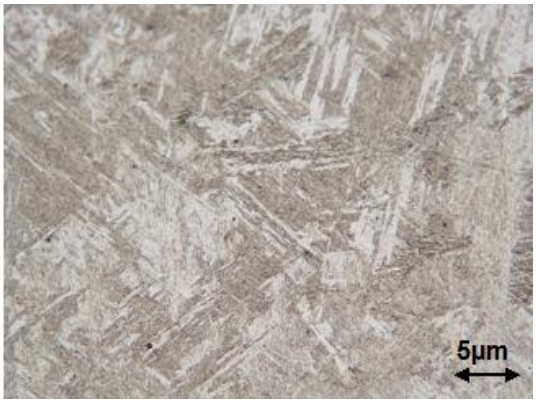

Sample 4: T_1 = 510°C, H_1 = 5 min (Mag. 20x)

Sample 4: T_1 = 510°C, H_1 = 5 min (Mag. 20x)

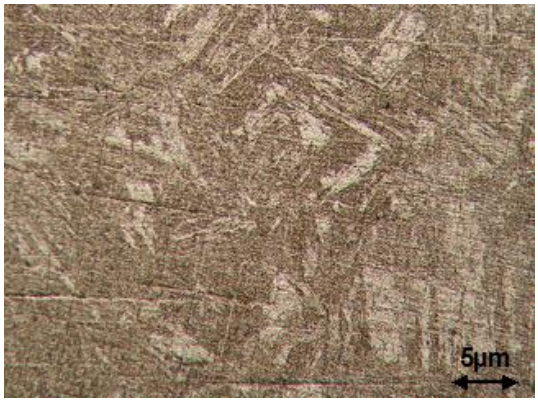

Sample 5: T_1 = 610°C, H_1 = 5 min (Mag. 20x)

Sample 5: T_1 = 610°C, H_1 = 5 min (Mag. 50x)

Micrographs of samples 6, 7 and 8.

Sample 6: T_1 = 650°C, H_1 = 5 min (Mag. 20x)

Sample 6: T_1 = 650°C, H_1 = 5 min (Mag. 20x)

Sample 7: T_1 = 510 ºC, H_1 = 2 min, T_2 = 810 ºC, H_2 = 2 min (Mag. 20x)

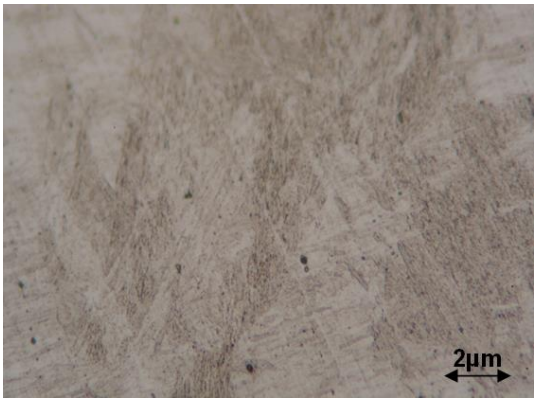

Sample 7: T_1 = 510 ºC, H_1 = 2 min, T_2 = 810 ºC, H_2 = 2 min (Mag. 50x)

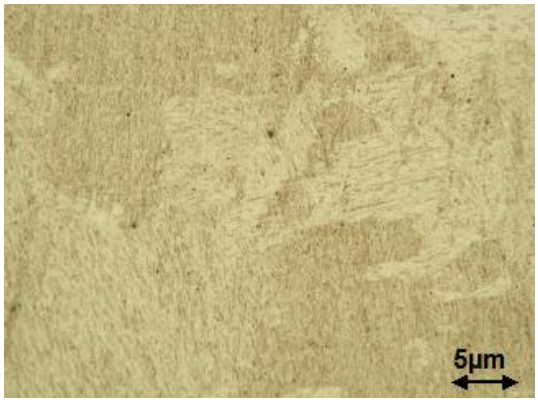

Sample 8: T_1 = 510 ºC, H_1 = 2 min, T_2 = 810 ºC, H_2 = 5 min (Mag. 20x)

Sample 8: T_1 = 510 ºC, H_1 = 2 min, T_2 = 810 ºC, H_2 = 5 min (Mag. 50x)

Micrographs of samples 9, 10 and 11.

Sample 9: T_1 = 510 ºC, H_1 = 2 min, T_2 = 915 ºC, H_2 = 2 min (Mag. 20x)

Sample 9: T_1 = 510 ºC, H_1 = 2 min, T_2 = 915 ºC, H_2 = 2 min (Mag. 50x)

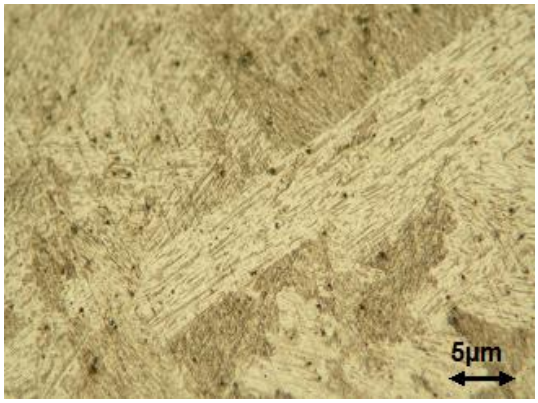

Sample 10: T_1 = 510 ºC, H_1 = 5 min, T_2 = 915 ºC, H_2 = 2 min (Mag. 20x)

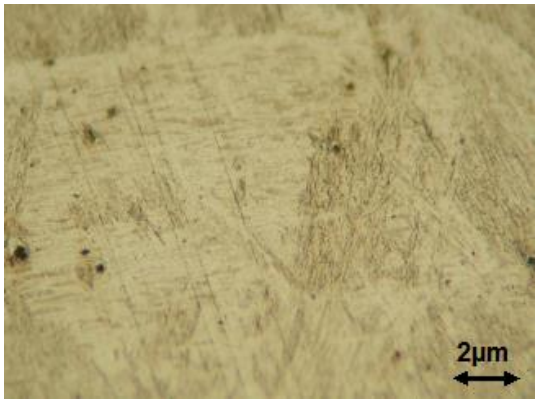

Sample 10: T_1 = 510 ºC, H_1 = 5 min, T_2 = 915 ºC, H_2 = 2 min (Mag. 50x)

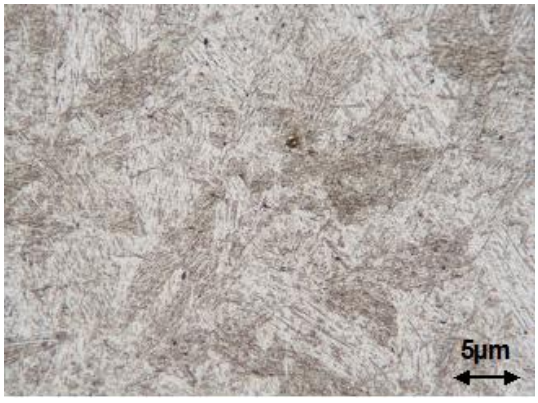

Sample 11: T_1 = 510 ºC, H_1 = 5 min, T_2 = 915 ºC, H_2 = 5 min (Mag. 20x)

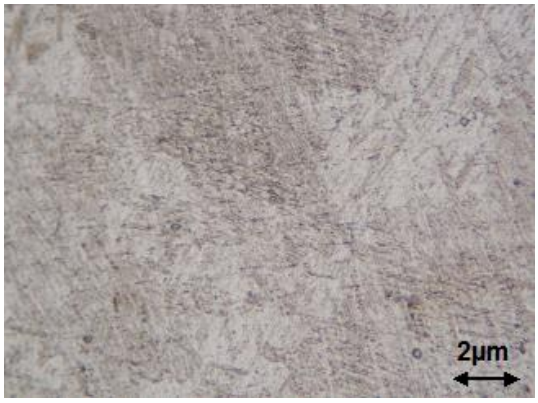

Sample 11: T_1 = 510 ºC, H_1 = 5 min, T_2 = 915 ºC, H_2 = 5 min (Mag. 50x)

Micrographs of samples 12, 13 and 14.

Sample 12: T_1 = 610 ºC, H_1 = 2 min, T_2 = 915 ºC, H_2 = 2 min (Mag. 20x)

Sample 12: T_1 = 610 ºC, H_1 = 2 min, T_2 = 915 ºC, H_2 = 2 min (Mag. 50x)

Sample 13: T_1 = 610 ºC, H_1 = 5 min, T_2 = 915 ºC, H_2 = 2 min (Mag. 20x)

Sample 13: T_1 = 610 ºC, H_1 = 5 min, T_2 = 915 ºC, H_2 = 2 min (Mag. 50x)

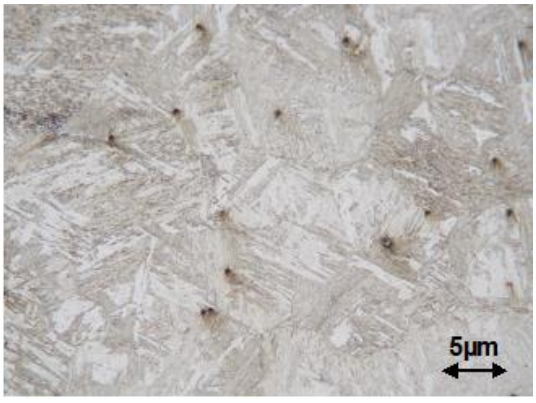

Sample 14: T_1 = 650 ºC, H_1 = 2 min, T_2 = 915 ºC, H_2 = 2 min (Mag. 20x)

Sample 14: T_1 = 650 ºC, H_1 = 2 min, T_2 = 915 ºC, H_2 = 2 min (Mag. 50x)

Micrographs of samples 15, 16 and 17.

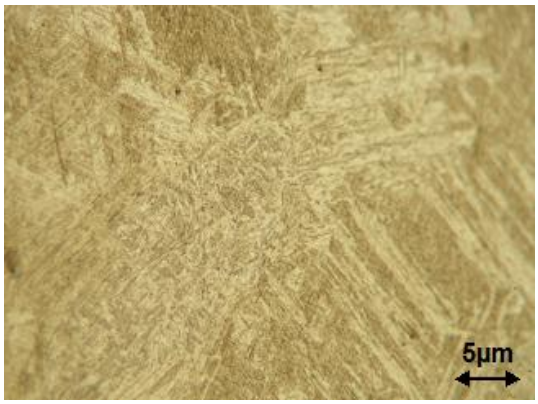

Sample 15: T_1 = 650 ºC, H_1 = 5 min, T_2 = 915 ºC, H_2 = 2 min (Mag. 20x)

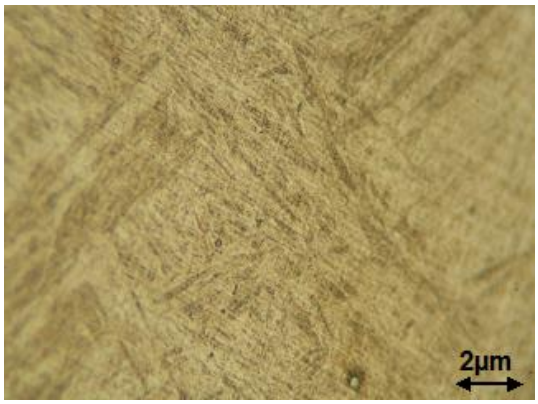

Sample 15: T_1 = 650 ºC, H_1 = 5 min, T_2 = 915 ºC, H_2 = 2 min (Mag. 50x)

Sample 16: T_1 = 650 ºC, H_1 = 2 min, T_2 = 915 ºC, H_2 = 5 min (Mag. 20x)

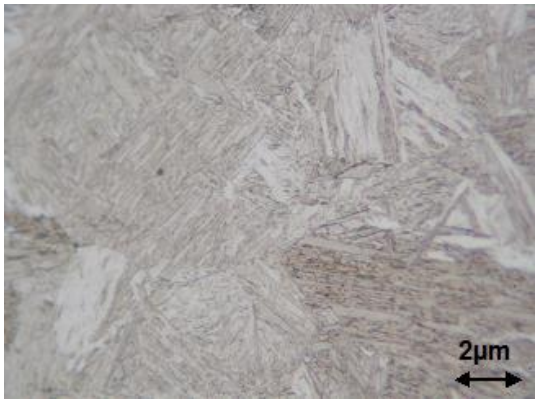

Sample 16: T_1 = 650 ºC, H_1 = 2 min, T_2 = 915 ºC, H_2 = 5 min (Mag. 50x)

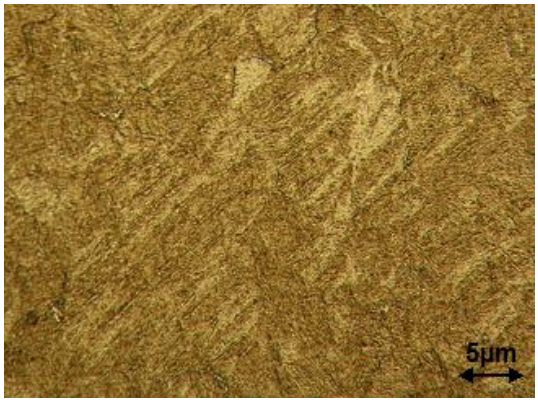

Sample 17: T_1 = 610 ºC, H_1 = 5 min, T_2 = 975 ºC, H_2 = 2 min (Mag. 20x)

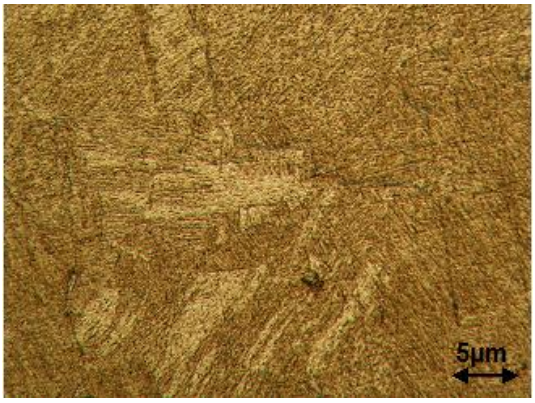

Sample 17: T_1 = 610 ºC, H_1 = 5 min, T_2 = 975 ºC, H_2 = 2 min (Mag. 20x)

Micrographs of samples 18, 19 and 20.

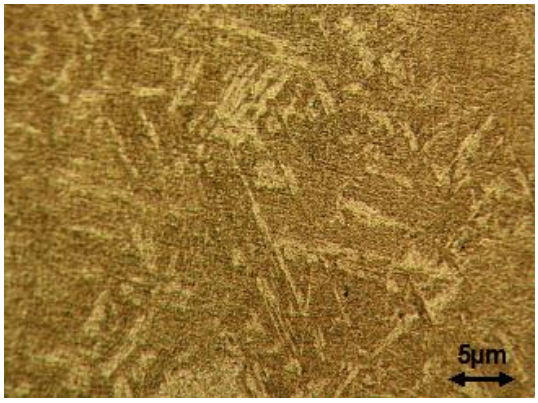

Sample 18: T_1 = 610 ºC, H_1 = 5 min, T_2 = 975 ºC, H_2 = 5 min (Mag. 20x)

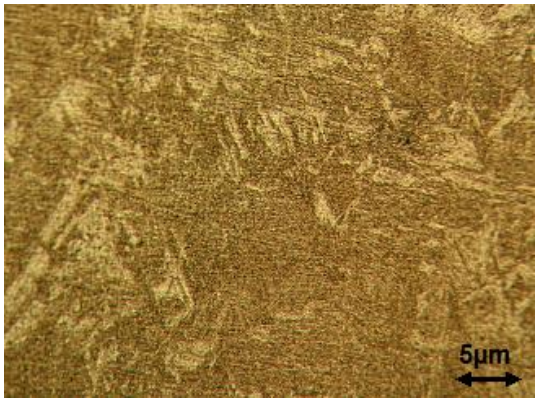

Sample 18: T_1 = 610 ºC, H_1 = 5 min, T_2 = 975 ºC, H_2 = 5 min (Mag. 20x)

Sample 19: T_1 = 610 ºC, H_1 = 5 min, T_2 = 975 ºC, H_2 = 2 min (Mag. 20x)

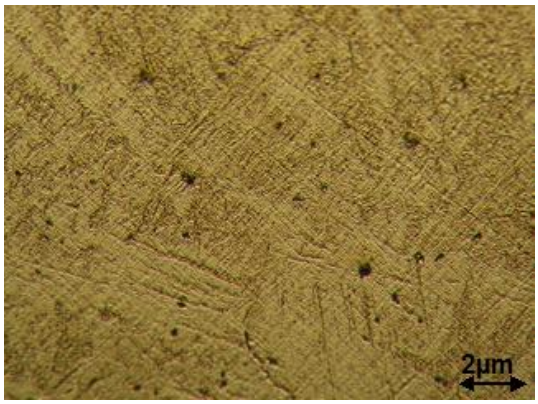

Sample 19: T_1 = 610 ºC, H_1 = 5 min, T_2 = 975 ºC, H_2 = 2 min (Mag. 50x)

Sample 20: T_1 = 610 ºC, H_1 = 5 min, T_2 = 975 ºC, H_2 = 5 min (Mag. 20x)

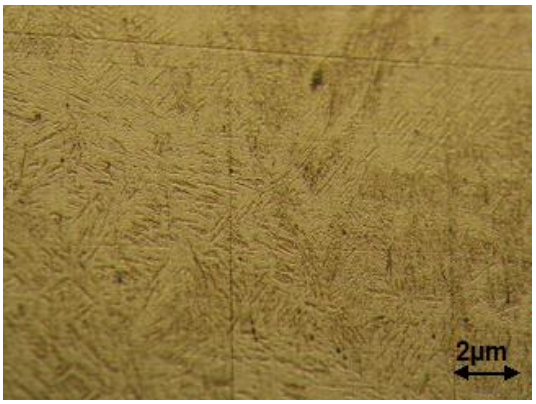

Sample 20: T_1 = 610 ºC, H_1 = 5 min, T_2 = 975 ºC, H_2 = 5 min (Mag. 50x)